解析下視丘投射至海馬回突觸中共同傳遞麩胺酸及γ-氨基丁酸的功能意義

Deciphering the Functional Significance of Hypothalamic Glutamate/GABA Cotransmission in the Hippocampus

研究生: Musa Iyiola Ajibola

指導教授：連正章 博士 (Lien, Cheng-Chang, M.D., Ph.D.)

共同指導教授：陳志成 博士 (Chen, Chih-Cheng, Ph.D.)

國立陽明交通大學

跨領域神經科學學位學程

博士論文

A Dissertation
Submitted to Taiwan International Graduate Program in Interdisciplinary Neuroscience
National Yang Ming Chiao Tung University
in Partial Fulfilment for the Requirements for the Degree of Doctor of Philosophy
in
Interdisciplinary Neuroscience

November 2021

Taiwan, Republic of China

中華民國一一○年十一月

National Yang Ming Chiao Tung University

Authorization to Copyright of Thesis/Dissertation and ETD(Electronic Thesis/Dissertation)

(For authors to bind after the title page)

The authorized thesis/dissertatione is my PH.D thesis/dissertation at Department of Taiwan International Graduate Program in Interdisciplinary Neuroscience of National Yang Ming Chiao Tung University in 1 (semester) 110 (academic year)

Title：Deciphering the Functional Significance of Hypothalamic Glutamate/GABA Cotransmission in the Hippocampus

Advisor：Cheng-Chang, Lien

1. Authorization to Copyright of Thesis/Dissertation (Hard copy)

   All the thesis/dissertations of National Yang Ming Chiao Tung University complies with Subparagraph 3, paragraph 2, Article 15 of the Copyright Act. In principle, all the thesis/dissertations shall be open resource for academic knowledge exchange.

2. Authorization to Copyright of ETD (Electronic Thesis/Dissertation)

   I hereby authorize, non-exclusive and free of charge, the said dissertation to National Yang Ming Chiao Tung University(NYCU), University System of Taiwan (UST) and the National Certral Library.

ElectronicThesis/Dissertation Publish Scope and Time	
Abstract (Chinese & English)	■ available to the public immediately
Fulltext for NYCU and UST	■ available to the public immediately
Fulltext for Internet & National Central Library	■ available to the public immediately

Note: Based on the concept of "resource sharing, mutual benefit cooperation" and the purpose of giving back to society and academic research, the thesis/dissertation is open. Any reader can search, download or print the thesis/dissertation within the limits permitted by the copyright law.

Authorized by: 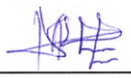 (Signature)

2022 / 02 / 08 (YYYY/MM/DD)

National Yang Ming Chiao Tung University
Thesis Approval Form

Student name: Ajibola, Musa Iyiola (English) 伊木夏 (hinese)

Program: ☐ Master Program ■ Ph.D. Program

Department/Institute: ıterdisciplinary Neuroscience

Title of the thesis:

(Chinese Title) 解析下視丘投射至海馬回突觸中共同傳遞麩胺酸及γ-氨基丁酸的功能意義

(English Title) Deciphering the Functional Significance of The Hypothalamic Glutamate/GABA Cotransmission in the Hippocampus

Approved by the Thesis Defense Committee

Committee Convener: _____ (Signature)

Additional Committee member

_____ (Signature) _____ (Signature)

_____ (Signature) _____ (Signature)

_____ (Signature) _____ (Signature)

_____ (Signature) _____ (Signature)

This thesis has been satisfactorily revised.

Signature of the Thesis Advisor: _____

Signature of the Director of Institute/ Program: 跨領域神經科學國際研究生博士學位學程主任 連正章

2022/02/08 (Date)

110.07 版

ACKNOWLEDGMENTS

All praises and adorations are due to Allah (SWT), the God of the universe.

First and foremost, I express my profound gratitude to my advisor, Professor Cheng-Chang Lien, who has painstakingly supervised this work. I thank you for your enormous guidance, direction, and encouragement. Throughout my Ph.D. study, you invested a lot of time in teaching and training me to achieve this feat. Thank you for the opportunity to do science with you. I am very proud to be your first international Ph.D. student and appreciate you for creating an international student-friendly lab environment. I have learned a lot from you, it is indeed a life-changing experience. I will forever be grateful.

I would also like to thank all the Lien lab members for your help with my research, constructive criticism, and scientific feedback. Especially for helping with animal management. You guys are wonderful. I also thank CJ who was the first to show me how to do local field recordings. My appreciation goes to KY for always being ready to help and have some scientific discussions with me. I thank Wahab and Daron for helping me with some experiments and analysis. I also thank Yu-Ling, TYY, HC, George, Jimmy, JD, ZS, SM, Wendy, WL, and everyone that have stayed in Lien Lab with me. I also thank all the past Lien lab members that our paths have crossed during my stay in the lab. You have all contributed to the success of this project in one way or another.

In the course of executing my project, I was blessed with amazing thesis committee members, Professor Min-Yuan, Min (National Taiwan University), Dr. Chih-Cheng, Chen (Academia Sinica), Professor Shih-Chieh, Lin (National Yang Ming Chiao Tung University), Dr. Hau-Jie, Yau (National Taiwan University) and Dr. Ching-Lung, Hsu (Academia Sinica). Thank you all for your time and scientific contributions.

My sincere thanks to the Taiwan International Graduate Program (TIGP) of Academia Sinica for giving me the scholarship to do science in such a multidisciplinary research environment. I also appreciate the management and the program assistants of the TIGP-interdisciplinary Neuroscience program (Vira and Ya-Jen) for their support right from the beginning of my study. I would also like to appreciate the Office of International Affairs (OIA) of National Yang Ming Chiao Tung University for their assistance during my stay at NYCU. I would also like to thank Nigerian students at National Yang Ming Chiao Tung University for their support and friendship.

A big thank you and gratitude to my parents and siblings. I appreciate your prayers, encouragement, and support at all times.

Finally, my heartfelt gratitude and appreciation to my lovely wife (Habeebat Aderonke Mustapha) and my adorable daughter (Khadijah Oladunni Ajibola). You have sacrificed and shared in my pains. Thank you for your understanding and tremendous support.

THANK YOU ALL!

CITATION TO OWN PREVIOUSLY PUBLISHED WORK

Parts of this thesis have been previously published:

Journal articles:

- **Ajibola MI,** Wu JW, Abdulmajeed WI, Lien CC (2021) Hypothalamic Glutamate/GABA Cotransmission Modulates Hippocampal Circuits and Supports Long-term Potentiation. J Neurosci 41:8181-8196.

Abstracts presented at conferences:

- **Ajibola MI,** Lien CC (2018) Differential glutamate and GABA release onto hippocampal dentate cells by supramammillary nucleus neurons. Poster session presented at the 2018 11th FENS Forum of Neuroscience, Berlin, Germany.
- **Ajibola MI,** Lien CC (2018) Differential glutamate and GABA release onto hippocampal dentate cells by supramammillary nucleus neurons. Poster session presented at the 2018 EMBO Neural development Workshop, Taipei, R.O.C

中文摘要

海馬回為負責認知及情緒功能的關鍵腦區。齒狀回為海馬回次核區中的第一個訊號處理器其會接受來自大腦皮質及皮質下核區傳來的訊號。其中，大腦皮質至海馬回路徑會在記憶獲得及提取時傳遞記憶相關的訊息；然而，來自皮質下的訊號參與了調控皮質及海馬回間的訊息溝通。下視丘乳頭上核藉由共同釋放兩種截然不同的快速神經傳遞物質，也就是麩胺酸及γ-氨基丁酸，來實質上的支配齒狀回活性，因而能協助空間定位及空間記憶的形成。然而乳頭上核中神經元是藉由何種突觸機制來調控齒狀回活性及其突觸可塑性尚未被釐清。齒狀回由興奮性的顆粒細胞及抑制性的中間神經元所組成。在這本論文中，我用光遺傳學、電生理及藥理學的方法，證明來自乳頭上核的訊號會透過不同的突觸機制差異性地調控齒狀回中不同種細胞的活性。選擇性活化乳頭上核會在所有的突觸後神經元產生突觸興奮及突觸抑制作用，然而這兩種作用的比例是會依突觸後細胞種類的不同而改變的。具體來說，樹突抑制型中間神經元主要接收突觸興奮作用，然而體抑制型中間神經元及顆粒細胞則主要接收突觸抑制訊號。雖然單獨活化乳頭上核並不足以興奮顆粒細胞，但是在有興奮性驅動力的情況下，活化乳頭上核可使顆粒細胞產生動作電位的時間更精準並縮短其產生動作電位所需的時間。此外，在有皮質訊號輸入時活化乳頭上核會增加顆粒細胞動作電位的產生，進而促使皮質到顆粒細胞突觸間的長期增強作用。總結來說，這些發現顯示了乳頭上核共同傳遞的麩胺酸及γ-氨基丁酸對於維持齒狀回中興奮/抑制的動態平衡是有貢獻的，並且能透過提升皮質到顆粒細胞突觸間的長期增強作用來幫助記憶的編碼。

關鍵字: 海馬回、乳頭上核、光遺傳學、電生理、麩胺酸、γ-氨基丁酸

ABSTRACT

The hippocampus is a key brain structure for cognition and emotion. Among the hippocampal subregions, the dentate gyrus (DG) is the first information processor that receives inputs from cortical and subcortical brain areas. The cortico-hippocampal pathways transfer mnemonic information during memory acquisition and retrieval, whereas subcortical inputs engage in the modulation of communication between the cortex and the hippocampus. The hypothalamic supramammillary nucleus (SuM) substantially innervates the DG by coreleasing two contrasting fast neurotransmitters, glutamate and GABA, and thereby supports spatial navigation and contextual memory. However, the synaptic mechanisms by which SuM neurons regulate the DG activity and synaptic plasticity are not well understood. The DG comprises excitatory granule cells (GCs) as well as inhibitory interneurons (INs). In this study, I combine optogenetic, electrophysiological, and pharmacological approaches, and demonstrate that SuM input differentially regulates the activities of different cell types in the DG via distinct synaptic mechanisms. Selective SuM activation results in synaptic excitation and inhibition in all postsynaptic targets, the ratio of these two components is variable and cell type-dependent. Specifically, dendrite-targeting INs receive predominantly synaptic excitation, whereas soma-targeting INs and GCs receive primarily synaptic inhibition. Although SuM excitation alone is insufficient to excite GCs, it enhances the GC spiking precision and reduces the latencies in response to excitatory drives. Furthermore, SuM excitation enhances the GC spiking in response to the cortical input, thereby promoting the induction of long-term potentiation at cortical-GC synapses. Taken together, these findings show that SuM glutamate/GABA cotransmission contributes to the maintenance of excitation/inhibition dynamics in the DG, and could as well support memory encoding via enhancement of long-term potentiation at the cortical-GC synapses.

Keywords: Hippocampus, Supramammillary nucleus, Optogenetics, Electrophysiology, Glutamate, GABA

GRAPHICAL ABSTRACT AND HIGHLIGHTS

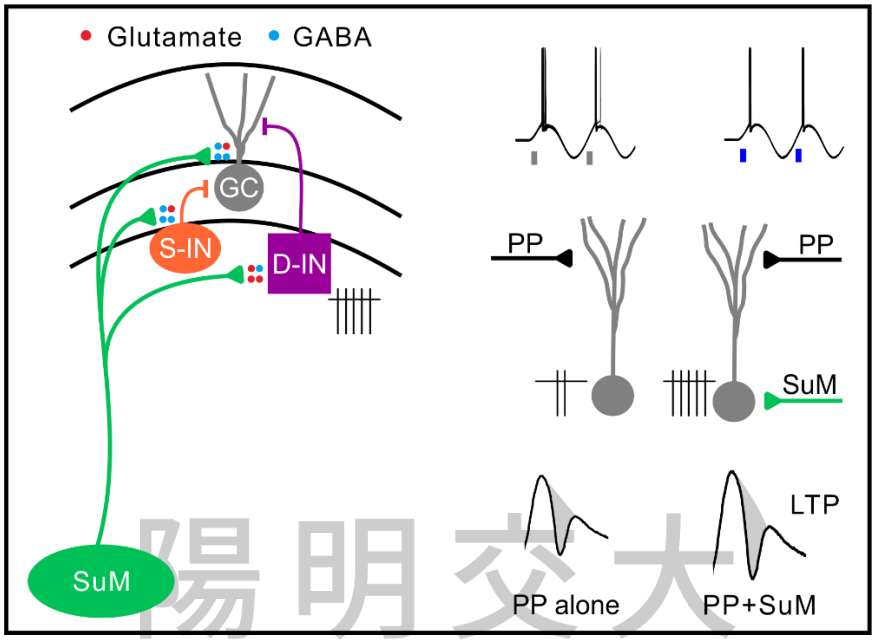

Highlights

- SuM neurons cotransmit glutamate and GABA onto DG cells in a target-dependent manner.
- Activation of the SuM input preferentially recruits dendrite-targeting INs over GCs and soma-targeting INs.
- SuM excitation, although weak, enhances GC spike generation and spike-timing precision.
- SuM input co-activated with the cortical input supports synaptic potentiation at cortical-GC synapses.

TABLE OF CONTENTS

LIST OF FIGURES

LIST OF TABLES

ABBREVIATIONS

AAC: axo-axonic cell

AAV: adeno-associated virus

AAV5: AAV serotype 5

ACSF: artificial cerebrospinal fluid

AMPA: α-amino-3-hydroxy-5-methyl-4-isoxazolepropionic acid

BC: basket cell

CA: cornu Ammonis

ChR2: channelrhodopsin-2

Cre: Cre recombinase

DG: dentate gyrus

D-IN: dendrite-targeting IN

EC: entorhinal cortex

EPSC: excitatory postsynaptic current

eYFP: enhanced yellow fluorescent protein

fEPSP: field excitatory postsynaptic potential

GABA: γ-aminobutyric acid

GC: granule cell

GCL: GC layer

HICAP: hilar commissural–associational pathway

HIPP: hilar PP-associated

IML: inner molecular layer

IN: interneuron

IPSC: inhibitory postsynaptic current

LEC: lateral entorhinal cortex

LS: lateral septum

LTD: long-term depression

LTM: long-term memory

LTP: long-term potentiation

MC: mossy cell

MEC: medial entorhinal cortex

ML: molecular layer

MML: medial molecular layer

MPP: medial PP

MS: medial septum

mt: mammillothalamic tract

NMDAR: N-methyl-D-aspartate receptor

OML: outer molecular layer

PN: principal neuron

PP: perforant path

PR: perirhinal cortex

pSpike: population spike

PV: parvalbumin

Rin, input resistance

RMP: resting membrane potential

SEM: standard error of the mean

S-IN: soma-targeting IN

SST: somatostatin

STM: short-term memory

SuM: supramammillary nucleus

TLE: temporal lobe epilepsy

TML: total molecular layer

TTX: tetrodotoxin

VGAT: vesicular GABA transporter

VGluT2: vesicular glutamate transporter 2

VMAT2: vesicular monoamine transporter 2

VIP: vasoactive intestinal polypeptide

VTA: ventral tegmental area

WT: wild-type

1. INTRODUCTION

1.1. Brain networks

The human brain comprises about 86 billion neurons complexly organized into interconnected neuronal networks whose activation characterizes a decipherable linear pathway (Callaway, 2002; Herculano-Houzel, 2012; Hilgetag et al., 2016). These neurons communicate through the generation of electrical signals and inspire complex behaviors which are excellently executed in the brain such as learning, memory, motivation, movement, perception, and cognition. A healthy brain self-organizes towards ‘‘small-world networks’’ consisting of a pattern of dense local microcircuits and critical long-range connections (Buxhoeveden and Casanova, 2002)**.** While the local microcircuits ensure proper neural information processing within a given brain region, the long-range connections facilitate interregional communications essential for complex brain functions. Brain structures are not isolated highlands, they receive inputs and give outputs that modulate their neural functions and the functions of other brain areas. This complex design has been demonstrated to arise under genetic control (Stam and van Straaten, 2012). Understanding the organization of distributed brain networks and how they communicate to produce complex functions during behaviors has been a major challenge to neuroscientists. However, in recent decades substantial progress has been made with the development of disruptive modern tools and techniques that have helped in identifying functions of individual brain structures, their cellular compositions, and connectivity. These have contributed remarkably to our understanding of complex brain functions including learning and memory formation, and some complex mechanisms underlying neurological disorders.

1.2. Concept of learning and memory

For survival, we need to acquire knowledge and remember events in place and time. What are learning and memory? How do we learn, store, remember and forget things we have learned? These are fascinating questions that have always been of interest to neuroscientists for decades. To neuroscientists, learning is an act of acquiring information that engages specific brain areas and results in specific changes in the brain cells that outlast the learning experience. During learning, a small population of brain cells (called an ensemble) is activated and they undergo persistent biological/physical/chemical changes (called engrams) that are reactivatable by appropriate recall cues leading to retrieval of specific memory. Therefore, memory is an act of storage of neural representation acquired by experience and its retrieval when needed to guide ongoing behaviors. Learning and memory are cognitive functions essential in our interaction with the environment and entail an interaction of large, interconnected brain networks. They are conceptualized in three stages. 1, encoding; the initial registration, acquisition of information, and persistent trace (engram). 2, storage; the maintenance and consolidation of information over time. 3, retrieval; the process of reactivation of stored information to influence ongoing behavior.

Over the years, Psychologists and Neuroscientists have designed several behavioral paradigms in animals and human studies to assess, classify and identify the neurological substrates of learning and memory (Eichenbaum, 1997; Tulving and Schacter, 1990; Squire, 1987; Thompson and Krupa, 1994). A notable and key advancement in the neurobiology of memory was the classification by Squire (1987, 2004) that defined the differences between declarative memory (explicit) and non-declarative memory (implicit) based on their variable dependence on distinct brain areas (Cohen and Squire, 1980). The non-declarative memory involved procedural skills, and the train-

ing of reflexive motor skills (such as driving a car, or riding a bicycle) and does not require conscious recall of the memory. It is believed that it depends largely on the cerebellum, striatum, and cortical association areas. Declarative memory (explicit) on the other hand is a memory of general facts and their meanings, knowledge of people, places, time, and things. It requires a deliberate and conscious recall effort. It is considered to be mostly carried out by the hippocampus and amygdala. Explicit memory has been further classified as semantic memory, a memory of facts that are learned and independent of context and individual relevance, or episodic memory, a memory of events. Episodic memory is experienced and dependent on context and individual relevance.

Based on the temporal dimension, memory is further classified into short-term memory (STM) and long-term memory (LTM). STM lasts for a while from a few seconds, minutes to hours such as working memory, and does not require consolidation. On the contrary, LTM lasts for many hours, months, or years and requires consolidation. It has been shown that STM and LTM share the same neural representation during encoding and retrieval. Medial temporal lobe structures (including the hippocampus) were demonstrated to be responsible for the formation of new representations regardless of their duration, and that similar processes are active in both STM and LTM (Jonides et al., 2008; Wheeler et al., 2000). However, how memories are formed and maintained is still unclear. In 1949, Donald Hebb proposed a synaptic plasticity-based mechanism as the memory substrate. This mechanism suggests that the strengthening of synaptic connectivity among a group of neurons by feedforward circuits is the persistent changes (engrams) underlying learning and memory. Moreover, other cellular and molecular mechanisms such as protein synthesis have been demonstrated to underlie memory formation (Abel et al., 1998; Davis, 1996; Kandel and Schwartz, 1982). Memory storage and processing are brain areas specific. The neocortex and the amygdala are known to play a role in semantic memory (Merzenich and Sameshima, 1993) and

associative learning (Damasio, 1995), respectively. The strengthening of synaptic connectivity between the entorhinal cortex (EC) and the hippocampus is thought to be crucial in the formation of episodic memory (Squire, 2004, Zhang et al., 2013).

1.3. Hippocampus

The hippocampus is a brain structure situated deep in the medial temporal lobe of the human brain and forms an essential component of the brain limbic system. The famous Venetian human anatomist, Julius Caesar Aranzi discovered the hippocampus. He named it "hippocampus" due to its seahorse-like shape (in Greek, hippo means "horse" and kampos means "sea monster"). Anatomically, the hippocampus is divided into the dentate gyrus and hippocampal proper. The hippocampus is well conserved in evolution. Biologists in primatology and Zoology fields also confirmed the existence of a similar structure in other primates, mammals, and birds years after Julius Caesar Aranzi, discovery (Colombo and Broadbent, 2000; West, 1990). Interestingly, despite the structural variations that exist in the vertebrate's forebrains, their hippocampus still conserved the characteristic, highly laminated histology similar to that of birds and mammals (Ocana et al., 2017; Rodriguez et al., 2002). Although some differences in species were reported in a few studies (Ahn et al., 2016; Lensjo et al., 2017; Rodriguez-Exposito et al., 2017), the hippocampus is proposed to be crucial for spatial cognition (Bingman, 1992) which is critical for survival across species. However, with the evolving and constant change in the environment, the functions of the hippocampus are getting more complicated.

1.3.1. Functions of the hippocampus

For the mammalian hippocampus, olfaction is the first proposed hippocampal function because of the observed anatomical projections between the hippocampus, lateral EC, and the olfactory bulb (van Groen and Wyss, 1990). Olfaction as the primary function of the hippocampus is not widely

accepted by neuroscientists (Otto et al., 1991). The declarative theory and the spatial recognition theory were later promulgated regarding the functions of the mammalian hippocampus. The declarative theory is based on phenotypic manifestations especially those that accompany pathological hippocampal damage. The most famous among the hippocampal pathological studies is the well-known patient Henry Molaison's (H.M) clinical report (Scoville and Milner, 1957), who suffered a severe memory loss of anterograde and partial retrograde amnesia after bilateral medial temporal lobe resection. The surgery relieved H.M of epilepsy but suffer distinct memory while his working memory and procedural memory were not affected. After the clinical case report of H.M, the hippocampus has been widely recognized as the main brain area responsible for memory acquisition and recall.

The spatial recognition theory describes the hippocampus as the global positioning system (GPS) of the brain. O'Keefe and Dostrovsky promulgated the spatial recognition function of the hippocampus and supported it with experimental data in 1971. They discovered some principal neurons in the rat hippocampus that exhibit spike activities only at a particular location of the room and not anywhere else. They named these location-specific spiking cells "place cells" and locations, where they fire, are called "place fields" (O'Keefe and Dostrovsky, 1971). Their experiments showed that in a freely moving rat, different groups of place cells encode different locations in the room. Place-modulated cells have been identified in all hippocampal subfields while the most prominent spiking fields are observed in the CA1 area (Barnes et al., 1990; Senzai and Buzsáki, 2017). However, strong evidence to support the presence of "place cells" in the hippocampal subfields of primates is relatively lacking, this can be attributed to technical challenges in recording brain activities in freely moving monkeys or humans. In addition to location recognition, other features such as relative spatial orientation, the distance between locations, landmarks recognition,

and head direction are also vital in spatial navigation (Stachenfeld et al., 2017). How spatial signals are conveyed to the hippocampus remained enigmatic until the discovery of another group of spatial encoding cells called "grid cells" in the medial EC (MEC) by May-Britt and Edvard Moser's group in 2005. They recorded the activities of neurons in the MEC while animals freely explored the recording chamber. The grid cells were described as a group of cells that fire action potential at multiple locations when the animal location coincides with the vertex of a periodic grid across the entire space. These cells provide the coordinate system for mapping the distance between different locations (Fyhn et al., 2008; Hafting et al., 2005). Border cells were described as cells activated when an animal approaches a specific visible boundary of the recording space. These cells encode and provide information about the surroundings of the boundaries (Brun et al., 2008; Meister and Buffalo, 2018; Solstad et al., 2008; Taube et al., 1990). The head-direction cells were characterized as cells that generate action potentials only when an animal faces a specific direction and is independent of its location in space. They were first identified in the postsubiculum (Taube et al., 1990) followed by MEC, and later in other brain regions (Moser et al., 2017; Sargolini et al., 2006). The outstanding phenomenon that is yet to be understood is how the spatial coding cells interact with each other and get coordinated by other brain areas to bring about effective spatial navigation (Moser et al., 2017; Zhang et al., 2013). Collectively, the aforementioned mounting evidence supports that in addition to memory, the hippocampus is also central to spatial navigation.

The hippocampus has a long, curved structure that is evolutionarily conserved in all mammalian brains. Along the longitudinal hippocampal axis, different parts have been shown to have distinct connectivity with other brain areas, and therefore, they may be responsible for distinct functions. Early studies that involved lesions along the long hippocampal axis suggest a functional

dichotomy between the dorsal and ventral parts of the hippocampus. The dorsal (or posterior) hippocampus was demonstrated to be involved in spatial navigation while the ventral (or anterior) is crucial in anxiety-based behaviors (Moser et al., 1993, Wang et al., 2021). Available evidence from structural and physiological studies which are now being corroborated by the emerging gene expression profiles suggest clear functional gradients across the longitudinal hippocampal axis (Strange et al., 2014).

1.3.2. Organization of the hippocampus

In mammals, the hippocampus is anatomically made up of two major parts; the dentate gyrus (DG) and the hippocampal proper, that is the *Cornu Ammonis* (CA; including CA3, CA2, and CA1). The great neuroanatomist Santiago Ramon y Cajal described the trisynaptic circuit as the pivotal circuit in the hippocampus. The trisynaptic circuit consists of granule cells (GCs) and pyramidal cells of the CA3 and CA1 (Amaral et al, 2007). The 1st synapse in the circuit is formed between the axonal projections from layer II of the EC called the perforant pathway (PP) and the distal dendrites the GC (the PP-GC synapse). The 2nd synapse between the mossy fibers, main axonal projections of GCs, and the CA3 pyramidal cells proximal dendrites (the mossy-CA3 synapse). The 3rd synapse is between the Schaffer collaterals, axonal projection from CA3 pyramidal cells, and CA1 pyramidal cells dendrites (the Schaffer collateral-CA3 synapse). Other excitatory circuits that also contribute to hippocampal functions are the direct PP-CA3 pathway, EC layer III to CA1 pathway, CA1-subiculum pathway, and DG feedback loop consisting of semilunar GC, GC, and mossy cells (Amaral et al., 2007; Strange et al., 2014).

Considering the laminated arrangement of the hippocampus, over the years, the hippocampus remains an excellent brain structure of choice by neurophysiologists to understand fundamen-

tal brain activities such as neurotransmission, synaptic plasticity, and electrophysiological properties of neurons. Moreover, the hippocampus is one of the most vulnerable brain regions in neurological disorders such as Alzheimer's disease, Huntington's disease, and temporal lobe epilepsy, thus, it has been implicated in the pathological processes associated with these diseases (Moodley and Chan, 2014; Ramaswamy, 2015; Ransome et al., 2012). The elaborate interactions exist between the hippocampus and other brain areas involved in several behaviors (Prasad and Chudasama, 2013), therefore, hippocampal damage has been linked to many behavioral deficits (Chudasama et al., 2009; Small et al., 2011; Zucker and Ranganath, 2015).

1.3.3. Dentate Gyrus

The DG is the first input region and information processor among the hippocampal subfields (Amaral et al., 2007; Treves et al., 2008). It plays a critical role in pattern separation (Berron et al., 2016; Leutgeb et al., 2007; Kheirbek et al., 2013; Yassa and Stark, 2011) and has also been shown to play a key role in cognitive and emotional behaviors such as spatial navigation, novelty recognition, exploration, anxiety, depression, and fear (Gilbert, et al., 2001, Amaral et al., 2007, Wang et al., 2021; Kesner, 2007, Kheirbek, et al., 2013). In neurological disorders including epilepsy, depression, dementia, anxiety, depression, and schizophrenia; impairment of the DG has been strongly implicated (Amaral, et al., 2007, Scharfman, 2007, Tamminga, et al., 2010).

In rodents, the DG is a well-layered structure and comprises two groups of neurons; the excitatory principal neurons and the inhibitory GABAergic interneurons. It is laminated into three layers of neuronal tissue; the molecular layer (ML), the granule cell layer (GCL), and the hilus. The ML is composed of GABAergic interneurons, GC dendrites, and axonal inputs from other brain regions. It is well laminated into the inner molecular layer (IML), middle molecular layer (MML), and outer molecular layer (OML). While the GCL is primarily constituted by polarized

glutamatergic principal neurons, the GCs. The hilus contains another glutamatergic neuron, mossy cells (MCs), and diverse GABAergic interneuron subtypes. The subgranular zone between the granule cell layer and the hilus houses the neural progenitor cells capable of dividing and generating functional, mature GCs throughout life (Ming and Song, 2011; Altman and Das, 1965, Jurkowski et al., 2020). The new mature GCs are integrated into already established DG circuitry (Paton and Nottebohm, 1984; Vivar et al., 2013).

GCs constitute the majority of glutamatergic cells in the DG with about 1,000,000 in the GCL of rats (Boss et al., 1985; West, 1990; Patton and Mcnaughton, 1995; Freund and Buzsáki, 1996). The other glutamatergic cells, MCs are approximately 30,000 (Buckmaster and Jongen-Relo, 1999). The GCs morphologically have small, round cell bodies localized in the GCL, monopolar dendrites in the ML, and their axonal output, the mossy fibers, that form synapses on CA3 neurons (Henze et al, 2000). GC axonal collaterals in the hilus primarily target the parvalbumin (PV)-expressing interneurons and the MCs. The PV^+ interneurons drive recurrent inhibition on the perisomatic region and axon initial segments of GCs, and the MCs that provide recurrent excitation on the proximal dendrite of GCs (Ascády et al., 1998; Blasco-Ibanez et al., 2000; Espinoza et al., 2018; Gulyas et al., 1992).

1.3.4. Diversity of GABAergic Interneurons in the DG

GABAergic interneurons (INs) are the arbiter of information flow in the hippocampus. They release γ-aminobutyric acid (GABA) as the main neurotransmitter which exerts a primarily inhibitory effect on targets by either hyperpolarizing or shunting mechanisms. GABA activates fast ionotropic $GABA_A$ or slow metabotropic $GABA_B$ receptors and controls neuronal excitability. GABAergic inhibition has been demonstrated to play a vital role in excitation/inhibition balance, information routing, ensemble selection, shaping the spatiotemporal dynamics of neuronal circuitry,

and generation of rhythmic activity (theta and gamma) (Klausberger and Somogyi, 2008; Lapray et al., 2012; Zaitsev, 2013).

The DG GABAergic INs are remarkably heterogeneous in terms of morphological, electrophysiological, neurochemical, and synaptic properties (Freund and Buzsáki 1996; Hosp et al., 2014; Booker and Vida, 2018). Individual class of DG INs innervates specific subcellular domains (perisomatic and dendritic domains) of the GCs suggesting their distinctive structural and functional characteristics (Pelkey et al., 2017; Liu et al, 2014; Halasy and Somogyi, 1993; Hefft and Jonas, 2005). Following this, DG INs that innervate the perisomatic region of the GCs are called soma-targeting interneurons (S-INs) while those innervating the dendritic domain are referred to as dendrite-targeting INs (D-INs). In addition, a small population of DG INs preferentially target other INs and are termed "IN-specific" interneurons. The S-INs, also called perisomatic inhibitory INs, include the basket cells (BCs, with axonal distribution in the GCL and make baskets of collaterals around the soma of GCs); and axo-axonic cells (AACs, with axonal distribution also in the GCL but target the axon initial segments of the GCs). BC is the most extensively studied GABAergic INs in the DG. BCs and AACs express Ca^{2+}-binding/buffer protein, parvalbumin (PV), and their firing pattern is characterized by fast-spiking, high-frequency action potentials. They control GC output by regulating spiking rates and spike-timing precision (Freund, 2003). PV-BC and PV-AAC receive strong synaptic inputs from the medial perforant path, commissural fibers of MCs, and axonal collaterals of mossy fibers of GCs (Hsu et al., 2016; Gulyas et al., 1992, Ascády et al., 1998, Blasco-Ibanez et al., 2000), and consequently drive fast feedforward and feedback inhibition to GCs (Penttonen et al., 1998; Pouille and Scanziani, 2001; Bartos et al., 2007). They exhibit synchronous synaptic transmission that is mediated by P/Q-type Ca^{2+} channels (Bucurenciu et al., 2010; Jonas et al., 2004; Hefft and Jonas, 2005). However, whether BCs and AACs are

recruited by subcortical inputs to the DG, and how their recruitment could contribute to the input-output transformation of GCs and behaviors remain open questions.

On the other hand, D-INs exhibit spatial selectivity in their axonal arborizations and dendritic compartment (Han et al., 1993; Freund and Buzsáki, 1996). They are classified into various types according to their layer-specific axonal density and soma locations. They exhibit distinct morphology and express different neurochemicals. They include the hilar commissural-associational path cells (HICAP, with soma in the hilar border and axonal density in the IML), the hilar perforant path cells (HIPP, with soma in the hilar border and axonal density in the OML), the total molecular layer cells (TML, with soma in the hilar border and axonal density in the in the spread in the entire ML), the molecular layer perforant path cells (MOPP, with soma in the ML and axonal density in the MML and/or OML), the hilar cells (HIL, with soma in the hilus and axonal density in the hilus), the neuroglioform cells (NGFC, with soma in the ML, short dendrites, about 100 um, axon branches profusely around the soma), the molecular layer commissural-associational path cells (MOCAP, with both the soma and axonal density in the IML), the outer molecular layer cells (OML, with soma in the OML and axonal density in the OML and extend beyond the hippocampal fissure to the subiculum) (Hefft and Jonas 2005; Halasy and Somogyi 1993; Han et al. 1993; Hosp et al. 2014; Savanthrapadian et al. 2014; Armstrong et al. 2011; Markwardt et al. 2011; Liu et al, 2014; Booker and Vida, 2018). HIPP, TML, and HIL cells express somatostatin (SST) (Han et al, 1993; Yuan et al., 2017), HICAP cells express cholecystokinin, CCK, (Han et al., 1993; Hefft and Jonas, 2005). D-INs are differentially recruited by extrinsic fibers in DG, suggesting they drive distinct feedforward inhibition onto the GCs and other INs. Finally, “IN-specific” D-IN express vasoactive intestinal polypeptide (VIP), and preferentially innervate other INs over principal cells. They are classified into hilus-projecting cells, ML projecting neurons, bistratified neurons, and

trilaminar neurons (Hájos et al., 1996; Wei et al., 2021). IN-specific interneurons have also been identified and characterized in the CA1 area (Tyan et al., 2014). In the DG network, the specific role of VIP INs is still not well understood.

1.5.5. Neuronal inputs to the DG

The DG receives extra-hippocampal inputs from the EC, medial septum (MS), locus coeruleus, and hypothalamic supramammillary nucleus (Amaral et al., 2007), and intrinsic (intra-hippocampal) inputs from commissural/associational inputs of MCs and back axonal projection of CA3 pyramidal cells (Scharfman, 2007). These inputs primarily target distinct subcellular domains of the GCs, and also make synaptic contacts with INs. The layer II cells of the EC are the major source of excitatory inputs to the DG via the PP and account for about 85% of the axospinous termination in the DG (Nafstad, 1967; Hjorth-Simonsen and Jeune, 1972). Lateral PP fibers (LPP) from LEC, innervate the OML while the medial PP fibers (MPP) from the MEC, innervate the MML of the ML of the DG. The commissural/associational inputs from MCs innervate the IML, and form asymmetric synaptic connections with GC proximal dendrites, and INs (Buckmaster et al., 1992; Larimer and Strowbridge, 2008; Hsu et al., 2016; Scharfman, 2016; Wang et al., 2021).

In addition to cortical inputs, DG also receives relatively few neurochemically distinct subcortical inputs such as cholinergic input from the MS/diagonal band of Broca (Bilkey and Goddard, 1987; Nyakas et al., 1987), dopaminergic/norepinephrinergic inputs from the locus coeruleus (Harley, 1991; Blackstad et al., 1967; Seo et al., 2021), and glutamate-GABA input from the supramammillary nucleus (Borhegyi and Leranth, 1997; Chen et al., 2020; Leranth and Hajszan, 2007; Magloczky et al., 1994; Nitsch and Leranth, 1994; Pan and McNaughton, 2004; Segal and Landis, 1974; Vertes, 2015). These inputs are known to play a modulatory role by interacting with both the principal neurons and GABAergic INs and participate in neural information processing within

the DG. However, considering the morpho-electrophysiological heterogeneity of INs, how subcortical inputs interact with different GABAergic INs remains an interesting question.

Cortico-hippocampal pathways play a central role in memory encoding, retrieval, pattern separation, and emotion (Amaral et al., 2007; Henze et al., 2002; Liu et al., 2012; Nakashiba et al., 2012). However, little is known regarding the functions of subcortical inputs to the hippocampus compared to cortical inputs. Among the subcortical brains, hypothalamic SuM provides substantial direct innervation to the supragranular layer of the DG.

1.4. Supramammillary nucleus

1.4.1. Anatomy and Physiology of SuM

The SuM is made up of relatively thin, neurochemically distinct cells situated dorsal to the hypothalamic mammillary bodies. (Pan and McNaughton, 2004**)**. SuM is bounded rostrally by the posterior and lateral hypothalamic nuclei, caudally by the interfascicular nucleus and the ventral tegmental area (VTA), dorsally by the posterior hypothalamic nucleus and the periaqueductal gray matter, ventrally by the mammillary body. Topographically, SuM is divided into medial parts (SuMM) and lateral parts (SuML) by the thalamomammillary tract (Swanson, 2018). Although there is no clear boundary between SuMM and SuML, SuMM is described as the SuM area between right and left SuML (Swanson, 2018). In terms of neuronal soma size, neurons in SuMM region are small (10-15 μm) and termed parvicellular while those in SuML are large neurons (20–30 μm) called grandicellular in rats (Pan and McNaughton, 2004; Risold and Swanson, 1997).

Although a small nucleus, SuM has wide anatomical connectivity with extensive ascending and descending afferents to several brain areas and receives inputs from different brain areas. Therefore, like monoamine systems, SuM may play some global modulatory role, especially in

emotion and mood behaviors. SuM provides major afferents to the hippocampus, septum, amygdala, some hypothalamic nuclei, EC, intralaminar thalamic nuclei, lateral habenula (LHb), medial preoptic area, and cingulate cortex (Chen et al., 2020) and receive inputs mainly from subcortical regions such as the lateral septum, MS, accumbens nucleus, zona incerta, lateral hypothalamus, medial preoptic nucleus, lateral preoptic nucleus, paraventricular hypothalamus, VTA, dorsal and median raphe nucleus.

The neuronal populations in the SuM are diverse in terms of their neurochemical properties, intrinsic properties, and synaptic connectivity, and are topographically distributed. They include glutamatergic cells, dopaminergic cells, calretinin-expressing neurons, substance P neurons, CCK-expressing neurons, VIP-expressing neurons (Pan and McNaughton, 2004), and recently described glutamate/GABA releasing cells (Boulland et al., 2009). The dopaminergic neurons are located mainly in the SuMM and project to the lateral septum and mammillary bodies (Gonzalo-Ruiz et al., 1999; Shepard et al., 1988; Swanson, 1982). The calretinin neurons are spread throughout the SuM areas. The glutamatergic positive and calretinin neurons are mainly located in the SuMl (Haglund et al., 1984, Boulland et al., 2009). The substance P fibers from SuMM terminate only in the CA2 region (Borhegyi et al., 1998)**,** and are formed prenatally (Berger et al., 2001). In the SuMl, the majority of large glutamatergic neurons co-express marker of GABAergic transmission, vesicular GABA transporter (VGAT) (Root et al., 2018, Boulland et al., 2009).

1.4.2. Functions of the SuM

Although SuM has comparatively few neurons, its neuronal populations have recently attracted attention due to their prominent role in the modulatory control of the hippocampus. For instance, the SuM was reported to contain neurons controlling hippocampal plasticity via monosynaptic

input (Nakanishi et al., 2001) and another group of SuM neurons modulating the frequency of hippocampal theta rhythm have also been described (Kirk and McNaughton, 1991; Kocsis and Vertes, 1994). SuM neurons have also been shown to be activated during behaviors such as learning (Ikemoto et al., 2005), Memory (Santin et al., 2003), anxiety (Silveira et al., 1993), exploration of novel environment (Ito et al., 2009; Vann et al., 2000), REM sleep and arousal (Pedersen et al., 2017; Renouard et al., 2015) and social interactions (Chen et al., 2020).

The hippocampal theta oscillation, a rhythmic slow-wave activity, which is the prominent feature of the hippocampal EEG has long been associated with hippocampal-dependent behaviors, such as mnemonic processes (Buzsaki, 2005; Kirk and Mackay, 2003). The resultant theta frequency from the synchronous firing of the hippocampal neurons is essentially dependent on the inflow of impulses from other brain areas such as the septum, EC, and SuM (Buzsaki, 2005; Buzsaki and Moser, 2013; Pan and McNaughton, 2004). Accumulating evidence has demonstrated that physiological generation and magnitude of hippocampal theta oscillation are related to and modulated by activation of reticular formation to the basal forebrain (Bland and Oddie, 1998; Pignatelli et al., 2012; Vertes and Kocsis, 1997) via, ascending brainstem-hippocampal pathway, a pathway in which SuM is central. (Vertes et al., 1986). The neural circuitry by which SuM modulates the hippocampal theta remains poorly understood.

The SuM neurons fire action potential *in vivo* in a pattern that phase lock with the theta activities of the hippocampus (Kocsis, 2006; Kocsis and Vertes, 1994; Vertes, 2015). Surprisingly, SuM lesion does not result in the complete abolition of the hippocampal theta oscillation (McNaughton et al., 1995; Thinschmidt et al., 1995), but a significant reduction in the theta frequency was widely reported (Kirk and McNaughton, 1993; Kocsis and Vertes, 1997). The multiple activities recorded from SuM were observed to be rhythmic at hippocampus theta frequency and

phase-locked to the ongoing hippocampal theta (Ito et al., 2018; Kirk, 1998; Kirk and McNaughton, 1991; McNaughton et al., 1995). SuM has been shown to make diverse long and short-range connections, and control the theta oscillation, however, the precise functions of SuM concerning specific connections to a given brain area are still scanty. Recently, SuM was reported as a key node that controls theta-frequency spike time coordination in the mPFC-NR-CA1 circuit, coordination that enhances the trajectory information transfer from the prefrontal cortex to the hippocampus during route decisions (Ito et al., 2018).

1.4.3. Supramammillary-hippocampal pathway

SuM afferents are among the notable subcortical long-range projections to the hippocampus and their roles in information processing by the GCs and pyramidal neurons are yet to be identified. The SuM neurons provide substantial direct innervation to the hippocampal DG and CA2 areas as well as indirect projections via the medial and lateral septum (Leranth and Kiss, 1996; Maglocky et al., 1994; Segal and Landis, 1974, see also Figure 1A and B). The majority of direct SuM projections terminate heavily on the somatodendritic area of GCs of DG and the pyramidal layer of CA2/CA3 (Magloczky et al., 1994), there is also light innervation of the hilus of the DG. While the SuM-DG projections signal contextual information during mnemonic memory, the SuM-CA2 is important for social interaction (Chen et al., 2020). The neurotransmitter signaling system at the SuM-hippocampal pathway remains controversial. Some reports stated that it is an exclusively glutamatergic system (excitatory) based on anatomical evidence that SuM afferent fibers form asymmetrical synapses (Dent et al., 1983; Magloczky et al., 1994; Stanfield and Cowan, 1984). Supporting this notion, SuM neurons axon terminals innervating DG, IML and CA2 were shown to lack GABA but express calretinin (Kiss et al., 2000; Leranth et al., 1999; Magloczky et al.,

1994). However, recent studies revealed that SuM-DG axon terminals co-express markers of glutamate and GABA release, vesicular glutamate transporter (VGluT2) and VGAT, respectively (Boulland et al., 2009; Root et al., 2018; Soussi et al., 2010) and make both asymmetric and symmetric synapses on the somatodendritic region of the GCs (Boulland et al., 2009, Soussi et al., 2010). Interestingly, the SuM-DG pathway co-releases glutamate/GABA while the SuM-CA2 pathway exclusively releases glutamate (Hashilomotodani et al., 2018; Robert et al., 2021). However, the specific cellular targets, synaptic properties, how SuM interacts with different cell types in DG, and the consequence of glutamate/GABA cotransmission on hippocampal information processing remain elusive.

1.5. Synaptic transmission

1.5.1. Synaptic organization

Synaptic transmission is communication between a neuron and other neurons, or muscle cells at a specialized site called a synapse. It forms the basis of complex functions of the brain. There are two major types of synaptic transmission, electrical and chemical transmissions. At an electrical synapse, communication between neurons is instantaneous, stereotypic, and occurs through specialized intercellular channels called gap junctions that directly allow a flow of ions between their cytoplasm. At chemical synapses, a presynaptic neuron releases chemical neurotransmitter(s) into a small space called a synaptic cleft, which then bind to receptors on the membrane of target postsynaptic neurons. Most neurons are identified based on the neurotransmitter they release such as glutamatergic, GABAergic, dopaminergic, and cholinergic neurons among others. However, neurons releasing multiple neurotransmitters have been identified in the brain.

At the presynaptic terminals, neurotransmitters are stored in the synaptic vesicles, each vesicle is filled with several thousand neurotransmitter molecules. When action potential arrived

at presynaptic terminals, voltage-gated Ca^{2+} channels open at the active zone, a region of synaptic vesicle clusters, and allow Ca^{2+} to enter. The rise in intracellular Ca^{2+} concentration triggers a biological process that causes the fusion of vesicles to the presynaptic membrane and thereby neurotransmitter release into the synaptic cleft, a process termed exocytosis. The transmitter molecules then diffuse across the synaptic cleft and bind to their receptors on the target postsynaptic cell membrane. This results in the opening or closing of ion channels followed by the ionic flux that changes the conductance and potential of the postsynaptic cell membrane. A synaptic vesicle release is capable of opening thousands of ion channels on the postsynaptic target, a process responsible for the amplifying effect at chemical synapses. Classically, two transmitter molecules are needed to open a given postsynaptic ion channel (Kandel et al., 2013). The strength of the synaptic connection is plastic depending on the activities or experience.

1.5.2. Corelease and cotransmission of neurotransmitters

Over the years, one neuron, one neurotransmitter idea conventionally classifies neurons into excitatory, inhibitory, and modulatory neurons according to neurotransmitter release at synapses. This idea is associated with Sir Henry Dale's concept (Dale, 1935) and was later termed Dale's principle by Eccles (Eccles, 1957). Our understanding of fast chemical communication among neurons and neural circuit functions has been based on this impression. This principle has been challenged and modified with the discovery of neurons with multiple neurotransmitter profiles. For instance, the release of neuropeptides along with classical neurotransmitters has long been recognized (Jan and Jan, 1982; Hokfelt et al., 1984; Sulzer and Rayport, 2000). Recently, the corelease and cotransmission of two or more classical neurotransmitters have been gaining attention. Subsets of neurons co-expressing multiple classical neurotransmitter markers in their axon terminals (Boulland et al., 2004) and capable of cotransmitting two or more classical neurotransmitters

have been demonstrated (Fattorini et al., 2015; Somogyi, 2006). Two inhibitory neurotransmitters, GABA and glycine, are simultaneously released from the same vesicles in the spinal cord (Jonas et al., 1998) and brainstem (O Brien and Berger, 1999; Russier et al., 2002; Nabekura et al., 2004; Awatramani et al, 2005). Two opposing neurotransmitters, glutamate and GABA are also reported to share the same synapse in LHb (Root et al., 2014; Shabel et al., 2014). Glutamate/GABA releasing neurons are reported to be most abundant in specific brain areas such as VTA, entopeduncular nucleus (EP), and SuM, and form distinctive synaptic architecture with their postsynaptic targets (Root et al., 2018). In addition, acetylcholine was reported to be coreleased with either glutamate (Li et al., 2004) or GABA (Takacs et al., 2018) by septal neurons.

Although cotransmitting neurons have been identified in many brain areas, the functional significance of cotransmission in neuronal computation and behaviors has been difficult to dissect. This can be largely attributed to; first, differential spatial and temporal profiles of the individual neurotransmitter being transmitted. Second, pre-and post-synaptic responses are modulated by co-releasing neurotransmitters. Third, the plastic nature of cotransmission depends on stimulus dynamics, developmental stage, injury, and neurological disorders. All these make the analysis of dual-transmitting synapses in neural circuits and behaviors complicated.

On the other hand, the mechanisms governing the packaging, release, and recycling of multiple neurotransmitters may determine the functional impact on circuit functions. For instance, corelease involves the packaging of two or more neurotransmitters into a single synaptic vesicle and their subsequent release simultaneously (Figure 2A) while cotransmission is believed to be the release of multiple neurotransmitters from distinct non-overlapping pools of synaptic vesicles at the same synapse (Figure 2B) or different neuronal processes (see Figure 2C). In cotransmission, release from different sets of synaptic vesicles might be differentially regulated either as a result

of differential vesicular Ca^{2+} sensitivities or neurotransmitter segregation into different neuronal terminals. A typical case of corelease was demonstrated at the VTA to striatal spiny neuron synapses where dopamine and GABA are corelease in a VGAT-independent manner (Tritsch et al., 2012). The conditional knockout of VGAT in the striatal-projecting VTA dopamine neurons did not abolish GABA release, however, conditional knockout of vesicular monoamine transporter VMAT2, known to package monoamines, eliminates GABA release (Tritsch et al., 2012, Chaudhry et al., 1998). This indicates GABA could have been loaded into synaptic vesicles via VMAT2 acting as a non-canonical vesical transporter of GABA. Cotransmission has also been demonstrated at septo-hippocampal synapses where acetylcholine and GABA cotransmitted are sorted into distinct synaptic vesicles and their release is regulated by distinct calcium channels (Takács et al., 2018). Similarly, a subpopulation of starburst amacrine neurons of the retina also cotransmit acetylcholine and GABA suggested by the non-uniform distribution of their receptors on the postsynaptic targets (spatial segregation) and differential Ca^{2+} sensitivities (differential release) (Lee et al., 2010). Ostensibly, cotransmission of multiple neurotransmitters could allow a neuron to engage in distinct circuit functions in the central nervous system.

An emerging line of evidence suggests segregated sorting of glutamate and GABA to different synaptic vesicles at SuM axon terminals in the DG (Boulland et al., 2009; Root et al., 2018), and that their release could be differentially regulated. The puzzling possibilities would be that a glutamate-GABA releasing neuron could cotransmit glutamate and GABA in equal proportion at some synapses, purely glutamatergic or GABAergic, or with one neurotransmitter dominating over the other at some synapses.

1.5.3. Modulation of synaptic plasticity

Synaptic plasticity involves the alteration of the strength of connectivity between neurons as a result of activities or experiences. It is a fundamental brain function that is widely thought to be the mechanism of information storage in activated neural networks enabling animals and humans to learn. The synapses are plastic, they can either be strengthened or weakened by activities, that is, synaptic facilitation or depression. The changes in synaptic efficiency can span a wide range of time (short-term to long-term) from milliseconds, minutes, hours to days, or even longer. Synaptic plasticity is necessary for animal survival, development, and neuronal injury recovery. Its impairment has been implicated in certain neurological disorders. Synaptic plasticity can be homosynaptic (intrinsic) plasticity and heterosynaptic (extrinsic) plasticity. While homosynaptic plasticity occurs when a change in synaptic strength of a neuron is a result of its activity, heterosynaptic plasticity involves a change in the synaptic strength as a result of activities occurring in another pathway. At the level of the synapse, persistent strengthening or weakening can occur which are termed long-term potentiation (LTP) or long-term depression (LTD). Both have been extensively studied and demonstrated as the substrate for learning and memory formation in the brain (Martin et al., 2000; Neves et al., 2008; Malenka, 1994). Activity-dependent plasticity is extensively studied in the synapses along the classical hippocampal trisynaptic pathways (Hebb, 1949; Malenka, 1994; Gruart et al., 2006; Whitlock et al., 2006). LTP and LTD can be regulated by intracellular signaling molecules such as catecholamines, GABA, acetylcholine, cytokines, and hormones or other inputs. This is called synaptic plasticity modulation. When the regulations by molecules or activities (priming) occur across time and altered the ability to induce LTP or LTD at a later time is termed metaplasticity, that is, the plasticity of synaptic plasticity (Abraham and Bear, 1996; Abraham, 2008).

1.5.4. Synaptic potentiation at cortical-GC synapses

The MEC and LEC massively innervate the MML and OML of the DG, respectively, via PP and make synapses with the distal dendrites of the GCs (Amaral et al., 2007). LTP has been demonstrated at the PP-GC synapses using high-frequency stimulation of the PP (Bliss and Lomo, 1973, McNaughton et al., 1987; McHugh et al., 2007; Schmidt-Hieber et al., 2004). Theoretical models proposed that synaptic plasticity at PP-GC synapses is required for pattern separation and minimizing memory interference (McNaughton and Morris, 1987; Treves and Rolls, 1994; Leutgeb et al., 2007). This was corroborated by impairment of contextual recognition and inability to differentiate between similar previous memories after conditional knockout of N-methyl-D-aspartate (NMDA) receptors in GCs (McHugh et al., 2007). Therefore, understanding the LTP at the PP-GC synapses and how it is enhanced or modulated is fundamental to an in-depth knowledge of learning and memory formation in the hippocampus.

Given that associative mechanisms represent reliable means of modifying synaptic strength during synaptic plasticity. They predominantly depend on excitatory postsynaptic potentials (EPSPs) at the presynaptic cell and action potential at the postsynaptic cell; which is mainly provided by the backpropagating axosomatic action potential at the synapse for effective induction of LTP (Hebb, 1949; Dan and Poo, 2006). Associative learning is regulated mainly by the state of the postsynaptic cell controlled by the interactions of synaptic inputs from different sources. This form of synapse-specific plasticity has been reported to contribute to long-lasting learning (Bi and Poo, 2001), motor learning (Carey and Lisberger, 2002), and spatial learning (Dragoi et al., 2003). In addition to PP fibers arriving at the distal dendrites, GCs also receive substantial inputs from the MCs and SuM at the proximal dendrites. It is still not clearly understood, how the interaction of PP with other inputs enhances LTP induction at synapses of PP and GC, and consequently learning and memory.

2. THE AIMS OF THIS STUDY

Early functional studies demonstrated that SuM terminals in the DG exert inhibitory effects (Segal, 1979). However, a follow-up study reported a net excitatory effect (Nicoll et al., 1980). Other early anatomical studies showed that the SuM-DG pathway is exclusively excitatory because its fibers form asymmetrical synapses and that SuM neurons do not express GABA (Dent et al., 1983; Magloczky et al., 1994; Stanfield and Cowan, 1984; Nitsch and Leranth, 1993). Moreover, it was also reported using anatomical methods that the postsynaptic targets of the SuM input in the DG are exclusively principal neurons (Magloczky et al., 1994). These initial contradicting data were attributed to the inability to specifically activate SuM terminals in the hippocampus and investigate the synaptic organization and physiological relevance. The recent availability of advanced neuronal tracing tools that allow specific labeling, identification, and manipulation of the SuM terminals in the DG, revealed that SuM terminals in the DG express VGluT2 and VGAT sorted into separate populations of vesicles (Boulland et al., 2009, Soussi et al., 2010; Root et al., 2018). However, several questions remain unanswered about the precise neurotransmitter signaling, cellular targets, synaptic properties, and circuit mechanisms of the functional relevance of SuM input in the DG circuitry. This study set out to understand the functional connectivity between the SuM input and diverse cell types in the DG and the functional relevance of glutamate/GABA cotransmission in the DG networks. These were dissected under the following specific aims.

2.1. Aim 1: Elucidation of neurotransmitter signaling, synaptic targets, and functional connectivity of SuM input in the DG

SuM input massively innervates the supragranular layer of the GCL with axonal branches in the IML that overlap with other cortical and subcortical inputs to the DG. Therefore, the conventional electrical stimulation and chemical lesions are not ideal methods to spatiotemporally activate SuM input and elucidate its neurotransmitter signaling and synaptic connectivity. To achieve selective

activation of SuM axon terminals and investigate synaptic transmission, an optogenetics approach was combined with *ex vivo* slice electrophysiology.

2.2. Aim 2: Investigation of synaptic mechanisms by which SuM input regulates the activities of DG cells

Extrinsic excitatory inputs to the DG differentially regulate the input-output transformation of the GCs via the recruitment of a distinct population of GABAergic INs (Liu et al., 2014). In addition, dendritic inhibition is proposed to control electrogenesis, synaptic plasticity, and activity states in their targets (Chiu et al., 2013; Hosp et al., 2014; Miles et al., 1996; Xu et al., 2013). S-INs and D-INs are reported to control spike probability and timing of action potential generation in the principal cells (Pouille and Scanziani, 2001). Given that SuM also provide dense axonal projection in the DG, it could regulate the excitability and spiking dynamics of GCs and GABAergic INs.

2.3. Aim 3: Investigation of the functional relevance of SuM glutamate/GABA cotransmission

SuM has long been identified to play a key role in the generation of theta rhythm, a brain wave that is central to hippocampal functions (Kirk and McNaughton, 1991; Kocsis and Vertes, 1994). Synaptic strengthening is widely believed as the basis of memory encoding and retrieval in the hippocampus, however, how SuM input in the DG contributes to synaptic plasticity is still not well understood. Here, I investigated how selective activation of SuM input interacts with the cortical inputs to modulate long-term potentiation at cortical-GC synapses.

3. MATERIALS AND METHODS

3.1 Experimental models

3.1.1. Animals

We used the VGluT2-Cre driver line (*Slc17a6*$^{tm2(cre)Lowl}$/J, stock# 016963), VGAT-Cre driver line (*Slc32a1*$^{tm2(cre)Lowl}$/J, stock# 028862), Gad2-Cre driver line (*Gad2*$^{tm2(cre)Zjh}$/J, stock# 010802) obtained from Jackson Laboratory (Bar Harbor, ME, USA), and wild-type (WT) mice with C57BL/6J genetic background obtained from National Laboratory Animal Center (Taipei, Taiwan). *Crlr-Cre* mice (C57BL/6N-Tg(Calcrl,cre)4688Nkza/J) obtained from Dr. Kazu Nakazawa were also used. Both male and female mice (3-5 months old) were used for the electrophysiological experiments. The mice were housed in a room with a 12-h light-12-h-dark cycle and were provided with food and water *ad libitum*. The protocols and procedures for the animal experiments were in accordance with the national and institutional guidelines and were approved by the Animal Care and Use Committee of National Yang Ming Chiao Tung University.

3.2. Experimental designs

3.2.1. Viruses

For the optogenetic experiments, we virally expressed channelrhodopsin (ChR2)-eYFP on SuM neurons by injecting an adeno-associated virus (AAV) serotype 5-CaMKIIα-ChR2(H134R)-eYFP (4.1×10^{12} vector genomes/mL, University of North Carolina, Chapel Hill, NC, USA) into the SuM of WT mice. To target glutamatergic and GABAergic neurons in the SuM selectively, an AAV5 vector carrying a Cre-inducible ChR2-eYFP transgene (AAV5-EF1α-DIO-hChR2-(H134R)-eYFP) (4.3×10^{12} vector genomes/mL, University of North Carolina, Chapel Hill, NC, USA) was injected into the SuM of VGluT2-Cre, VGAT-Cre, and Gad2-Cre mice.

3.2.2. Stereotaxic injection

For the retrograde tracer and virus injections, the mice were anesthetized with 4% isoflurane (v/v; Halocarbon Laboratories, North Augusta, SC, USA) in a 100% oxygen-containing induction chamber. The scalp was shaved and the mice were transferred to a stereotaxic frame (IVM-3000; Scientifica, Uckfield, UK) for the surgery. The mouth and nose of each mouse were covered using an anesthetizing mask that was supplied with approximately 1.5% isoflurane and had an airflow rate of 4 mL/min. To maintain the body temperature of the mice at 34–36°C, a biological temperature controller pad (Physitemp Instruments, New Jersey, USA, or TMP-5b, Supertech Instruments, Budapest, Hungary) remained placed under the body of each mouse throughout the surgical procedure. The head was fixed using two ear bars; 75% ethanol was applied to the scalp to sterilize the surgical area, and an ophthalmic gel was applied to the eyes to avoid dryness. An analgesic (ketorolac, 6 mg/kg) was administered intraperitoneally. For the delivery of the tracer, unilateral or bilateral craniotomy was performed at the antero-posterior (AP) and medio-lateral (ML) coordinates of the dorsal DG (AP: -1.80 mm, ML: ± 1.30 mm). Then the tracer was delivered into the DG at the dorso-ventral (DV) coordinate (DV: -2.20 and -2.0 mm). To target the SuM neurons, unilateral or bilateral craniotomy was performed over the SuM (AP: -2.85 mm, ML: ± 0.15 mm). Then viral vectors were delivered into the SuM at DV, -4.86 mm. The viral vectors (0.2–0.4 µL) and red retrobeads (0.2 µL) (LumaFlour, North California, USA) were delivered to the SuM and DG, respectively, using a 10-µL NanoFil syringe (World Precision Instruments, Sarasota, FL, USA) and a 34-G beveled metal needle. The injection volume (0.2–0.4 µL) and flow rate (0.1 µL/min) were controlled using a nanopump controller (KD Scientific, Holliston, MA, USA). Subsequently, the needle was raised 0.1 mm above the site of injection for an additional 10 min to minimize the upward flow of the viral solution. Finally, the needle was gradually withdrawn. After

the injection was performed, the incision was sutured, and the mice were transferred to the cage for recovery.

3.2.3. Brain slice preparation for electrophysiology

Acute brain slices containing the hippocampal and SuM sections were prepared one week after the retrograde tracer injection or at least three weeks after the viral injection. Transverse brain slices were used for whole-cell patch-clamp recording of the DG neurons, while coronal brain slices were used for the recording of retrobeads positive SuM neurons. The mice were anesthetized using isoflurane and decapitated rapidly. The brains were quickly removed and transferred to an ice-cold oxygenated (95% O_2 and 5% CO_2) sucrose solution containing (in mM): 87 NaCl, 25 $NaHCO_3$, 1.25 NaH_2PO_4, 2.5 KCl, 10 glucose, 75 sucrose, 0.5 $CaCl_2$, and 7 $MgCl_2$. Next, 300 µm thick slices were cut using a vibratome (DTK-1000; Dosaka, Kyoto, Japan). After sectioning, the slices were recovered at 34°C for 25 min in a holding chamber filled with an oxygenated sucrose solution, then transferred to room temperature (25 ± 2°C) for further experiments.

3.2.4. Patch-clamp recording and photostimulation

For the recordings, individual slices were transferred to a submerged chamber and were continuously perfused with oxygenated artificial cerebrospinal fluid (ACSF) containing the following (in mM): 125 NaCl, 25 $NaHCO_3$, 1.25 NaH_2PO_4, 2.5 KCl, 25 glucose, 2 $CaCl_2$, and 1 $MgCl_2$. The ChR2-eYFP expression pattern was confirmed using fluorescence and the neurons in the DG were selected visually for recording under an infrared differential interference contrast microscope (IR-DIC, BX51WI, Olympus). The axonal terminals that expressed ChR2 were stimulated with 470-nm light transmitted through the objective from an LED source (LED4D162, driven by DC4104, Thorlabs, Newton, NJ, USA).

Whole-cell patch-clamp recordings were performed using a Multiclamp 700B amplifier (Molecular Devices, Sunnyvale, CA, USA). The recording electrode pipettes (4–7 MΩ) pulled from borosilicate glass tubing (outer diameter, 1.5 mm; inner diameter, 0.86 mm; Harvard Apparatus) were filled with a high-Cl^- internal solution, containing the following (in mM): 15 K-gluconate, 140 KCl, 0.1 EGTA, 2 $MgCl_2$, 4 Na_2ATP, 10 HEPES, 0.5 Na_3GTP, and 0.4% biocytin (w/v, Life Technologies, Grand Island, NY, USA). In certain set experiments for the determination of spike-timing precision and spike phase, a low Cl^- internal solution containing (in mM): 136.8 K-gluconate, 7.2 KCl, 0.2 EGTA, 4 MgATP, 10 HEPES, 0.5 Na_3GTP, 7 Na_2-phosphocreatine (pH 7.3 with KOH) and 0.4% biocytin was used. The pipette capacitance was compensated in the cell-attached mode. To measure the excitatory postsynaptic current (EPSC) and the inhibitory postsynaptic current (IPSC), the whole-cell recording was performed using a high Cl^- internal solution (E_{GABA} = ~0 mV, E_{AMPA} = ~0 mV), the EPSC and IPSC were isolated using a pharmacological approach. Bath application of SR95531 (1 μM) and CGP55845 (1 μM) were used to block $GABA_A$ and $GABA_B$ receptors, respectively, while an ionotropic glutamate receptor blocker, kynurenic acid (Kyn, 2 mM) was used to block ionotropic glutamatergic transmission. The GABAergic component (IPSC) traces were obtained by digital subtraction of traces recorded after bath application of SR, CGP from the baseline traces recorded in the presence of ACSF. The glutamatergic component (EPSC) traces were obtained by digital subtraction of traces recorded in the presence of SR, CGP, and Kyn from the traces recorded in the presence of SR and CGP.

Cell-attached was performed with patch pipettes filled with a high Cl^- internal solution before the whole-cell recording of current spikes in GCs and INs. A 5-Hz, 5 ms light pulse was applied with a 15-s inter-sweep interval and 6 sweeps were recorded. The spike probability was determined as the percentage of spikes among 6 sweeps. In the dual recording experiments, the

distance between the recorded pair was less than 200 μm. Although the serial resistance was not compensated, it was monitored continuously during the recording process. The recordings with the serial resistance < 25 MΩ were analyzed. The fast-spiking phenotype of hippocampal INs at room temperature (21-24°C) was defined by their maximal firing rate > 65 Hz and coefficient of variation (CV) of < 0.2 in response to 1-s depolarizing current injection (Lien and Jonas, 2003). The recording electrode (tip diameter, ~5 μm) filled with ACSF was placed in the GCL to monitor the population spike (pSpike) in response to PP stimulation. Further experiments were performed at stimulus intensities that evoked 30–50% of the maximum pSpike amplitude and paired with the 10-ms light pulse for activation of the SuM input.

For the spike-timing precision experiments, sinusoidal waveforms were created and customized using Clampfit 10.3 (Molecular Devices). To test the ability of the SuM input to enhance spike-timing precision and phase, theta frequency (5-Hz trains of 5 pulses) sinusoidal current pulses were delivered into the GCs and were paired with 5-Hz square photostimulation of the SuM input. The 5-ms photostimulation was delivered during the ascending phase (31°–39°) of the sinusoidal waveform. The current injected (peak to trough, 50–150 pA) was set to evoke a single action potential close to the peak of the sinusoidal waveform while the membrane potential of the GCs was held at approximately -80 mV. Twenty sweeps were recorded at 15-s intervals and superimposed to observe the precision of AP generation. To determine the spike jitter and phase, the time point for the peak in each spike was converted to phase (angle) using the customized Python codes. The mean and the standard deviation represented spike phase (latency) and spike jitter, respectively. All cells used for spike-timing precision experiments reliably generated excitatory postsynaptic potential (EPSP) in response to 5-Hz photostimulation of the SuM input. The signals

were recorded using Multiclamp 700B amplifiers (Molecular Devices), filtered at 4 kHz, and sampled at 10 kHz using a digitizer (Digidata 1440A, Molecular Devices), which was controlled using pCLAMP version10.3 (Molecular Devices).

3.2.5. Biocytin labeling and morphological reconstructions

To identify the recorded neurons (filled with 0.4% biocytin), brain slices were fixed overnight with 4% paraformaldehyde (w/v) in phosphate-buffered saline (PBS). After rinsing with PBS 3 times, 0.3% Triton X-100 (v/v; USB Co., Cleveland, OH, USA) in PBS (PBST) was added for 30 min. Then, blocked with 0.3% PBST and 10% normal goat serum (NGS, S-1000, Vector Laboratories, Burlingame, CA, USA) for 2 h. Slices were incubated with streptavidin-conjugated Alexa Fluor 594 or 555 or 488 (1:400; Life Technologies) in 0.3% PBST and 5% NGS at 4°C overnight or 2 h at room temperature. After rinsing 6 times with PBS, slices were mounted onto slides with mounting medium Vectashield with 4′,6-diamidino-2-phenylindole (DAPI, H-1200, Vector Laboratories, Burlin-game, CA, USA). Confocal image stacks were reconstructed with Neuromantic 1.6.5 software (developed by Darren Myatt, University of Reading, Reading, Berkshire, UK).

3.2.6. Immunohistochemistry

WT mice (3 months old) with AAV5-CaMKIIα-ChR2-eYFP injected into the SuM were deeply anesthetized using isoflurane and perfused transcardially with 20 mL of ice-cold PBS, followed by 50 mL of 4% PFA. The fixed brain specimens were excised and post-fixed in 4% PFA for an additional 6 h or overnight. Next, dehydration was performed by incubation in 15% sucrose for 4 h, followed by 30% sucrose in PBS for 2 h. The brain specimens were sectioned coronally into 50-μm slices using a microtome (SM2010R, Leica, Wetzlar, Germany). The brain slices were rinsed with PBS three times and blocked by treating with 0.3% PBST and 5% NGS for 2 h. The slices were then incubated in a cocktail of rabbit anti-GFP antibody (1:1000, Abcam, ab290), rabbit anti-

VGluT2 antibody (1:500, VGluT2-135 403, Synaptic System, Germany), and mouse anti-VGAT antibody (1:250, VGAT-131 011; Synaptic System, Germany) at 4°C for 24 h.

Next, the slices were rinsed three times with PBS and incubated in cocktails of fluorescent secondary antibodies, Alexa Fluor 488 anti-rabbit, Alexa Fluor 594 anti-rabbit, and Alexa Fluor 647 anti-mouse at room temperature for 2 h or overnight at 4°C. The procedures were performed under continuous shaking conditions. After rinsing six times with PBS, the sections were mounted using the mounting medium Vectashield with DAPI. Fluorescent images were taken using a confocal microscope (Leica SP5 module, Leica Microsystems, Germany) or (LSM 700, Zeiss, Germany) using 20×, 40×, or 63× objectives and analyzed using ImageJ (NIH, USA, 1.52t). Single plane coronal sections with bead expression were imaged using a Research High-Class Stereo Microscope System (SZX16, Olympus, Tokyo, Japan). For colocalization analysis of ChR2-eYFP expressing boutons with VGluT2 and VGAT, boutons along ChR2-eYFP expressing axons were identified in z-stack images and examined for colocalization and were counted using a cell counter plugin in Fiji (a distribution of ImageJ software, NIH, USA, 1.53c) (Billwiller et al., 2020).

3.3. Data analysis and statistics

Data were analyzed using Clampfit 10.3 (Molecular Devices), Prism 6.0 (GraphPad Software, La Jolla, CA, USA), or customized Python codes. The synaptic latency was determined as the time elapsed from the light onset to the onset of the synaptic response (Hsu et al., 2016). The onset of the synaptic response was determined by the intersection of a line through the 20% and 80% points of the rising phase of the EPSC or IPSC and the baseline. To calibrate evoked IPSCs during successive 5-Hz photostimulation, the EPSC obtained after bath application of SR95531 (1 μM) and CGP55845 (1 μM) was digitally subtracted from the mixed postsynaptic current (baseline). To calculate the conductance, the EPSC and the IPSC amplitude were divided by their respective

driving forces. The input resistance was determined by the ratio of a steady-state (the last 100 ms of a 1-s pulse) voltage response versus the injected 1-s hyperpolarizing (10 pA) current pulse (Liu et al., 2014). The magnitude of LTP was calculated 30-40 min after LTP induction. Data are presented as mean ± standard error of the mean (SEM). Error bars in the figures also show SEMs. Statistical significance was tested using the unpaired t-test, Mann–Whitney test, Wilcoxon signed-rank test, or two-way repeated-measures ANOVA followed by Bonferroni's *post-hoc* tests. Significance levels were set at $p < 0.05$ (*), $p < 0.01$ (**), $p < 0.001$ (***), and $p < 0.0001$(****) for the statistical comparisons.

4. RESULTS

4.1. Morpho-electrophysiological properties of DG-projecting SuM neurons

To label and characterize the electrophysiological and morphological properties of DG-projecting SuM neurons, I bilaterally injected a retrograde tracer (red retrobeads) into the hippocampal DG (Figure 3A, left, three mice). The precision of the injection sites was confirmed by preparing *post hoc* serial coronal sections (Figure 3A, middle). It was observed that the injected retrobeads were restricted to the GCL and the hilus of the DG (Figure 3A, right top). After waiting for 7 to 10 days post-injection, the retrogradely labeled DG-projecting neurons were found largely in the SuML above the mammillothalamic tract (mt) (Figure 3A, right bottom). In addition, few bead-positive cells were also detected in the SuMM (Figure 3A, right bottom). The retrogradely labeled DG-projecting SuM neurons are distributed along the antero-posterior axis of the SuM (Figure 3B). Bead-positive neurons were also detected in other brain areas known to project to the DG such as perirhinal cortex (PR), LEC, MS, and MEC (Figure 3C).

In another set of mice, the red retrobeads were then injected unilaterally into the right DG (Figure 4A), it is noteworthy that the labeled DG-projecting SuM cells were mainly observed in the right SuML (Figure 4B), that is, ipsilateral to the injection site. Quantification of the number of bead-positive cells further revealed that DG-projecting SuM neurons were symmetric in their projection pattern (Figure 4C, data from 12 slices, 3 mice). Next, to characterize the electrophysiological properties and the morphological features of the DG-projecting SuM neurons, I performed whole-cell recordings from bead-positive SuM neurons in the SuML (Figure 5A) in prepared acute brain slices from mice injected bilaterally and unilaterally. These cells had relatively large soma ($\geq$ 20 μm in diameter; Figure 5B), with a resting membrane potential of -58.0 ± 1.7 mV (n = 11 cells from 5 mice) and input resistance of 508.3 ± 69.4 MΩ (n = 11 cells from 5 mice). They exhibited a bursting firing pattern (at a holding potential of -70 mV) in response to a small current

injection (10–30 pA) and displayed an accommodating firing pattern in response to increased depolarizing current (Figure 5C; n = 11 cells from 5 mice). The biocytin-filled SuM cells exhibited axonal projection extending toward the dorsal brain areas with dendrites located within the mammillary region (Figure 5D; n = 5 cells from 4 mice).

Next, I used an optogenetic approach to investigate the function of SuM projections to the DG. A CaMKIIα-ChR2-eYFP virus was injected into the SuM of wild-type (WT) mice (Figure 6A, left). The virus expression was restricted to the SuM area (Figure 6A, middle). The SuM neuron axonal terminals were observed to form a dense pattern in the supragranular layer of the GCL and CA2 pyramidal layer (Figure 6A, right, from three mice). To confirm that the ChR2-expressing SuM neurons respond to light stimulation, I made whole-cell recordings from these neurons (Figure 6B). When the recorded neurons were illuminated with blue light pulses (470 nm, 5 ms at 5 Hz), they generated spikes in the current-clamp at -70 mV (Figure 6C, traces; n = 7 cells, 5 mice). Similarly, a light-evoked ChR2-mediated inward current was recorded in a voltage-clamp in the presence of an ionotropic glutamate receptor antagonist, kynurenic acid (Kyn, 2 mM) (Figure 6C, traces). 6 of 7 cells recorded from 5 mice show multiple spikes in response to 5 ms photostimulation in the current-clamp at a holding potential of -70 mV. The burst response was composed of 2-4 spikes (mostly 2) with an interspike interval of 12.5 ± 1.3 ms (corresponding to 85 ± 10 Hz). This could be due to the bursting firing pattern of DG-projecting SuM neurons (at a holding potential of -70 mV) in response to a small current injection (10–30 pA) as shown in figure 5C.

4.2. Selective labeling of the SuM and MC inputs in the DG

To investigate whether the axon terminals of SuM and MC inputs overlap in the DG, a dual viral strategy was used. To selectively label MC axon terminals in the DG, a Cre-dependent virus construct carrying ChR2-mCherry was unilaterally injected into the dorsal hilus of a Crlr-Cre mouse,

with Cre expression on MCs (Figure 7A). In the same mouse, a non-Cre dependent virus carrying CaMKIIα-ChR2-eYFP was unilaterally injected into the SuM (Figure 7A). We observed that the axon terminals of the DG-projecting SuM neurons were exclusively in the supragranular layer of the GCL (Figure 7B, left) while those of MCs are strictly in the IML (Figure 7B, middle). The merged image (Figure 7B, right) shows that the two inputs are largely nonoverlapping in the DG.

The ChR2-eYFP-expressing axon terminals in the DG (Figure 8A) co-expressed VGluT2 and VGAT (Figure 8B). A total of 1381 putative boutons (from 9 slices, 2 mice) were identified along the ChR2-eYFP-expressing axons. Overall, 92 ± 1.4% (85-98%) of the boutons expressed VGluT2, 88 ± 2.3% (82-97%) expressed VGAT while 84 ± 2.3% (78-94%) expressed both VGluT2 and VGAT, similar to previous reports (Boulland et al., 2009; Billwiller et al., 2020; Root et al., 2018; Soussi et al., 2010).

4.2. SuM input preferentially excites dendrite-targeting INs

Next, we examined SuM-DG synaptic transmission by recording field postsynaptic potentials (fEPSPs) along the somatodendritic axis of GCs (Figure 9A, top). The fEPSPs exhibited downward at the GCL (-0.10 ± 0.01 mV; n = 7) and inner molecular layer, IML (-0.06 ± 0.01 mV; n = 7). The polarity of fEPSP reversed at the middle molecular layer, MML (0.03 ± 0.00 mV; n = 7) and exhibited upward at the outer molecular layer, OML (0.03 ± 0.00 mV; n = 7). This was consistent with the observation that SuM axons mainly innervated the somatic and proximal dendritic regions of GCs (Hashimotodani et al., 2018). Then, we checked whether photostimulation of SuM axon terminals was enough to excite different cell types in the DG. To achieve this, I injected a CaMKIIα-driving ChR2-eYFP viral construct into the SuM of WT mice or EF1α-DIO-ChR2-eYFP viral construct into VGluT2-Cre mice. Next, cell-attached recordings were performed from various cell types in DG such as GCs, S-INs, and D-INs (Figure 9A, bottom) and followed by

biocytin-filled whole-cell recordings for *post hoc* morphological identification of recorded cells (Hsu et al., 2016; Lee et al., 2016; Liu et al., 2014). Dentate GCs receive coherent theta (4–10 Hz)-band EPSCs *in vivo* (Pernía-Andrade and Jonas 2014) and the SuM synchronizes with the DG at a theta range (Li et al., 2020). Thus, we investigated the response of DG cells to SuM activation at a physiologically relevant frequency (e.g., 5 Hz). Upon photostimulation of SuM axons (5 Hz, 5 ms pulses), no spikes were evoked in all recorded GCs (Figure 9B; 21/21 cells) and S-INs (Figure 9C; 5/5 cells). In contrast, the majority of D-INs reliably generated spikes in response to SuM terminal activation (Figure 9D; 22/27 cells). Several morphological subtypes of D-INs have been well characterized (Freund and Buzsáki, 1996; Hsu et al., 2016, see also figure 10A and B). According to their soma locations and the input layers where their axons innervate, there are at least four distinct subtypes, including the TML cells, HIPP cells, MOPP, and HICAP cells (Figure 10A). Based on the results of morphological reconstructions, the spike probability of each subtype was plotted against the stimulus number (Figure 10B). The five nonresponsive D-INs including two HICAP, two HIPP, and one MOPP were not included in the plots. Collectively, the SuM input alone was sufficient to activate most D-INs, but not GCs and S-INs.

4.3. SuM input excites S-IN, but not GC, under blockade of synaptic inhibition

Given that the interplay between intrinsic properties of each cell type and the synaptic properties including strength, dynamics, and excitatory conductance determines the firing and the recruitment of neurons. Therefore, blocking inhibition may enhance the spike probability of various cell types. To check whether SuM input will recruit GCs and S-INs under blockade of GABAergic transmission, cell-attached recordings were performed in the presence of GABAergic blockers, 1 μM SR95531 and 1 μM CGP 55845. To confirm this, additional experiments were performed, that is, cell-attached recordings from GCs and an S-IN in the presence of GABAergic blockers (1 uM SR

and 1 uM CGP; Figure 11). We observed that all GCs (n = 10) recorded in the presence of blockers of synaptic inhibition did not generate a spike in response to photostimulation of the SuM input (Figure 11A). To further confirm that these GCs receive SuM input, we recorded the EPSCs after the cell-attached recording (Figure 11A, bottom trace) and calculated their corresponding EPSGs (Figure 11A, bar graph). Unlike GCs, an S-IN recorded generated spikes in the presence of GABAergic blockers (Figure 11B, top trace). Although GCs and S-INs receive similar synaptic inputs from SuM, the response after blocking inhibition is different. Overall, these results support that in addition to synaptic properties, the intrinsic properties of each neuron type also determine the firing probability.

4.4. Differential glutamate/GABA cotransmission is target cell-specific

Synaptic excitation and inhibition are critical for neuronal excitability and information processing in neural circuits (Bhatia et al., 2019; Iascone et al., 2020; Liu et al., 2004; Yizhar et al., 2011). SuM afferents are known to corelease glutamate and GABA onto both GCs and GABAergic INs (Hashimotodani et al., 2018; Li et al, 2020; Pedersen et al., 2017). Given that the SuM input preferentially excites D-INs, I next investigated whether synapse-specific excitatory and GABA conductances correlate with differential recruitment of DG cells. To address this question, ChR2-eYFP was virally expressed in SuM neurons of WT or VGluT2-Cre mice (Figure 12A, top) and recordings were made from GCs, S-INs, and D-INs in transverse slice sections of the DG (Figure 12A, bottom). The expression of ChR2-eYFP in the GCL was confirmed before recordings (Figures 12B, C, and D, top). To determine the synaptic property at the SuM-GC synapse, we performed whole-cell recordings from GCs, which exhibited regular spiking at -75 mV, ($[Cl^-]_i$ = 140 mM; E_{GABA} = ~0 mV as determined experimentally), in brain slices. Photostimulation of the SuM terminals (470 nm, 5 ms at 5 Hz) in the DG evoked inward currents in all recorded GCs (30 of 30

cells; 12 mice). The mean peak amplitude was 84.0 ± 7.0 pA (n = 30) at -75 mV. The mean response was largely reduced by co-application of a $GABA_A$ receptor blocker, SR95531 (1 μM), and a $GABA_B$ receptor blocker, CGP55845 (1 μM) to 22.6 ± 2.4 pA and finally almost abolished by Kyn (2 mM) (Figure 9B, traces). The pharmacologically isolated components, SR and CGP-sensitive component (hereafter called "IPSC") and Kyn-sensitive component (hereafter called "EPSC") were GABAergic and glutamatergic, respectively (Figure 9B, red trace, EPSC and blue trace, IPSC). The GABAergic component was slower (20 to 80% rise time, 2.79 ± 0.37 ms; n = 30; decay time constant, 30.67 ± 1.85 ms; n = 30; see also table 1) relative to the glutamatergic component (20 to 80% rise time, 1.10 ± 0.07 ms; n = 30; decay time constant, 6.87 ± 0.47 ms; n = 30; see also table 1). Nevertheless, both EPSC and IPSC components exhibited similar synaptic latencies in response to 5 ms photostimulation of SuM terminals (Figure 9E, $EPSC_1$, 2.60 ± 0.10 ms; $IPSC_1$, 2.56 ± 0.10 ms; n = 30; p = 0.875, U = 439.0; Mann-Whitney test), supporting the idea of glutamate and GABA co-transmission at the SuM-GC synapse. The EPSC and IPSC evoked by SuM terminal activation exhibited strong depression of the amplitude (Figure 12B, bottom traces). Notably, analysis of the first peak excitatory (E) and GABA (I) conductances (hereafter called $EPSG_1$ and $IPSG_1$, respectively) revealed that GABAergic transmission dominated at the SuM-GC synapse (Figure 12F, GCs, $EPSG_1$, 0.30 ± 0.03 nS; $IPSG_1$, 0.91 ± 0.08 nS; n = 30; $p < 0.0001$; U = 67.0; Mann-Whitney test). Moreover, the scatter plot of the individual relationship between $EPSG_1$ and $IPSG_1$ obtained from each cell showed a bias towards IPSG (Figure 12G, gray circles) and the slope of the linear regression line (gray line) was less than 1. Taken together, GABAergic transmission was predominant at the SuM to GC synapse.

Next, we investigated the synaptic property of different IN subtypes (Figures 12C and D). Photostimulation of the SuM terminals evoked variable inward currents (Figures 12C and D, black

traces) in different IN subtypes. Similar to GCs, the evoked postsynaptic current recorded from putative S-INs, which exhibited a fast-spiking firing pattern, was largely blocked by bath application of SR95531 (1 μM) and CGP55845 (1 μM) (Figure 12C, bottom traces). The remaining small excitatory component was blocked by Kyn (2 mM). The S-INs recorded exhibited a maximum firing rate of 74.0 ± 4.9 Hz (n = 6 cells; 5 mice). Overall, 3 of 6 fast-spiking INs were morphologically identified as S-INs. The pharmacologically isolated EPSC and IPSC in S-INs have similar synaptic latencies (Figure 12E, S-INs, $EPSC_1$, 2.78 ± 0.20 ms; $IPSC_1$, 3.07 ± 0.23 ms; n = 6; p = 0.571, U = 14.0; Mann-Whitney test). The 20 to 80 % rise time of the IPSC and EPSC was 1.73 ± 0.31 ms and 1.19 ± 0.08 ms (n = 6), respectively, while the decay time constant of IPSC and EPSC was 17.40 ± 1.53 ms and 7.94 ± 0.55 ms (n = 6), respectively, see table 1. Like SuM-GC synapses, analysis of $EPSG_1$ and $IPSG_1$ showed that GABA conductances dominated at the SuM-S-IN synapses (Figure 12F, S-INs, $EPSG_1$, 0.58 ± 0.08 nS; $IPSG_1$, 2.14 ± 0.67 nS; n = 6; $p < 0.05$; U = 4.0; Mann-Whitney test). However, the IPSGs at SuM-S-IN synapses were larger than that at SuM-GC synapses (S-INs, $IPSG_1$, 2.14 ± 0.67 nS; GCs, $IPSG_1$, 0.91 ± 0.08 nS, $p < 0.01$, unpaired t-test). Furthermore, the plot of $EPSG_1$ versus $IPSG_1$ showed a bias towards the $IPSG_1$, confirming the dominance of GABA conductance at the SuM-S-IN synapses (Figure 12G, orange regression line).

Intriguingly, unlike GCs and S-INs, the co-application of $GABA_A$ and $GABA_B$ receptor blockers SR95531 (1 μM) and CGP55845 (1 μM) slightly reduced the postsynaptic current recorded in most D-INs (Figure 12D, bottom). However, further bath application of Kyn completely blocked the remaining large current, indicating a dominant excitatory transmission at the SuM-D-IN synapses (Figure 9D). The pharmacologically isolated EPSC and IPSC (Figure 12D; EPSC, red trace and IPSC, blue trace) exhibited similar synaptic latencies (Figure 12E, D-INs, $EPSC_1$, 2.67 ± 0.09 ms; $IPSC_1$, 2.73 ± 0.10 ms; n = 22; p = 0.663, U = 223.0; Mann-Whitney test). The IPSC

kinetics was slower (20 to 80% rise time, 2.53 ± 0.23 ms; n = 25; decay time constant, 19.64 ± 2.40 ms; n = 25; also see table 1) relative to the EPSC kinetics (20 to 80% rise time, 1.25 ± 0.11 ms; n = 25; decay time constant, 6.38 ± 0.61 ms; n = 25, also see table 1). Contrary to the SuM-GC and SuM-S-IN synapses, analysis of $EPSG_1$ and $IPSG_1$ showed that excitation dominated the SuM-D-IN synapses (Figure 12F, D-INs, $EPSG_1$, 0.99 ± 0.08 nS; $IPSG_1$, 0.48 ± 0.08 nS; n = 22; $p < 0.0001$; U = 63; Mann-Whitney test). The plot of EPSG versus IPSG recorded from each cell revealed a clear shift towards excitatory conductance (Figure 12G, violet circles) and the slope was greater than 1 (Figure 12G).

To pharmacologically verify the monosynaptic cotransmission of glutamate and GABA, another set of experiments was performed in VGluT2-Cre transgenic mice injected with EF1α-DIO-ChR2-eYFP (Figure 13A) in the presence of tetrodotoxin (TTX), a voltage-dependent sodium channel blocker, and 4-aminopyridine (4-AP), a voltage-dependent potassium channel blocker (Figures 13B, GC and 13E, D-IN). The light-evoked postsynaptic current was completely blocked by bath application of TTX (1 μM) and was reversed by subsequent addition of 4-AP (1 mM; in the presence of TTX). Consistent with a previous report (Hsu et al., 2016), 4-AP significantly increased the synaptic latencies of light-evoked postsynaptic currents (Figure 13C; SuM-GC; synaptic latency, baseline, 2.24 ± 0.11 ms ms; TTX & 4-AP, 4.01 ± 0.28 ms; n = 9 cells; 5 mice; Figure 13F, SuM-D-IN; synaptic latency, baseline, 2.67 ± 0.21 ms; TTX & 4-AP, 3.66 ± 0.17 ms; n = 6 cells; 4 mice). Furthermore, EPSG and IPSG analysis confirmed GABAergic transmission dominance at the SuM-GC synapse (Figure 13D), while glutamatergic transmission predominates in the SuM-D-IN synapse (Figure 13G). Moreover, the scatter plot of all EPSGs and IPSGs obtained from individual cells revealed a slop of 0.14 at the SuM-GC synapse and a slop of 1.40 at the SuM-D-IN synapses (Figure 13H). To further confirm the monosynaptic connection between

SuM terminals and S-INs, light-evoked EPSC was obtained from the S-IN recorded in Figure 11B (Figure 11C). Bath application of TTX completely blocked the EPSC and this was reversed in the presence of 4-AP (Figure 11C, traces). This shows that SuM input monosynaptically formed connections with the S-INs in the DG.

In another set of experiments, VGAT-Cre and Gad2-Cre transgenic mice were injected with EF1α-DIO-ChR2-eYFP (Figure 14A). In these mice, ChR2-eYFP was selectively expressed on VGAT- and Gad-positive SuM neurons. Then whole-cell recording was made from GCs. Photostimulation of VGAT or Gad2 positive SuM terminals in the DG evoked an inward current that was largely blocked by SR and CGP (Figure 14B). Consistent with the data obtained from WT and VGluT2-Cre mice, isolated EPSC and IPSC demonstrated monosynaptic latencies (Figure 14C). The analysis of excitatory and GABAergic conductances (Figure 14D) further confirmed that GABAergic transmission is dominant at SuM-GC synapses.

4.5. MCs receive weak synaptic input from the SuM

In addition to GCs and INs, we also checked the functional connectivity between the SuM input and mossy cells (MCs), which are excitatory neurons located in the hilus and featured by prominent thorny excrescences at their proximal dendrites (Figure 15A). ChR2-eYFP expression in the GCL was confirmed (Figure 15A). Then, sequential whole-cell recordings were made from GCs and MCs (Figure 15A). Unlike other cell types in the DG, photostimulation of the SuM input could not reliably evoke a response in recorded MCs (Figure 15A, traces). Only 1 out of 5 MCs (4 mice) recorded received a discernible response and the current was small (-42 pA; Figure 15B, traces). The summary plot of the first EPSG and IPSG obtained from different cell types in the DG are shown in Figures 16A and B.

4.6. Synaptic responses from simultaneously recorded GCs and D-INs

To exclude the possibility that the distinct synaptic properties observed were due to variable viral expression from slices to slices, we performed some set of experiments in WT injected with CaMKIIα-ChR2-eYFP injected virus (Figure 17A), where simultaneous dual recordings of GCs and D-INs were obtained from the same slices (Figure 17B). We found that photostimulation of SuM input (5 ms, 470 nm, 5 Hz light pulses) in the DG evoked inward currents in both GCs and INs (Figure 17C, 6 of 7 pairs recorded, black traces). Co-application of SR95531 (1 μM) and CGP55845 (1 μM) blocked approximately 70.5 ± 5.0% of current in GCs, only about 25.5 ± 5.5% was blocked in D-INs and Kyn (2 mM) completely abolished the remaining current in both GCs and D-INs (Figure 17C). The synaptic strength was stronger at the SuM-D-INs synapses compared to that at the SuM-GC synapses (Figure 17D). Consistent with this, analysis of the peak excitatory and GABA conductances of the first pulses ($EPSG_1$ and $IPSG_1$) in some cells revealed that inhibitory transmission dominated at the SuM-GC synapses (Figure 17E, left, $EPSG_1$; 0.22 ± 0.05 nS, $IPSG_1$; 0.52 ± 0.10 nS; n = 5 cells; 4 mice; $p < 0.05$; U = 2.0; Mann-Whitney test), while excitatory transmission dominated at the SuM-D-IN synapses (Figure 17E, right, $EPSG_1$; 1.24 ± 0.26 nS, $IPSG_1$; 0.40 ± 0.09 nS; n = 5 cells; 4 mice; $p < 0.01$; U = 0.0; Mann-Whitney test). Taken together, these results demonstrated that the ratio of excitatory and inhibitory components at SuM-DG synapses depends on the subtypes of target cells.

4.7. Activation of SuM input increases spike generation in GCs and D-INs

Cortical principal neurons are known to fire action potentials with large variability in response to identical stimuli *in vivo* (Carandini, 2004; Fricker and Miles, 2001; Shadlen and Newsome, 1998).

The GABAergic transmission provides well-timed inhibition known to promote spike timing precision essential for hippocampal network rhythmic activities. The spiking precision of neurons is believed to be essential for accurate information representation and cognitive functions (Bacci and Huguenard, 2006; Hou et al., 2016; Woodruff and Sah, 2007). Here, we explored how SuM-driven synaptic excitatory and GABA conductances regulate spike generation in GCs and D-INs using the low chloride internal solution $[Cl^-]_i$ = 7.2 mM, which is close to the physiological intracellular chloride concentration (Chiang et al., 2012). To simulate *in vivo* membrane oscillations, GCs and D-INs were driven by injecting sinusoidal current steps at low theta (5 Hz) frequencies (Figure 18). Under this condition, photostimulation of the SuM input at the ascending phase of each theta cycle slightly increased spike numbers in GCs (Figures 18A and B). Given that D-INs received predominantly synaptic excitation upon SuM activation, we next examined the modulatory effect of SuM activation on spike generation in D-INs in response to the same oscillatory input. Compared with the light-off epoch, photostimulation of the SuM input remarkably increased spike numbers in D-INs in response to sinusoidal current injections (Figures 18C and D).

4.8. SuM input shortens spike latency and enhances spike-timing precision

To examine the impact of SuM input on spike latency and spike jitter of GCs and D-INs, a constant suprathreshold sinusoidal current near enough to generate single spikes near the peak of each theta cycle was injected (GCs, Figure 19A; D-INs, Figure 19D). Superimposition of spike trains from GCs (Figure 19A) showed that SuM stimulation shortened the spike latencies and decreased spike jitters (Figure 19E, traces). Both reductions in spike latencies and jitters were only significant in 1st spike (Figures 19B and C), which could be explained by strong synaptic depression at the SuM to GC synapses. Notably, superimposition of spike trains from D-INs showed that pairing the SuM input with the suprathreshold sinusoidal stimulation (baseline-to-peak current amplitude of 80 pA)

greatly reduced spike latencies (Figure 19D). In great contrast to GCs, photostimulation of the SuM input did not have a significant effect on spike jitters in D-INs (Figure 19F). This result was consistent with our observation of high synaptic excitation and low synaptic inhibition at the SuM-D-IN synapses. Collectively, activation of SuM input differentially regulates spike generation in GCs and D-INs.

4.9. SuM input enhances GC excitability, thereby supporting long-term potentiation

Subcortical inputs modulate GC responses to cortical inputs *in vivo* (Nakanishi et al., 2001; Li et al., 2020). In the DG circuits, the equilibrium potential of GABAergic conductance (E_{GABA}) is approximately -72 mV (Chiang et al., 2012), which is more depolarized than the resting potential of GCs (ranging from -80 to -90 mV). Thus, GABA, which is cotransmitted with glutamate by the SuM, could exert either the 'shunting inhibitory' or 'depolarizing (or excitatory)' effect on GCs. It has been previously reported from our lab (Chiang et al., 2012; Hsu et al., 2016) that GABA could enhance action potential generation in GCs. Therefore, I investigated the functional role of SuM input glutamate/GABA cotransmission on GC responses to the excitatory PP input. I performed local field potential recordings in the GCL in response to photostimulation of the SuM input and/or electrical stimulation of the PP input (Figure 20A). The evoked response consisted of the fEPSP and population spike (pSpike), a proxy of synaptic strength and GC activity, respectively. Photostimulation of the SuM input evoked the fEPSP, but was not strong enough to generate pSpike (Figure 20B, black trace), whereas electrical stimulation of the PP generated a compound response, which consisted of the fEPSP followed by pSpike (Figure 20B, gray area trace). Notably, paired activation of the PP and SuM inputs significantly increased the pSpike area (Figure 20B, blue area trace), indicating an increase in GC spike numbers. The summated trace obtained by digital summation of SuM-evoked fEPSP and PP-response was shown in the red trace (Figure 20B,

arithmetic sum). Finally, we overlaid all traces and revealed that the SuM-evoked fEPSP emerged before the onset of pSpikes (Figure 20B, overlay). In sum, the pSpike area induced by co-activation of SuM and PP inputs was significantly larger than that of summated trace suggesting a supralinear summation of the two inputs by the GC dendrites (Figure 20C, left). Notably, there was no significant change in the relative slope of fEPSP (Figure 20C, right). Further analysis of successive GC responses to either PP activation alone or co-activation of PP and SuM during the 5-Hz trains (Figure 20D, top traces) showed significant increases in the pSpike area (Figure 20D, bottom left plot), but not in the fEPSP slope (Figure 20D, bottom right plot). The lack of changes in the fEPSP slope during co-activation of PP and SuM supports the anatomical finding that SuM axons preferentially innervate the proximal part of GC dendrites.

Given that co-activation of SuM input and PP input enhanced the activities of GCs as demonstrated by increased pSpike areas in Figure 20. We hypothesize that the excitatory effect of SuM activation on GCs could enhance LTP induction. To test this hypothesis, we stimulated the cortical input to GCs using a weak protocol (e.g., 20-Hz train stimulation) without and with SuM activation (Figure 21A). After train stimulation, we measured the changes in the synaptic responses. For the SuM + PP protocol, the electrical stimulation of the PP and photostimulation of the SuM input were timed to occur simultaneously ($\Delta t = 0$ ms; Figure 21A, left). The pSpikes were monitored after induction of LTP (Figure 21B). Notably, 20-Hz PP stimulation alone could not induce LTP (black circles); however, pairing it with photostimulation of the SuM input (20 Hz, 4 trains, 470 nm, 10 ms) increased pSpike and fEPSP slope (Figures 21B and C). Collectively, the SuM input enhanced GC responses to cortical inputs, thereby facilitating induction of LTP at the PP-GC synapses.

5. DISCUSSION

5.1. Summary

At the SuM terminals in the DG, Glutamate and GABA are segregated and packed into distinct synaptic vesicles suggesting a differential synaptic transmission (Boulland et al., 2009; Root et al., 2018). Therefore, the vesicular loading, synaptic release, and recycling of these two classical neurotransmitters at the axon boutons are likely to be differentially regulated. In this study, we demonstrated that glutamate/GABA cotransmiting SuM neurons establish cell-type specific synapses with various subtypes of DG neurons. Photostimulation of SuM axon terminals reliably excites D-INs, but not S-INs and GCs. Notably, the synaptic excitation and inhibition at the SuM-DG synapses are target-specific. SuM-GC and SuM-S-IN synapses are predominantly GABAergic while SuM-D-IN synapses are mainly glutamatergic. Furthermore, we demonstrated that coactivation of SuM input and PP input enhances GC response to PP, and consequently facilitates induction of long-term synaptic plasticity at the PP-GC synapses.

5.2. The choice of optogenetics and technical considerations

The IML of the DG receives overlapping excitatory inputs from both intrahippocampal and extrahippocampal pathways (Buckmaster et al., 1996; Scharfman and Myers, 2012) including the MC commissural and associational fibers (Nakashiba et al., 2008), septal cholinergic input, perirhinal excitatory input and the SuM input (Boulland et al., 2009; Leranth and Hajszan, 2007; Soriano and Frotscher, 1994; Vivar et al., 2012). Therefore, electrical stimulation or chemical lesions are not suitable to selectively activate individual input, dissect their synaptic organizations, and contribute to information computation in the DG network. Here, we selectively express ChR2-eYFP on the SuM input in the DG and extensively study its neurotransmitter signaling, synaptic targets, and synaptic mechanism of its modulatory role in the DG circuitry.

5.3. Target-specific glutamate/GABA cotransmission at SuM-DG synapses

The target cell-dependent excitation and inhibition at the SuM-DG synapses could be essential for precision in neural information processing (Liu, 2004; Turrigiano and Nelson, 2004). In this study, I demonstrated a dominant inhibitory transmission at the SuM-S-IN synapses (Figure 9C), which might be responsible for weak disynaptic somatic inhibition in GCs (Hashimotodani et al., 2018). Feedforward inhibition is believed to enhance spike timing precision by curtailing EPSPs (Pouille and Scanziani, 2001). The reduced di-synaptic feedforward inhibition appears to be compensated by co-transmission of GABA along with glutamate at SuM-GC synapses. The imbalance of synaptic excitation and inhibition has been associated with neurological disorders, including epilepsy, autism spectrum disorders, schizophrenia, addiction, depression, and social dysfunction (Meye et al., 2016; Shabel et al., 2014; Yizhar et al., 2011). Moreover, disruption of GABA and glutamate co-release has been implicated in depression and addiction behaviors (Meye et al., 2016; Shabel et al., 2014). Consistent with this notion, the SuM fibers in the supragranular layer extend aberrant axonal sprouting to the IML and are mostly $VGluT2^{+}$ in an epileptic rat model (Soussi et al., 2015).

The observed target-specific Glutamate/GABA contransmission at the SuM-DG synapses is another piece of evidence supporting the idea that specialized information is routed along the long hippocampal axis. Therefore, DG-projecting SuM neurons could play an important role in hippocampal homeostatic plasticity (Turrigiano and Nelson, 2004) as well as regulation of the balance between glutamatergic and GABAergic afferents under physiological and pathological conditions (Liu, 2004). In addition, in terms of metabolic energy cost and error of neurotransmitter signaling, glutamate-GABA releasing neurons are at an advantage as differential regulation can be achieved (Somogyi, 2006). Some of the possible mechanisms for differential release of the excitatory and inhibitory neurotransmitters at synapses may be dictated by the nature of the postsynaptic

neurons, receptor composition of postsynaptic neurons, and membrane potential of postsynaptic neurons at the time at which glutamate and GABA are coreleased.

5.4. Cell-type-specific recruitment of distinct types of DG INs

Cortical and subcortical extrinsic excitatory inputs in the DG differentially excite subtypes of GABAergic INs and play crucial roles in gating transmission of neural information to the hippocampal proper (Armstrong et al., 2011; Chiang et al., 2012; Ewell and Jones, 2010; Hefft and Jonas, 2005; Hsu et al., 2016; Lee et al., 2016; Liu et al., 2014). BCs and AACs are known to provide powerful feedforward inhibition to perisomatic region and axon initial segment of the GCs, respectively. It has been previously reported that HIPP and HICAP cells dynamically regulate the dendritic excitability of GCs (Liu et al., 2014). They weakly inhibit GCs when they fire sparsely, whereas they inhibit GCs robustly in the burst spiking mode (Liu et al., 2014). The medial PP (MPP) and commissural fibers of hilar MCs have been demonstrated to strongly excite BCs and drive powerful feedforward inhibition onto GCs (Hsu et al., 2016). On the contrary, selective photoactivation of MPP and commissural fibers of hilar MCs could not recruit HIPP and HICAP cells (Hsu et al., 2016). The extrinsic excitatory inputs that activate HIPP and HICAP cells and their consequent integration into DG circuitry are still unknown. Our current findings revealed that selective activation of the SuM input can reliably recruit HIPP and HICAP cells. Overall, cortical and subcortical inputs may engage in hippocampal-dependent functions such as cognition and affective behaviors through distinctive recruitment of different types of DG INs. Although INs primarily innervate principal neurons, a growing body of evidence shows that DG INs connect and inhibit each other (Bartos et al., 2007; Liu et al., 2014; Wang and Buzsáki, 1996). Here, we show that the SuM input robustly recruits HIPP, TML, MOPP, and HICAP cells in the DG. These types of D-INs especially HIPP and HICAP are known to form synaptic connections with fast-spiking basket cells

(BCs) (12.8% connectivity at HIPP-BC synapses and 16.3% connectivity at HICAP-BC synapses) and effectively inhibit spike generation and reduce spike jitters in BCs (Acsady et al., 2000; Savanthrapadian et al., 2014). Therefore, their direct or indirect activation could cause somatic disinhibition in GCs and result in increased GC excitability. The DG ensembles are highly sensitive to the change in contextual cues (Danielson et al., 2016; Pignatelli et al., 2019). SST-expressing cells, including HIPP and TML cells, control the size of memory ensembles (Stefanelli et al., 2016). Therefore, activation of HIPP cells by the SuM input could regulate the size and specificity of the memory engram.

5.5. Potential role of D-INs recruitment in hippocampal theta oscillation

GABAergic INs are believed to generate and maintain hippocampal theta activity (Freund, 2003; Freund and Buzsáki, 1996; Fricker and Miles, 2001; Ito et al., 2018; McBain and Fisahn, 2001). Given that the SuM plays an essential role in the generation and regulation of hippocampal theta activity, it would be interesting to determine the process by which D-INs are selectively recruited by SuM neurons *in vivo*. It will be more physiologically relevant to determine the process by which target cell-specific cotransmission of glutamate and GABA at the SuM-DG synapses contributes to brain computation in different behavioral states. The high excitatory (E)/low GABAergic (I) conductances (E > I) at the SuM-D-IN synapses can promote dendritic inhibition, whereas the low excitatory/high GABAergic conductances (E < I) at the SuM-GC synapses may help maintain the minimal excitatory drive to GCs on one hand, and ensure high spiking precision on the other hand. The differential co-transmission of these two contrasting neurotransmitters at these two synapses may be crucial to the sparsity of GC activation, which plays a central role in pattern separation.

5.6. Physiological Relevance of glutamate/GABA cotransmission in the DG circuity

On a broad view, the role of SuM input in the DG will mostly depend on the net effect of SuM projections. Correct representation of sensory information relies on the precise temporal firing of neurons (Kara et al., 2000; Reich et al., 1997; Reinagel and Reid, 2002). Here, we demonstrated that SuM-mediated glutamate-GABA co-transmission promotes spike-timing fidelity and reduces AP latency in GCs. This could be essential for ensuring the temporal precision of cognition and fidelity in separating the barrage of sensory information into distinct outputs, as described in pattern separation. Moreover, the interaction among coincident inputs gives rise to associative plasticity and long-term regulation of information flow. Consistent with this view, pairing the SuM input with the PP enhances the responses of GCs to cortical inputs, and also promotes a long-lasting increase in the excitability of GCs. The pSpike area reflects the firing of the GC population, and coactivation of PP and SuM significantly increased the pSpike area. Current findings further showed that simultaneous photostimulation SuM input and electrical stimulation of the PP produced a supralinear GC response, indicating SuM input could enhance the resultant effects of the PP in the DG. During LTP induction (Figure 21A), spikes are reliably generated in GCs. After the LTP induction, the PP-GC synapse is strengthened and there is a long-lasting increase in the excitability of GCs. In addition to synaptic summation, the observed net enhancement of GCs activity could be explained by IN network functions as illustrated in the proposed network models (Figure 22). Given that fast-spiking BCs in the DG provide powerful inhibition of GCs, suppression of their activities increases the response of GCs to the cortical input (Lee et al., 2016). Notably, dendritic inhibition driven by HIPP cells can reduce spike generation in BCs (Savanthrapadian et al, 2014). Our study showed that activation of the SuM input reliably excites HIPP and TML cells, which could suppress BCs activities, leading to somatic disinhibition of GCs and consequently,

enhanced spike generation. Therefore, SuM can potentially modulate the hippocampal network and improve spatial information processing during navigation.

5.7. Proposed network mechanisms for the modulatory role of SuM in the DG

The net excitatory/modulatory influence of SuM input observed could be explained by both the direct effect of glutamate and GABA as well as network mechanisms. Based on the results obtained in this study, we proposed network mechanisms by which the SuM input modulates the input-output logic of the DG (Figure 22). The synaptic connectivity data showed that DG-projecting SuM neurons cotansmit glutamate and GABA in a target-specific manner (Figure 12). The S-INs receive greater synaptic inhibition (GABA conductance) than excitation (excitatory conductance) (E < I), whereas D-INs receive stronger synaptic excitation than inhibition (E > I). Moreover, only D-INs generate spikes in response to SuM activation (Figure 22A), whereas S-INs respond with biphasic subthreshold potential changes (fast EPSP and slow IPSP). Our previous studies demonstrated that a single AP generation in D-INs hardly triggers synaptic release onto GCs (Liu et al., 2014) and is therefore ineffective in modulating the GC output (Lee et al., 2016). Thus, SuM activation alone primarily causes small excitatory (red) and large GABA (blue) conductance changes around the somata of GCs (Figure 22A). As shown by our previous study (Chiang et al., 2012), GABA is depolarizing as the E_{GABA} (approximately -72 mV) > resting membrane potential in GCs and could promote spike generation in GCs in response to the cortical input. The summation of the glutamate- and GABA-mediated conductances, therefore, results in subthreshold postsynaptic depolarization in GCs (Figure 22A). In great contrast to the SuM input, the PP input alone is sufficient to evoke spikes in S-INs (Lee et al., 2016; Liu et al., 2014). Accordingly, we propose that co-activation of SuM and PP inputs can trigger APs in both D-INs and S-INs (Figure 22B). Of note, D-INs and S-INs form reciprocal inhibition (Liu et al., 2014; Savanthrapadian et

al., 2014; Scharfman et al., 1990; Sik et al., 1997). Thus, activation of the PP, SuM, and S-INs results in monosynaptic glutamatergic, mono-synaptic glutamatergic-GABAergic, and disynaptic somatic GABAergic conductance changes in GCs, respectively (Figure 22B). In line with our experimental data, the synaptic summation of these inputs results in AP generation in GCs (Figure 22B). During 20-Hz co-activation of the PP and SuM inputs, both D-INs and S-INs generate repetitive spikes (Figure 22C). Notably, D-INs dramatically increase their synaptic output while they fire at burst frequency above 20 Hz (Liu et al., 2014). Accordingly, activation of the PP, SuM, S-INs, and D-INs results in mono-synaptic glutamatergic, mono-synaptic glutamatergic-GABAergic, disynaptic somatic, and disynaptic dendritic GABAergic conductance changes in GCs, respectively (Figure 22C). Overall, the synaptic summation of these inputs at 20 Hz results in multiple APs in GCs (Figure 22C), which is supported by our experimental data (Figure 20). The enhanced spike generation in GCs during LTP induction is believed to be essential during the induction of Hebbian LTP.

After LTP induction, the pSpike was greatly enhanced (Figure 21A and B), whereas the fEPSP was modestly enhanced (Figure 21C). Although several potential mechanisms could account for these changes, a parsimonious explanation is the formation of Hebbian LTP. Specifically, activity-dependent Hebbian LTP is accompanied by synaptic potentiation or a long-lasting increase in GC excitability as demonstrated by enhanced EPSP-spike (E-S) coupling (Figure 21B). Alternatively, the enhancement of E-S coupling after LTP induction could be mediated through network mechanisms. Given that the fEPSP at the PP-GC synapse was modestly increased (Figure 21C), we proposed that the D-IN-GC synapse may undergo weak long-term depression (iLTD), resulting in a slight increase in the fEPSP (Figure 21C) after LTP induction. In contrast, the S-IN-

GC synapse undergoes strong iLTD, resulting in a large decrease in somatic inhibition and therefore a large increase in the pSpike (Figure 21B). The future work is to investigate the changes in the synaptic efficacy at the individual synapse in the DG circuits after LTP induction.

5.8. Importance of glutamate/GABA cotransmission in behaviors

Neural information processing, integration, and consequent complex behaviors executed by the mammalian brain rely on the balance of excitation and inhibition within the neural circuitry (Liu, 2004). Interruption of this balance is implicated in epilepsy (Behr et al., 1998; Vreeswijk and Sompolinsky, 1996), depression (Shabel et al., 2014), and addiction (Meye et al., 2016). Therefore, cotransmission of classical fast excitatory and inhibitory neurotransmitters in the case of glutamate and GABA could promote the maintenance of excitation/inhibition balance. Glutamate is known as a classical excitatory transmitter; however, GABA has been widely demonstrated to be a versatile neurotransmitter that could exert excitatory, inhibitory, or modulatory influence on its target. This flexibility, combined with the multiple mechanisms of glutamate/GABA cotransmission supports potential multiple functions of cotransmission against a single, universal function. For instance, a population of VTA and EP are reported to corelease glutamate and GABA onto LHb neurons. Photostimulation of VTA terminals suppressed the firing of LHb neurons (Root et al., 2014). However, the EP fiber activation persistently evoked action potential in LHb neurons (Shabel et al., 2014). Disruption of inhibition/excitation ratio at EP-LHb synapse has been implicated in the pathogenesis of depression (Shabel et al., 2014). Here, I demonstrated that activation of SuM input in the DG, modestly enhanced the GC firing (Figure 18B). This suggests that in the DG network, GABA cotransmission has a modest depolarizing effect on GC. This could in part, explain the enhanced somatic excitability and support for LTP induction after activation of SuM input. LTP is the most studied form of synaptic plasticity, and it is believed to be the substrate of

learning and memory. Therefore, disruption of glutamate/GABA cotransmission could result in cognitive deficits. Indeed, a recent study demonstrated that silencing of the SuM-DG pathway resulted in deficient novel context recognition (Chen et al., 2020).

5.9. Conclusion and future perspectives

The data obtained from this study have advanced our knowledge of the synaptic organization of hypothalamic-hippocampal pathways, and signpost the multiplicity of sources via which the DG could integrate signals for the execution of cognitive functions. Moreover, we have illuminated the circuit mechanisms underlying how SuM could modulate the activities of GC in the DG and subsequent support for the long-lasting strengthening of cortical input to GC synapses, a process that is central in the routing of sensory signals to the hippocampus for effective memory storage, retrieval, spatial navigation, and social interactions. These findings further suggest that activation of SuM input could recruit silent GCs for memory storage by causing subthreshold membrane depolarization which is essential for somatic excitability and LTP induction.

The DG is among the few brain structures capable of continually generating new neurons during the entire adulthood. These adult-born neurons are integrated into existing neuronal circuitry and have been demonstrated to play a role in pattern separation as well as memory encoding (Deng et al., 2010). Excitatory inputs in the DG are demonstrated to contribute to adult neurogenesis in the DG. For example, MC input was reported to dynamically regulate quiescence and maintenance of DG neural stem cells via excitation/inhibition balance (Yeh et al., 2018). Also, activation of PP input enhances proliferation in the DG probably via feedforward inhibition (Stone et al., 2011; Li et al., 2013). It is also important to understand the contribution of subcortical inputs such as SuM to adult neurogenesis in the DG.

Future research using available labeling techniques in providing causal evidence of SuM recruitment during ongoing memory-related behaviors and how this alters the number of neuronal ensembles, their connectivity, and the maintenance of the engrams would be an interesting research focus. An emerging line of evidence has shown that in addition to cognitive functions, the hippocampus especially the ventral part participates in emotional behaviors evident by its involvement in anxiety-related behaviors (Bannerman et al., 2003; Jimenez et al., 2018). DG-projecting SuM neurons send axonal projection to the entire septotemporal axis of the hippocampus, an indication that they could modulate both hippocampal-dependent cognitive and emotional behaviors. For instance, neuronal activities were increased in SuM of rats undergoing elevated plus maze and open field tests (Ito et al., 2009; Silveira et al., 1993). Glucagon-like peptide-1 receptors expressing SuM neurons are reported to be crucial for the expression of anxiety-related behaviors (López-Ferreras et al., 2020). All of these are suggestive of the potential participation of SuM not only in memory circuits but also in anxiety-related circuitry. Although direct SuM-hippocampal projections have been established and shown to play a vital role in signaling contextual and social novelties via parallel pathways (Chen et al., 2020), strong evidence for indirect pathways via the septum and their functions has been lacking. Future studies focusing on the mono-transynaptic retrograde tracing approach combined with *in vivo* circuit interrogations are highly desired in elucidating the functional relevance of indirect SuM-hippocampal pathways.

The SuM is known to contribute to the generation and regulation of theta rhythm in the hippocampus, a brain oscillation that is generated, coordinated, and maintained by interneurons (McBain and Fisahn, 2001; Freund, 2003; Freund and Buzsaki, 1996; Fricker and Miles, 2001). It would be interesting to know in future investigation, how selective recruitment of D-INs by SuM

input participates in the generation and regulation of hippocampal oscillation, a brain wave that is believed as the substrate for many cognitive and emotional behaviors.

6. FIGURES AND TABLES

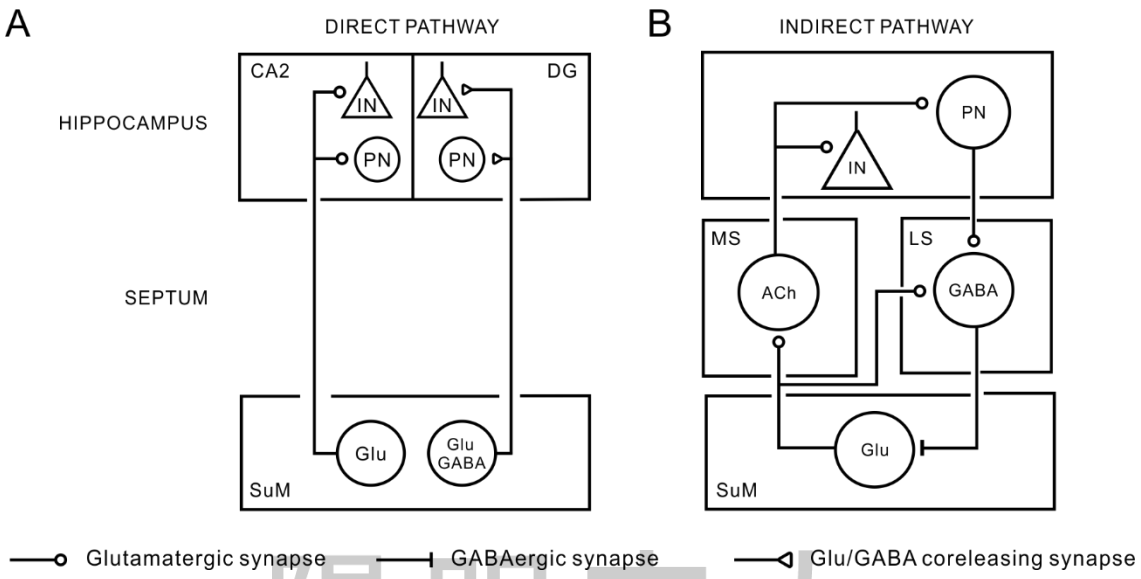

Figure 1. Schematic of wiring diagrams of direct and indirect SuM-hippocampal pathways

(A) Drawing depicts direct SuM-hippocampal pathway. Two distinct populations of SuM neurons project directly to CA2 and DG of the hippocampus. The glutamatergic neurons project to the CA2 while the glutamate/GABA-releasing neurons project to the DG.

(B) A schematic showing a proposed wiring diagram of the indirect SuM-hippocampal pathway. A SuM glutamatergic neuron innervating the hippocampal-projecting cholinergic and GABAergic neurons in the medial septum (MS) and lateral septum (LS), respectively. The recruited neurons in the septum subsequently form synapses with both principal neurons (PNs) and INs in the hippocampus. Modified from Leranth and Kiss, 1996.

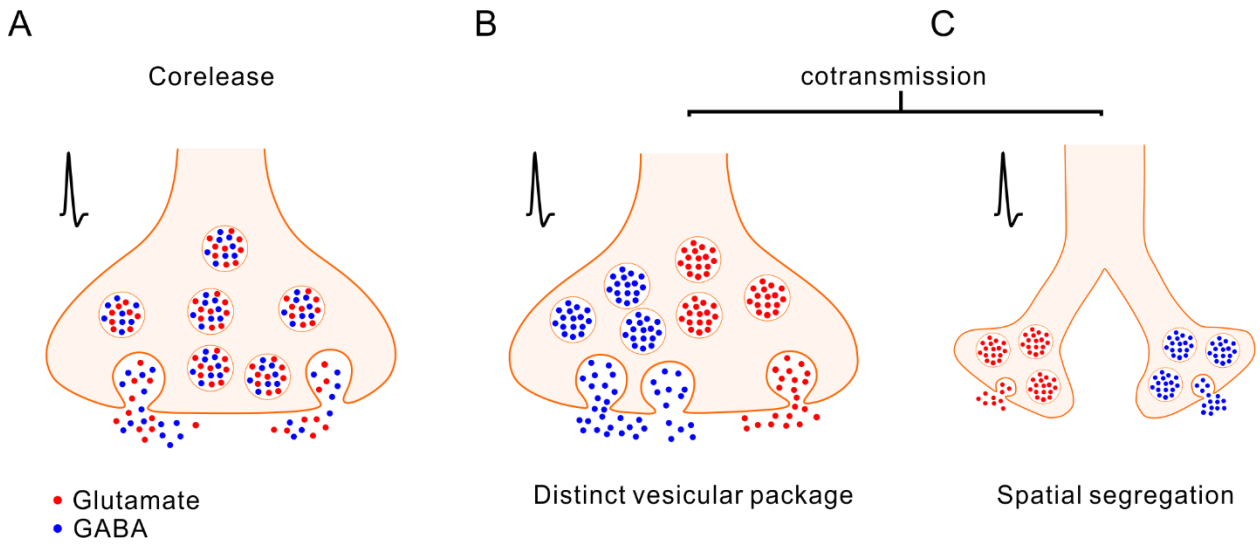

Figure 2. Corelease and cotransmission of neurotransmitters

(A) A model of corelease of two classical neurotransmitters, for example, glutamate (red circles) and GABA (blue circles) sorted into a single synaptic vesicle. The two neurotransmitters are released simultaneously into the synaptic cleft during exocytosis when the presynaptic terminal is activated and binding respective receptors on the postsynaptic neurons.

(B) A model of cotransmission where glutamate and GABA are packed into distinct populations of synaptic vesicles in the same bouton. Here, their release could be differentially regulated by differential Ca^{2+} sensitivities.

(C) A model depicting neurotransmitter spatial segregation model where synaptic vesicles containing distinct neurotransmitters are spatially segregated into different axon boutons which could be neighboring or distant.

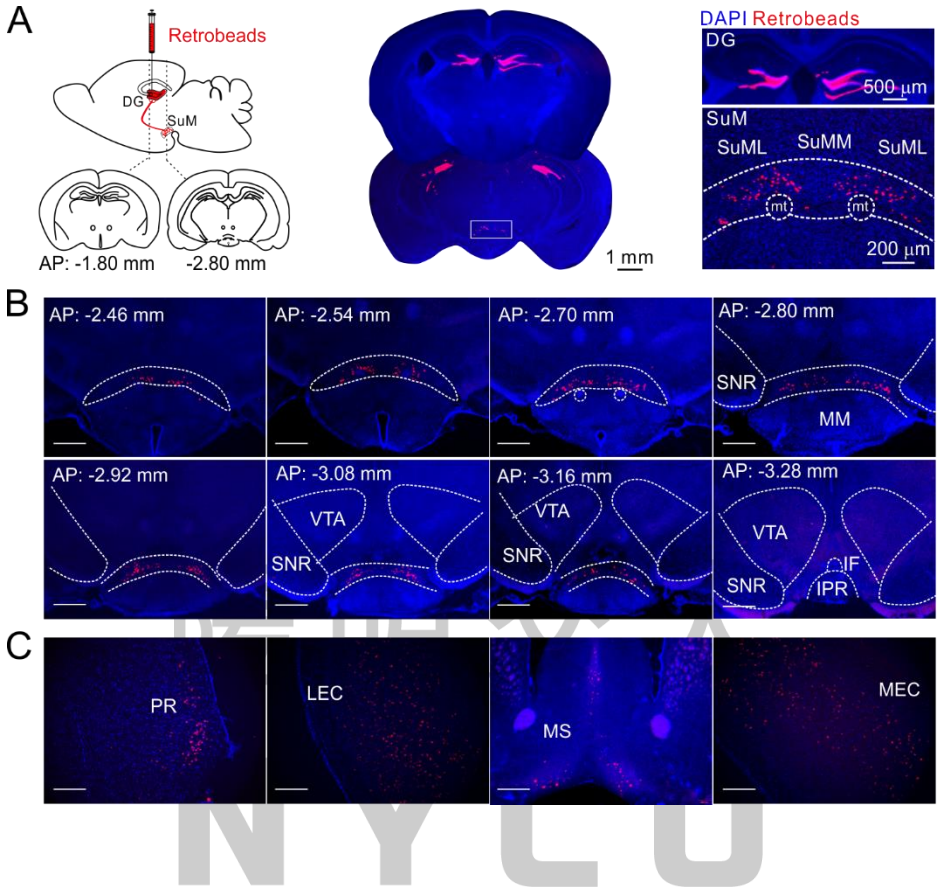

Figure 3. Retrograde labeling of DG-projecting SuM neurons

(A) Left, schematic showing the location of retrogradely labeled cells in the SuM after bilateral red retrobead injections into the DG. Middle, representative images of injection sites along the anteroposterior (AP) axis of the DG. Right top, a high magnification image of injection sites in the DG. Right bottom, retrogradely labeled DG-projecting SuM neurons in the SuM area.

(B) Antero-posterior distribution of labeled DG-projecting SuM neurons.

(C) Other brain areas with bead-positive neurons perirhinal cortex (PR), LEC, MS, and MEC.

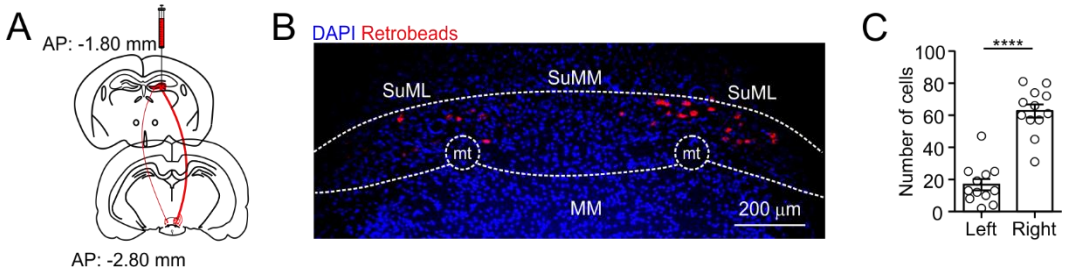

Figure 4. The suM-DG pathway is mainly symmetric

(A) Schematic of unilateral red retrobead injection into the DG.

(B) Retrogradely labeled DG-projecting SuM neurons were mainly located in the right SuML ipsilateral to the injection site.

(C) Quantification of retrogradely labeled DG-projecting SuM neurons in the right and left SuML. Right SuML, 63 ± 4.2 cells; left SuML, 17 ± 3.5 cells; 12 slices from 3 mice; $p < 0.0001$, $U = 2.0$; Mann-Whitney test.

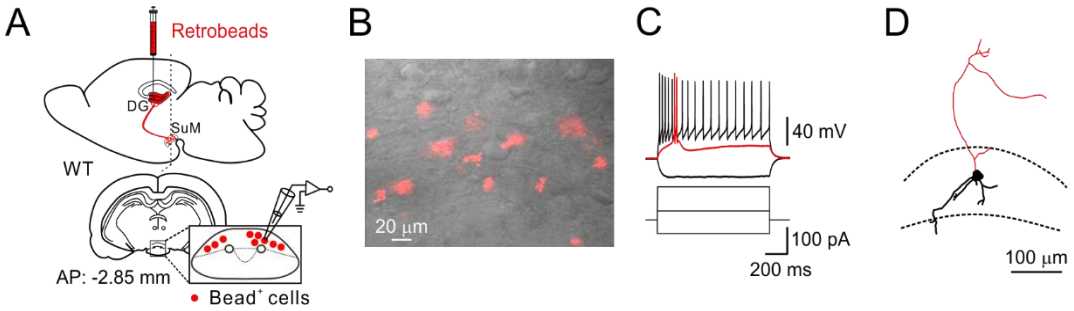

Figure 5. Morpho-electrophysiological properties of DG-projecting SuM neurons

(A) Experimental configuration of red retrobead injection into the DG and whole-cell patch-clamp recording of bead-positive cells in the SuM.

(B) IRDIC image showing retrogradely labeled DG-projecting SuM neurons in the SuM area.

(C) Representative firing pattern of a DG-projecting SuM neuron in response to 1-s current injection steps.

(D) Morphological reconstruction of a DG-projecting SuM neuron; soma and dendrites are depicted in black and axon in red. Black dotted lines depict the boundary of the SuM area.

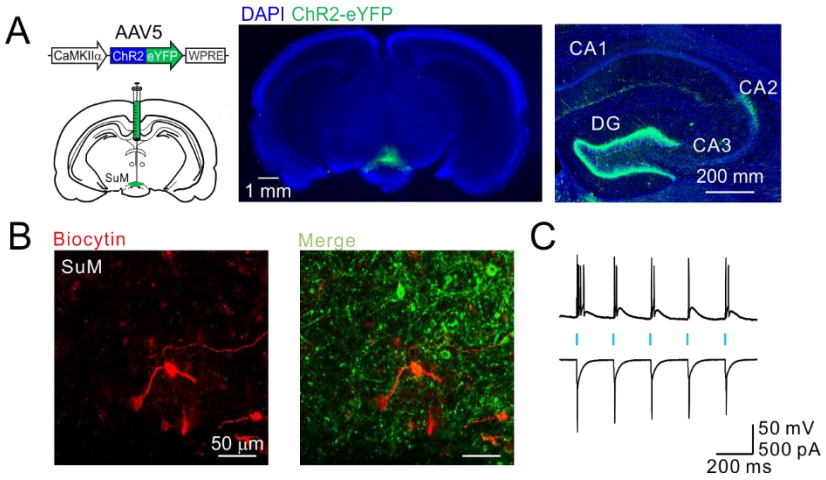

Figure 6. Selective expression of ChR2-eYFP on SuM terminals in the DG and CA2

(A) Left, schematic of injection of AAV5-CaMKIIα-hChR2-eYFP into the SuM. Middle, a representative of the whole-brain coronal section showing ChR-eYFP expression at SuM. Right, a representative coronal section showing ChR2-eYFP expression in the DG and CA2.

(B) Left, a biocytin-filled recording from a ChR2-expressing SuM neuron. Right, merged image of ChR2-eYFP and biocytin.

(C) Right, traces of light-evoked spikes were recorded from the same cell in the presence of Kyn (2 mM), in current-clamp at -70 mV (top), and ChR2-mediated photocurrent recorded at approximately -70 mV in voltage-clamp (bottom). Blue bars indicate the light pulses (5 ms, 470 nm, 5-Hz light pulse).

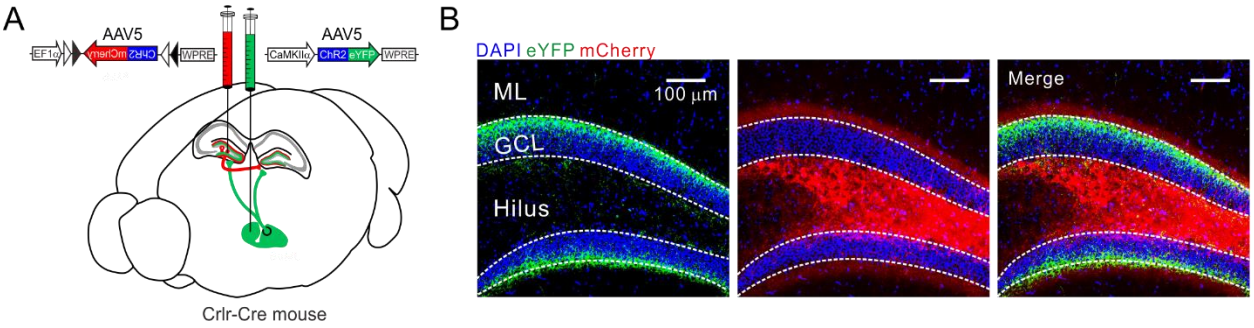

Figure 7. Selective labeling of SuM and MC axon terminals in the DG

(A) Schematic of virus injection showing injection of AAV5-Ef1α-DIO-ChR2-mCherry into the DG and AAV5-CaMKIIα-ChR2-eYFP into the SuM of a Crlr-Cre mouse.

(B) Confocal stack images showing SuM axon terminals on the supragranular layer of the GCL (left), MCs in the hilus, and MC terminals in the IML (middle), and merged image of non-over-lapping SuM and MC axon terminals (right).

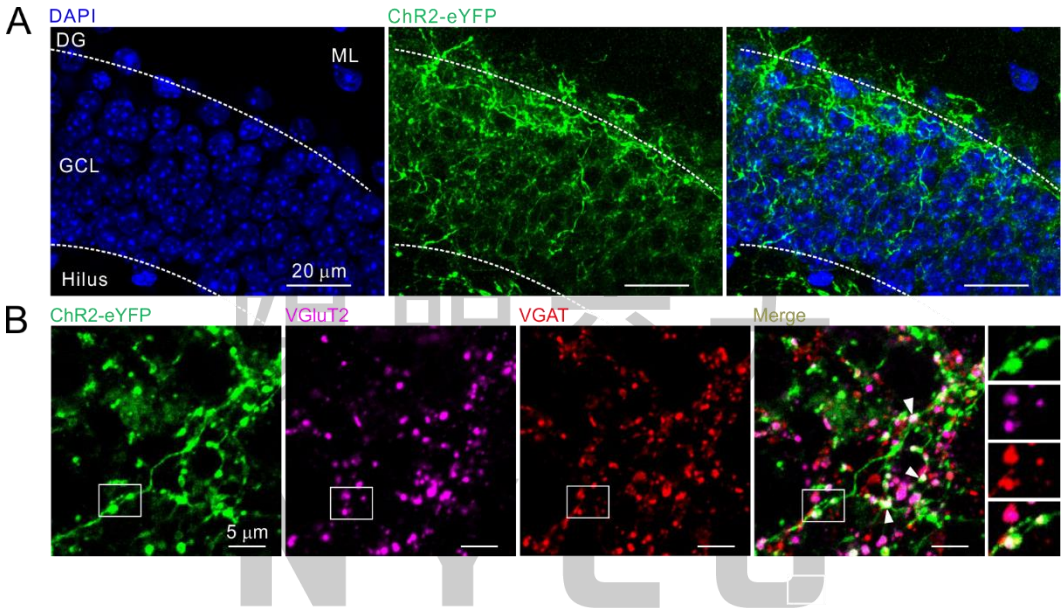

Figure 8. SuM axon boutons in the DG co-express VGluT2 and VGAT

(A) Confocal image stacks of a coronal section through the DG show the projection pattern of SuM terminals in the DG. DAPI (left), ChR2-expressing SuM terminals (middle), and merged image (right).

(B) Confocal image stacks of SuM axon terminals expressing ChR2-eYFP, VGluT2, VGAT immunofluorescence, and the merged image showing their co-localization on the labeled SuM terminals. Right, putative boutons in the box.

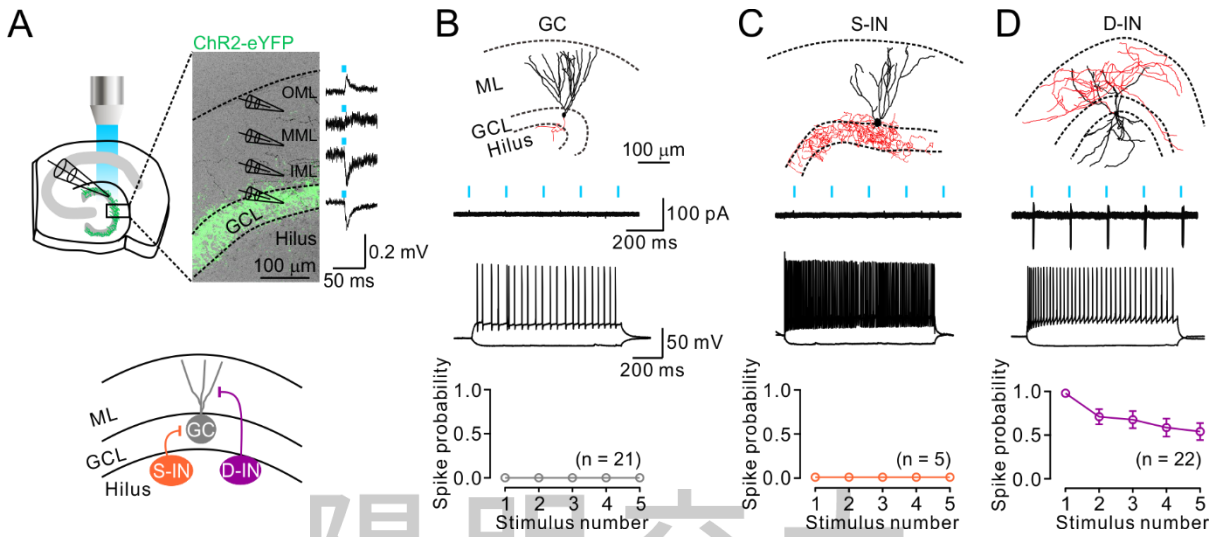

Figure 9. SuM input preferentially excites dendrite-targeting INs in the DG

(A)Top, the experimental configuration of local field potential (LFP) recordings and photostimulation. A transverse section across the DG showing ChR2-eYFP-expressing SuM fibers (green) in the GCL and light-evoked LFPs recorded along the somatodendritic axis of GCs in the DG. Bottom, schematic of the local network of the DG depicting GC (gray), S-IN (orange), and D-IN (violet).

(B-D) Top, representative morphological reconstruction of a GC, an S-IN, and a D-IN (soma and dendrites, black; axon, red) in the DG. Middle, sample traces of cell-attached responses (six overlaid sweeps) to 5-Hz photostimulation of the SuM input and firing pattern of a representative GC, S-IN, and D-IN. Bottom, the plot of spike probabilities of all recorded cells.

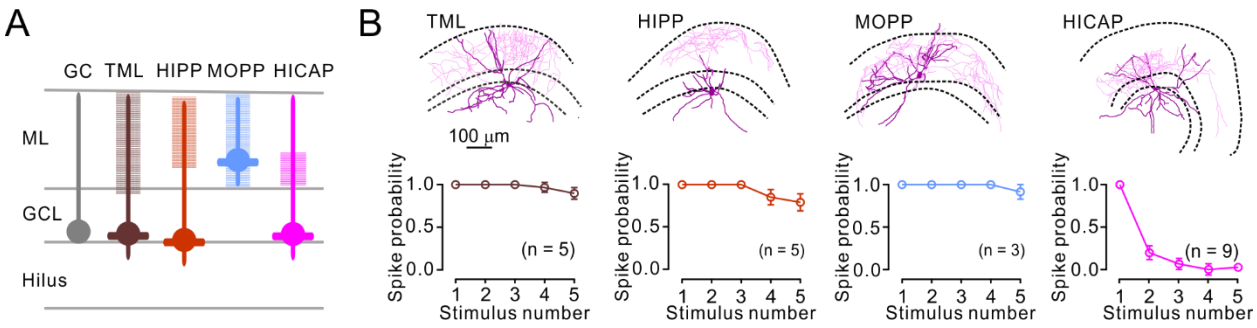

Figure 10. Morphological reconstruction of dendrite-targeting INs recruited by photostimulation of SuM terminals

(A) Summary of identified D-INs subtypes recruited by the SuM input is depicted. The filled circles (soma locations), the thick lines (dendrites), and the hatched boxes (axon distribution).

(B) Top, morphological reconstructions of representative TML, HIPP, MOPP, and HICAP in the DG. Bottom, the plot of spike probabilities of recorded cells in response to 5-Hz photostimulation of the SuM input. Data error bars represent mean ± SEM.

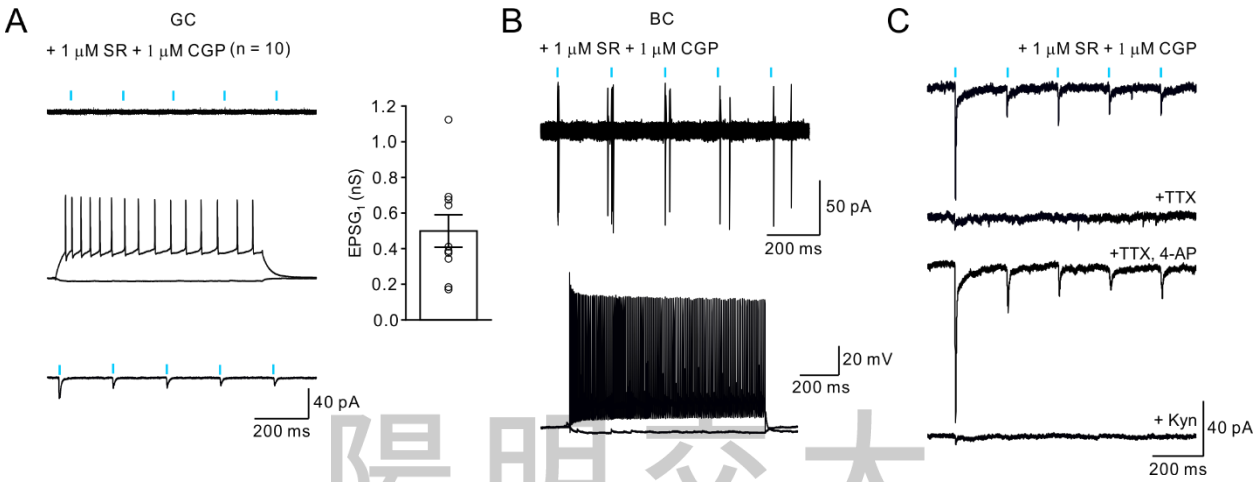

Figure 11. SuM input excites BC but not GCs under the blockade of synaptic inhibition

(A) Top, representative traces of cell-attached responses of a GC (six overlaid sweeps) to 5-Hz photostimulation of the SuM input in the presence of GABAergic inhibition blockers. Middle, the firing pattern of the recorded GC. Bottom, light-evoked EPSC in recorded GC. The bar graph shows the plot of EPSGs obtained from all the GCs recorded (n = 10).

(B) Top, representative traces of cell-attached responses of a BC (six overlaid sweeps) to 5-Hz photostimulation of the SuM input in the presence of GABAergic inhibition blockers. Bottom, the firing pattern of the recorded BC.

(C) Representative traces of light-evoked EPSC recorded from the BC in panel B in SR, CGP, TTX (1 μM), TTX, 4-AP (1 mM), and 2 mM Kyn. Notice that TTX completely blocked the responses and is recovered by 4-AP. Kyn completely abolished the responses.

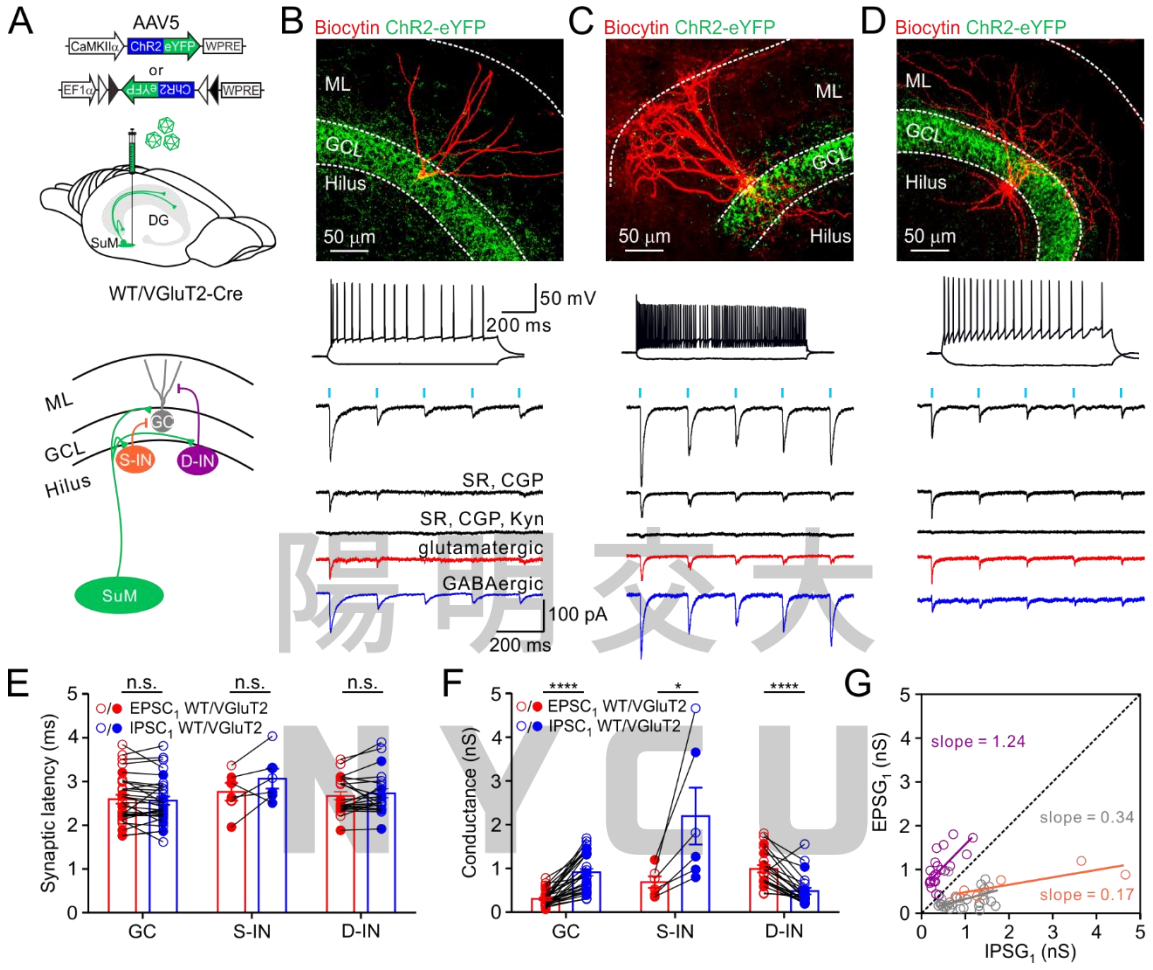

Figure 12. Differential glutamate/GABA cotransmission is target cell-specific

(A) Top, schematic of virus injection into SuM of VGluT2-Cre or WT mouse. Bottom, schematic of local DG network including the SuM input (green), GC, S-IN, and D-IN.

(B), (C), and (D) Top, confocal image stacks of transverse sections of the DG depicting selective expression of ChR2-eYFP in the GCL and a biocytin-filled GC, S-IN, and D-IN (red). Middle, firing pattern of the GC, S-IN, and D-IN. Bottom, sample traces showing the responses of a GC,

S-IN, and D-IN to the 5-Hz photostimulation of the SuM input. Black traces; average inward currents recorded in ACSF, in the presence of $GABA_A$ receptor blocker, SR95531 (1 μM, SR) and $GABA_B$ receptor blocker, CGP55845 (1 μM, CGP), and in the presence of SR, CGP, and 2 mM Kyn. The Kyn-sensitive component (glutamatergic, red), and SR & CGP-sensitive component (GABAergic, blue) obtained by digital subtraction from the above traces.

(E) Plot of synaptic latencies of $EPSC_1$ and $IPSC_1$ induced by the first light pulse in GCs, S-INs and D-INs. (GCs, $EPSC_1$, 2.60 ± 0.10 ms; $IPSC_1$, 2.56 ± 0.10 ms; n = 30; p = 0.875, U = 439.0; S-INs, $EPSC_1$, 2.78 ± 0.20 ms; $IPSC_1$, 3.07 ± 0.23 ms; n = 6; p = 0.571, U = 14.0; D-IN, $EPSC_1$, 2.67 ± 0.09; $IPSC_1$, 2.73 ± 0.10; n = 22; p = 0.663, U = 223.0; Mann-Whitney test. Circles connected by lines represent data collected from the same cell. Filled circles are data obtained from VGluT2-Cre line while open circles represent data from WT mice.

(F) Plot of excitatory and GABA conductances, $EPSG_1$ and $IPSG_1$ in GCs, S-INs and D-INs. (GCs, $EPSG_1$, 0.30 ± 0.03; $IPSG_1$, 0.91 ± 0.08; n = 30; p < 0.0001; U = 67.0; S-INs, $EPSG_1$, 0.58 ± 0.08 nS; $IPSG_1$, 2.14 ± 0.67 nS; n = 6; p < 0.05; U = 4.0; D-INs, $EPSG_1$, 0.99 ± 0.08 nS; $IPSG_1$, 0.48 ± 0.08 nS; n = 22; p < 0.0001; U = 63; Mann-Whitney test.

(G) Scatter plot of $EPSG_1$ versus $IPSG_1$ from GCs (gray circles), S-INs (orange circles), and D-INs (violet circles). The dashed line represents the equality diagonal. The gray, orange and violet lines are the linear regression lines for GCs, S-IN and D-INs respectively (the slope = 0.34; R^2 = 0.20 for GCs, slope = 0.17, R^2 = 0.68 for S-INs, and slope = 1.24, R^2 = 0.68 for D-INs). Data error bars represent mean ± SEM.

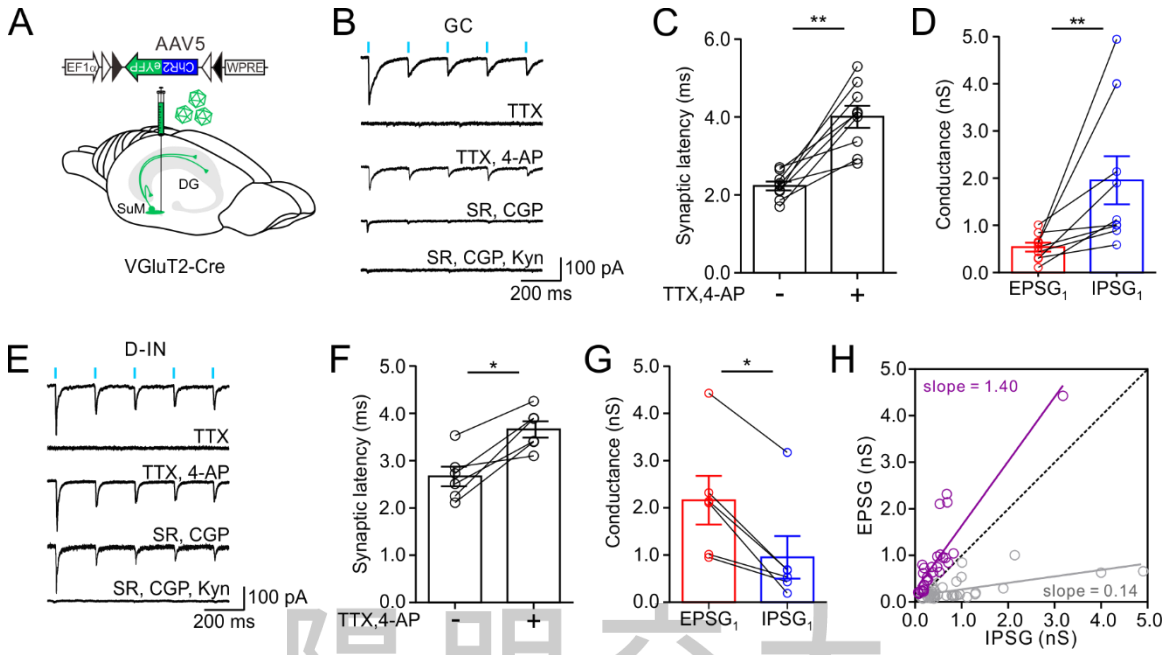

Figure 13. SuM input forms monosynaptic connections with GCs and D-INs

(A) Schematic of virus injection into the SuM of VGluT2-Cre mice.

(B) Representative traces of light-evoked responses recorded from a GC in ACSF, TTX (1 μM), TTX, and 4-AP (1 mM). Note that TTX completely blocked the response and recovered by 4-AP. The addition of SR (1 μM) and CGP (1 μM) largely block the response, Kyn (2 mM) completely abolished the remaining responses.

(C) Synaptic latencies before and after bath application of TTX, 4-AP at the SuM-GC synapse; ACSF, 2.24 ± 0.11 ms; TTX, 4-AP, 4.01 ± 0.28 ms; n = 9; p = 0.0039, Wilcoxon sign-rank test.

(D) Plot of $EPSG_1$ and $IPSG_1$ of GCs. $EPSG_1$, 0.53 ± 0.10 nS; $IPSG_1$, 1.95 ± 0.51 nS; n = 9; p = 0.0012; U = 6.0; Mann-Whitney test.

(E) Representative traces of light-evoked responses recorded from a D-IN in ACSF, TTX (1 μM), TTX, 4-AP (1 mM). TTX completely blocked the response and recovered by 4-AP. SR (1 μM)

and CGP (1 μM) slightly block the response, and finally, Kyn (2 mM) completely abolished the remaining responses.

(F) Plot of synaptic latencies before and after bath application of TTX, 4-AP at the SuM-D-IN synapses; ACSF, 2.67 ± 0.21 ms; TTX & 4-AP, 3.66 ± 0.17 ms; n = 6, p = 0.0313, Wilcoxon sign-rank test.

(G) Plot of $EPSG_1$ and $IPSG_1$ of D-INs. $EPSG_1$, 2.16 ± 0.51 nS; $IPSG_1$, 0.95 ± 0.06 nS; n = 6; p = 0.0411; U = 5.0; Mann-Whitney test.

(H) Scatter plot of EPSG versus IPSG from GCs (gray circles) and D-INs (violet circles) during 5-Hz photostimulation of SuM input. The dashed line represents the equality diagonal. The gray and violet lines are the linear regression lines for GCs and D-INs, respectively (the slope = 0.14; R^2 = 0.40 for GCs and slope = 1.40, R^2 = 0.78 for D-INs). Data error bars represent mean ± SEM.

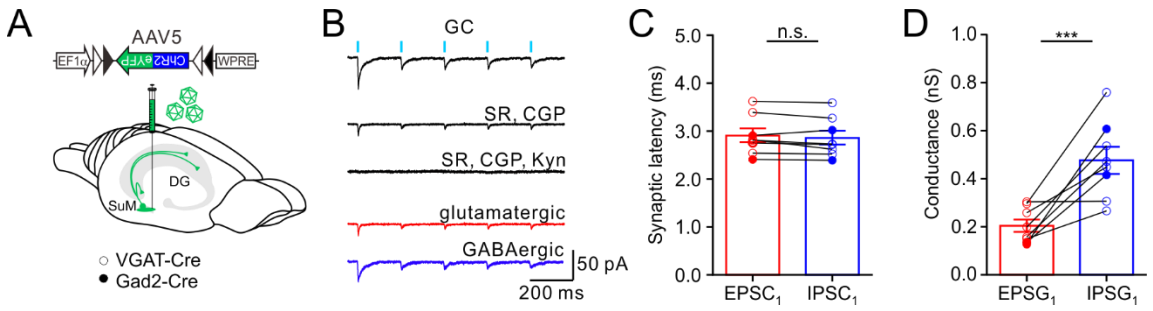

Figure 14. VGAT$^+$ and Gad$^+$ neurons in the SuM project to DG and corelease glutamate and GABA at SuM-GC synapses

(A) Schematic of virus injection into the SuM of VGAT-Cre (open circle) and Gad2-Cre (closed circle) mice.

(B) Sample traces showing the responses of a GC to the 5-Hz photostimulation of the SuM input. Black trace; average inward currents recorded in ACSF, in the presence of $GABA_A$ receptor blocker, SR95531 (1 µM, SR) and $GABA_B$ receptor blocker, CGP55845 (1 µM, CGP), and in the presence of SR, CGP and 2 mM Kyn. The Kyn-sensitive component (glutamatergic, red), and SR & CGP-sensitive component (GABAergic, blue) obtained by digital subtraction from the above traces.

(C) Plot of synaptic latencies of $EPSC_1$ and $IPSC_1$ of GCs. $EPSC_1$, 2.91 ± 0.14 nS; $IPSC_1$, 2.86 ± 0.14 nS; n = 8; p = 0.5604; U = 26.0; Mann-Whitney test.

(D) Plot of conductances $EPSG_1$ and $IPSG_1$ of GCs. $EPSG_1$, 0.20 ± 0.03 nS; $IPSG_1$, 0.48 ± 0.06 nS; n = 8; p = 0.0006; U = 2.0; Mann-Whitney test.

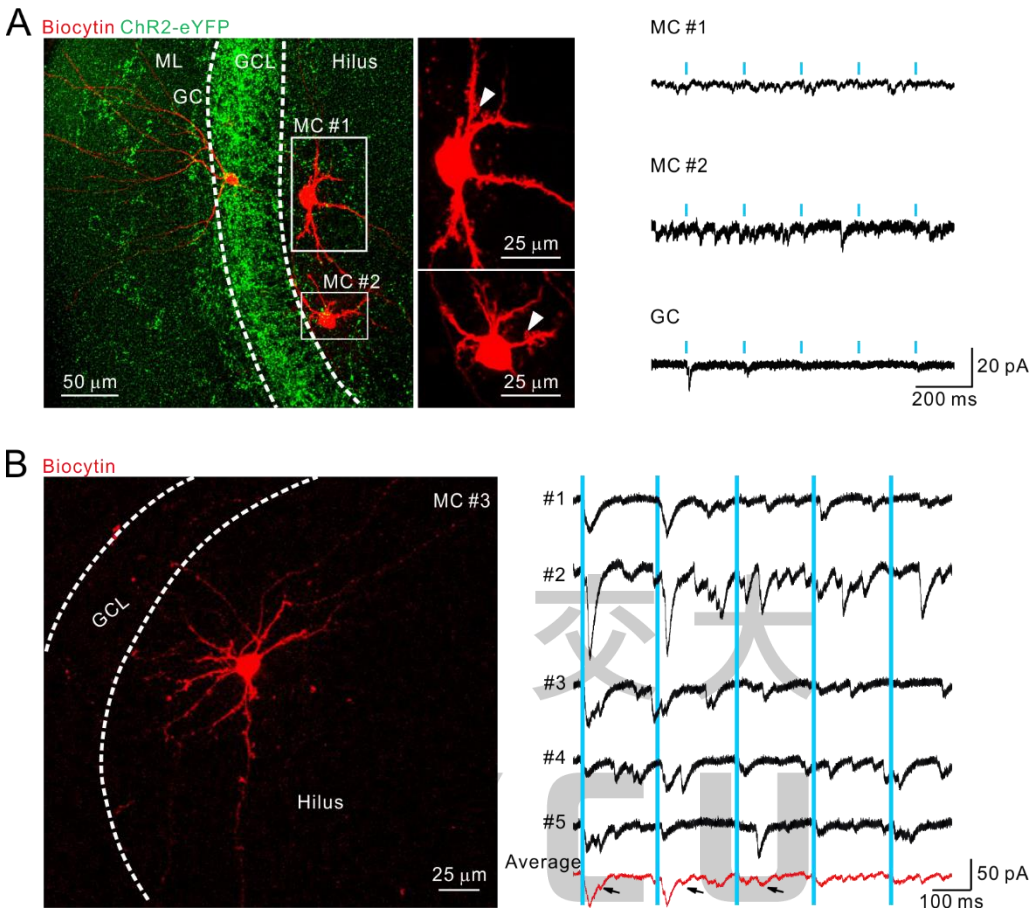

Figure 15. MCs receive weak synaptic input from the SuM

(A) Left, confocal image stacks of transverse sections through the DG depicting selective expression of ChR2-eYFP in VGluT2^{+} SuM fibers (green) in the GCL and sequentially recorded biocytin-filled MC #1, MC #2 (arrow heads, thorny excrescences), and a GC. Right, representative traces obtained from MC #1, MC #2, and a GC in response to the photostimulation of the SuM input.

(B) Left, the morphology of a biocytin-filled responsive MC #3. Right, black traces, individual traces of responses of the MC #3 to 5 Hz photostimulation of SuM input. The red trace is the average trace. The arrows denote disynaptic responses.

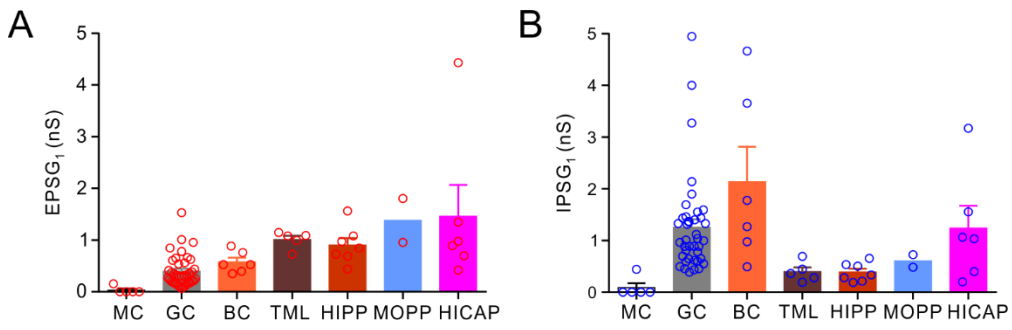

Figure 16. EPSGs and IPSGs of SuM-evoked responses in different dentate cells

(A) and (B) Summary of the $EPSG_1$ and $IPSG_1$ respectively, recorded from different cell types in the DG. Individual cells were shown in circles. Data error bars represent mean ± SEM

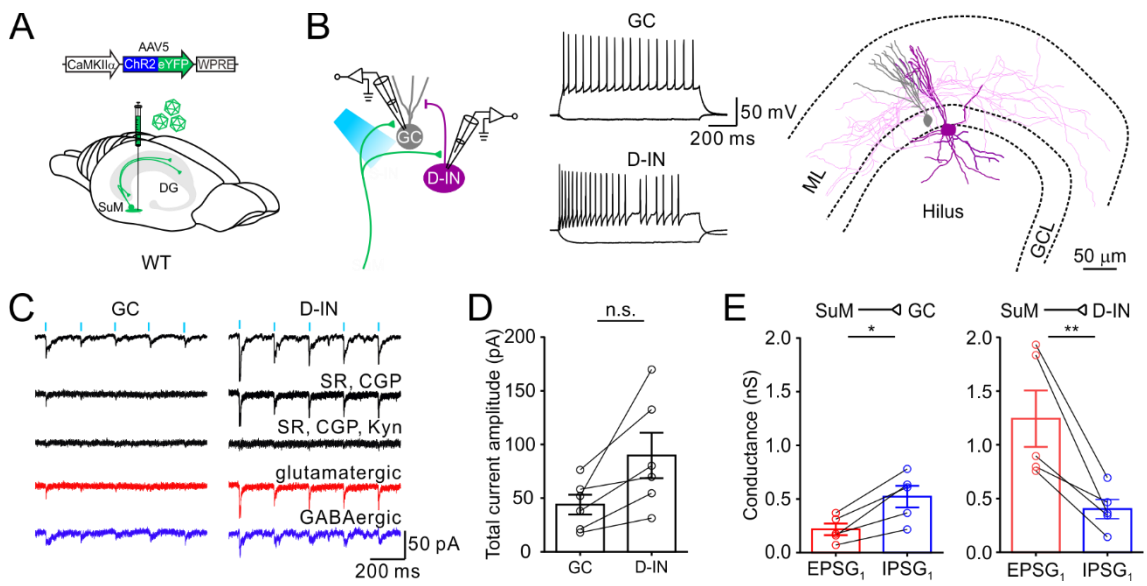

Figure 17. Synaptic responses from simultaneously recorded GCs and D-INs

(A) Schematic of virus injection into the SuM.

(B) Left, simultaneous whole-cell recording from a GC and a D-IN. Middle, the firing pattern of the recorded GC and D-IN. Right, the morphological reconstruction GC (gray color) and D-IN (violet color).

(C) Traces of light-evoked postsynaptic responses recorded in GC and D-IN in baseline, SR & CGP, SR, GCP & Kyn, glutamatergic component (red), and GABAergic component (blue).

(D) Plot of the total composite current amplitude in the GCs and D-INs simultaneously recorded. GC, 43.94 ± 9.24 pA; D-IN, 89.78 ± 21.13 pA; n = 6; p = 0.0931; U = 7.0; Mann-Whitney test. Circles connected by dashed lines represent data collected from cells recorded simultaneously from the same slice.

(E) Plot of conductances of EPSG and IPSG at the SuM-GC and SuM-D-IN synapses. SuM-GC, $EPSG_1$, 0.22 ± 0.05 nS; $IPSG_1$, 0.52 ± 0.10 nS; n = 5; $p < 0.05$; U = 2.0; SuM-D-IN, $EPSG_1$, 1.24 ± 0.26 nS; $IPSG_1$, 0.40 ± 0.09 nS; n = 5; $p < 0.01$; U = 0.0; Mann-Whitney test.

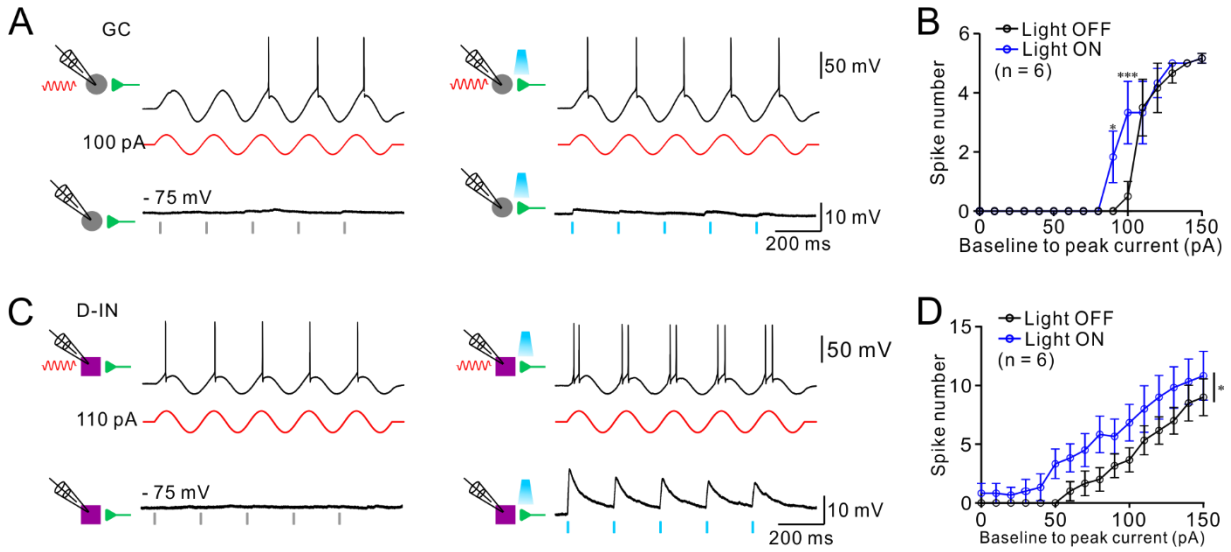

Figure 18. SuM input enhances the excitability of GCs and D-INs

(A) Top, representative traces of responses of GCs to sinusoidal current steps before (left) and after (right) photostimulation of SuM input. Middle, baseline to peak current amplitude of 100 pA sinusoidal protocol (red traces). Bottom, the EPSP evoked by photostimulation of SuM input. Gray bars represent light off while blue bars indicate the time of photostimulation at 5 Hz.

(B) Plot of spike number versus baseline to peak current in GCs.

(C)Top, representative traces of responses of D-INs to sinusoidal current steps before (left) and after (right) photostimulation of SuM input. Middle, baseline to peak current amplitude of 110 pA sinusoidal protocol (red traces). Bottom, the EPSP evoked by photostimulation of SuM input. Blue bars indicate the time of photostimulation at 5 Hz.

(D) Plot of spike number versus baseline to peak current in D-INs.

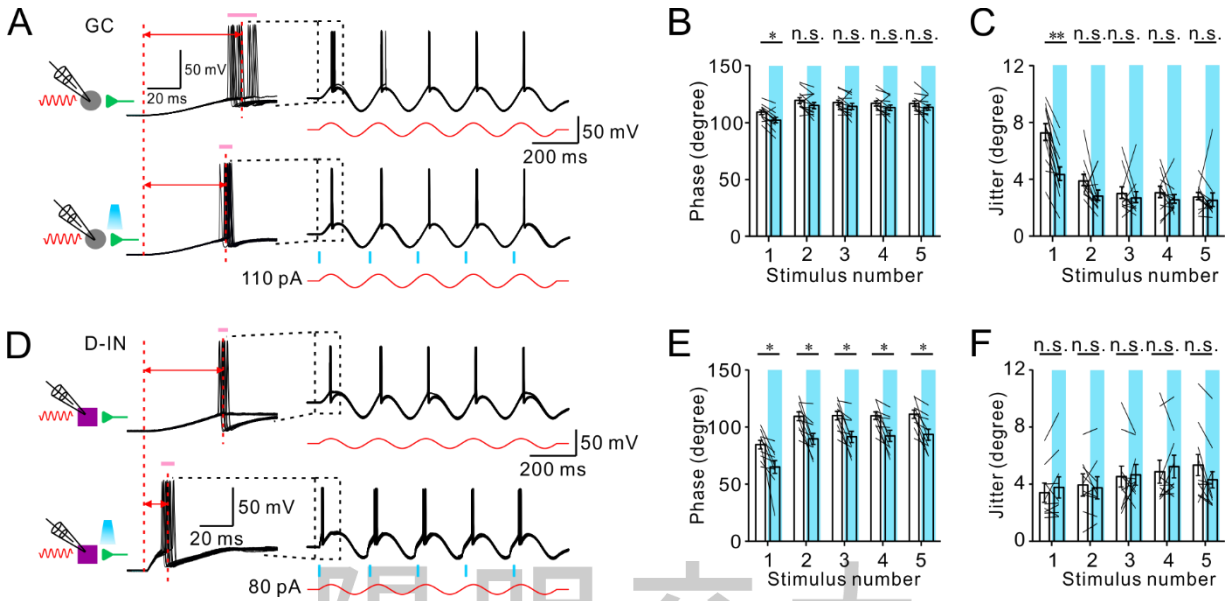

Figure 19. SuM input shortens spike latencies and enhances spike timing precision in GCs and D-INs

(A) Representative traces of responses of GCs (twenty overlaid sweeps) to constant suprathreshold sinusoidal current injection without (upper traces) and with (lower traces) photostimulation of SuM input. Left, enlarged traces of APs induced by the first stimulus without (upper traces) and with photostimulation of SuM input (lower traces). Red dotted lines and the red arrow lines show a shift in the mean spike latencies between the onset of sinusoid current injection and the mean time point of peak in each AP. The pink bars represent spike jitters.

(B) Summary plot of spike phase. n = 12; $F(4, 44) = 20.43$; $p < 0.0001$; n.s., no significant difference; two-way ANOVA with Bonferroni *post hoc test.* Data error bars represent mean ± SEM.

(C) Summary plot of spike jitter. n = 12; $F(4, 44) = 22.17$; $p < 0.0001$; n.s., no significant difference; two-way ANOVA with Bonferroni *post hoc test.*

(D) Representative traces of responses of D-INs (twenty overlaid sweeps) to constant suprathreshold sinusoidal current injection without (upper traces) and with (lower traces) photostimulation of the SuM input. Left, enlarged traces of APs induced by the first stimulus without (upper traces) and with photostimulation (lower traces). Red dotted lines and the red arrow lines show a shift in the mean spike latencies between the onset of sinusoid current injection and the mean time point of peak in each AP. The pink bars represent spike jitters.

(E) Summary plot of spike phase. $n = 10$; $F(4, 36) = 115.4$; $p < 0.0001$; two-way ANOVA with Bonferroni *post hoc test.* Data error bars represent mean ± SEM.

(F) Summary plot of spike jitter. $n = 10$; $F(4, 36) = 5.0$; $p = 0.0027$; n.s., no significant difference; two-way ANOVA with Bonferroni *post hoc test.*

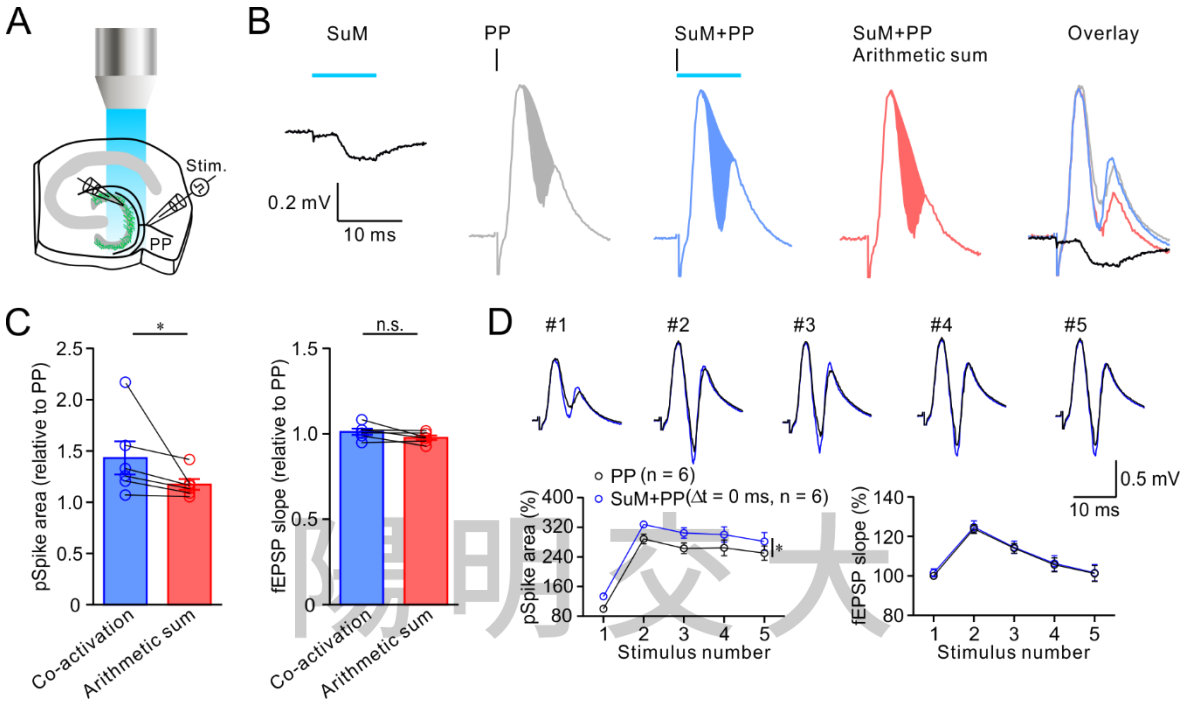

Figure 20. SuM input promotes GC responses to cortical input

(A) Experimental schematic showing a stimulation electrode (stim.) placed in the subiculum to electrically activate the PP fibers, a field-recording electrode in the GCL to monitor LFP and pSpike, and blue light for photostimulation of the SuM axon terminals in the GCL.

(B) Representative traces of SuM-mediated fEPSP (black trace) after photostimulation, PP-mediated pSpike (filled area in gray) upon electrical stimulation, and a pSpike (filled area in light blue) after the co-activation (Δt = 0 ms) of the SuM and PP. The arithmetic sum of fEPSP and pSpike was shown in red. The traces of pSpikes were superimposed and aligned with fEPSP.

(C) Left bar graph, summary plots of the pSpike areas evoked by SuM+PP co-activation (light blue) and arithmetic sum of SuM-evoked fEPSP and PP-evoked pSpike (light red). Areas were normalized to pSpike area evoked by the PP alone. SuM+PP co-activation, 1.43 ± 0.16; SuM+PP

arithmetic sum, 1.17 ± 0.05; n = 6; p = 0.0313. Right bar graph, summary plots of relative fEPSP slope, SuM+PP co-activation, 1.01 ± 0.02; SuM+PP arithmetic sum, 0.97 ± 0.01; n = 6; n.s., no significant difference; Wilcoxon signed-rank test.

(D) Top, representative traces of pSpike responses to PP stimulation alone (black traces) and SuM+PP (blue traces) during a 5-Hz train. Bottom**,** left, a summary of the effect of SuM activation on PP-evoked pSpikes versus stimulus number. PP, n = 6; PP + SuM, n = 6; $p < 0.05$; two-way ANOVA with Bonferroni *post hoc* test. Right, fEPSP slope before and after photostimulation of the SuM input. PP, n = 6; SuM+PP, n = 6; n.s., no significant difference, two-way ANOVA with Bonferroni *post hoc* test.

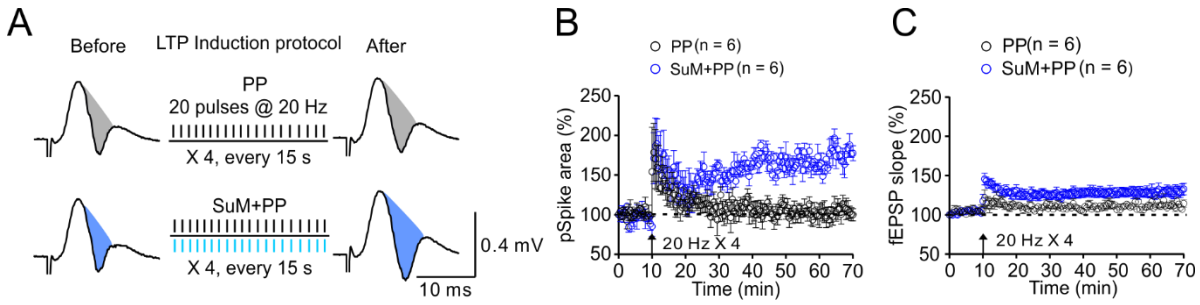

Figure 21. SuM input supports LTP at the PP-GC synapses

(A) Left, representative traces of baseline pSpikes in response to stimulation of PP alone. Middle, LTP induction protocol consists of four trains of 20-Hz electrical stimulation of the PP alone at 15 s inter-train interval (top) or co-activation of the PP and 20-Hz, 4 trains, 10 ms photostimulation of the SuM input (bottom). Right, sample traces of pSpikes after LTP induction.

(B) Time course of the normalized pSpike area recorded from the GCL in response to 20-Hz, 4 trains stimulation of PP inputs alone (black circles) or co-activation of the PP input stimulation and 20-Hz photostimulation of the SuM input (blue circles). PP alone, 104.8 ± 8.59%; n = 6; SuM+PP, 167.6 ± 5.30%; n = 6; p = 0.0009; paired t-test.

(C) Time course of the normalized fEPSP slope of pSpikes recorded from the GCL in response to 20-Hz, 4 trains stimulation of PP inputs alone (black circles) or co-activation of PP input stimulation with 20-Hz photostimulation of the SuM input (blue circles). PP alone, 110.6 ± 2.20%; n = 6; SuM+PP, 128.5 ± 5.19%; n = 6; p = 0.0598; paired t-test. Data error bars represent mean ± SEM.

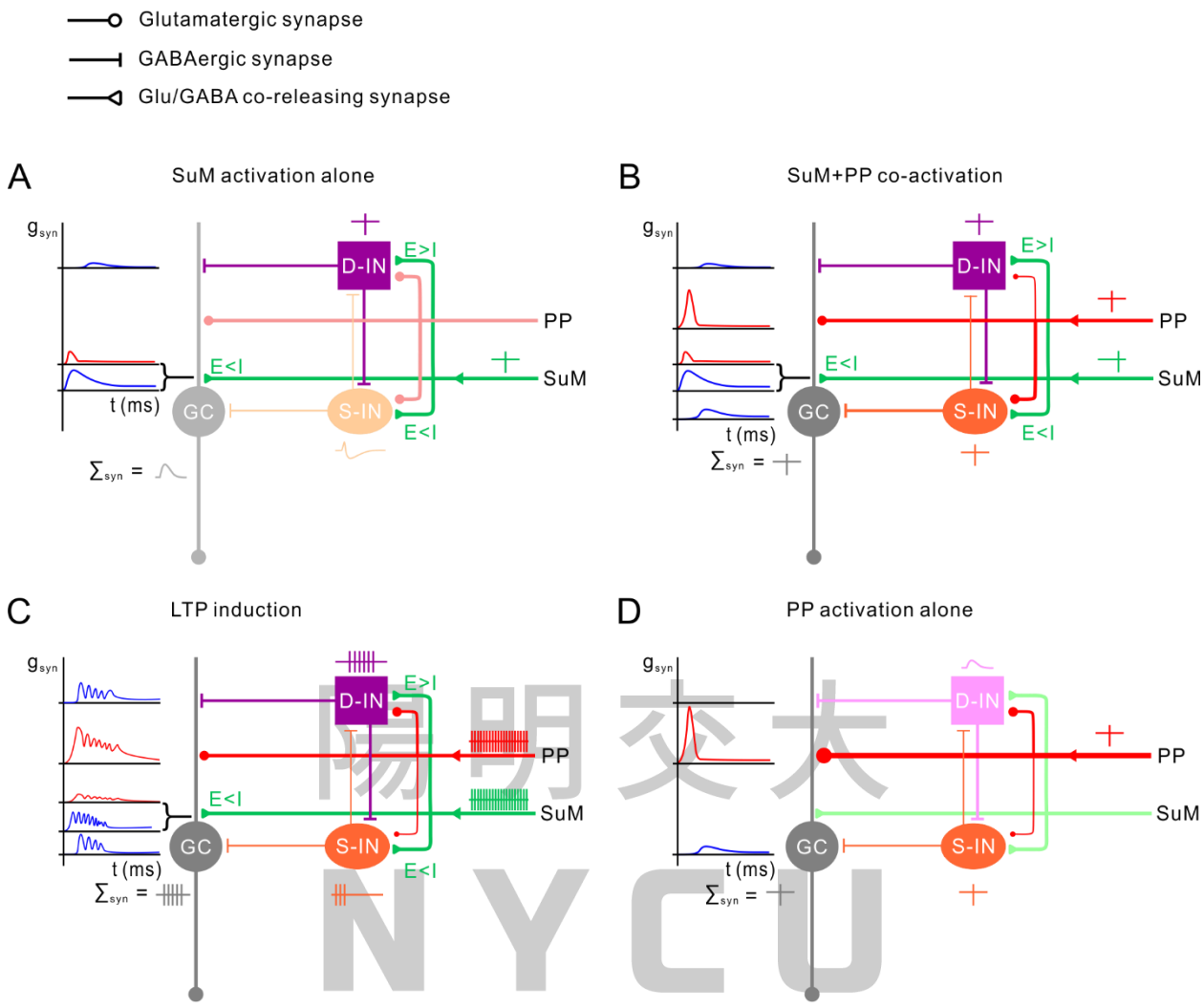

Figure 22. Proposed network mechanisms for the modulatory role of SuM input in the DG

(A) Schematic of the DG network model showing the synapses between the SuM input (green) and the GC (gray), the D-IN (violet square), and S-IN (orange oval). The SuM input forms monosynaptic excitatory and inhibitory connections with the GC, D-IN, and S-IN. At SuM-GC and SuM-S-IN, E<I while at SuM-D-IN, E>I. Activation of SuM input (green AP) results in spike generation in D-IN (violet AP), but only subthreshold depolarization in the GCs and S-INs. The synaptic summation in this model leads to a small subthreshold depolarization in the GCs.

(B) Co-activation of the SuM input (green) and PP input (red). The spike generation in the D-IN (violet AP) is reinforced by PP stimulation. S-IN is recruited into the network by the PP input (orange AP). The summation of the synapses results in enhanced EPSP (E)-spike (S) coupling (gray E-S coupling) in the GC.

(C) Co-activation of SuM and PP inputs during LTP induction. 20 Hz simultaneous activation of SuM (green spikes) and PP (red spikes). During this LTP induction protocol, spike generation in D-IN is strongly reinforced through the entire phase of the stimulation trains while S-IN generates spikes only at the early phase (orange spikes); this could result in late somatic disinhibition of GC. The synaptic summation during this induction protocol leads to the net increase in spike generation in GC (gray spikes).

(D) Synaptic output by PP activation alone after LTP induction. Both PP-GC synapse and E-S coupling are enhanced.

Table 1. Comparison of electrophysiological properties and synaptic responses in GCs, S-INs, and D-INs

	GC (30)	S-IN (6)	D-IN (25)	P-value
RMP (mV)	81.43 ± 0.66	55.81 ± 1.14	54.85 ± 2.44	a. < 0.0001 b. < 0.001 c. 0.3840
R_{in} (MΩ)	386.80 ± 20.30	144.90 ± 16.97	383.00 ± 31.74	a. 0.5197 b. < 0.0010 c.< 0.0010
EPSG (nS)	0.36 ± 0.06	0.58 ± 0.08	0.99 ± 0.08	a. < 0.0001 b. < 0.0500 c. 0.0741
IPSG (nS)	1.05 ± 0.11	2.14 ± 0.67	0.43 ± 0.06	a. < 0.0001 b. 0.5277 c.< 0.0100
E/I ratio	0.36 ± 0.05	0.40 ± 0.11	2.66 ± 0.21	a. < 0.0001 b. 0.2371 c.< 0.0010
EPSC (pA)	25.16 ± 4.01	42.21 ± 8.69	67.36 ± 5.81	a. < 0.0001 b. 0.1054 c. 0.0586
IPSC (pA)	67.27 ± 8.54	139.10 ± 43.80	27.75 ± 3.64	a. < 0.0001 b. 0.4912 c. <0.01
Q_{EPSC}(pC)	0.36 ± 0.08	1.31 ± 0.18	0.71 ± 0.14	d. < 0.0001 e.0.0649 f. 0.0301
Q_{IPSC}(pC)	3.41 ± 0.42	1.06 ± 0.39	3.28 ± 1.53	
Rise time EPSC (ms)	1.10 ± 0.07	1.19 ± 0.08	1.25 ± 0.11	d. <0.0001 e. 0.1255 f. <0.0001
Rise time IPSC (ms)	2.79 ± 0.26	1.73 ± 0.31	2.53 ± 0.23	

Tau EPSC (ms)	6.87 ± 0.47	7.94 ± 0.55	6.38 ± 0.61	d. <0.0001 e.<0.001 f. <0.0001
Tau IPSC (ms)	31.67 ± 1.85	17.40 ± 1.53	19.64 ± 2.40	

Note: Cell numbers are represented in parentheses. Data were obtained from VGLUT2-Cre and WT mice.

[a]GC versus D-IN, [b]GC versus S-IN, [c]S-IN versus D-IN.

[d]EPSC vs IPSC of GCs, [e]EPSC vs IPSC of S-IN, [f]EPSC vs IPSC of D-INs.

Mann-Whitney test was performed to determine statistical significance. All values are given as mean ± SEM.

Table 2. Key resources used in this study

REAGENT OR RESOURCE	SOURCE	IDENTIFIER
Antibodies		
Monoclonal mouse anti-VGAT	Synaptic systems	Cat# 131 011C3; RRID:AB_887868)
Polyclonal rabbit anti-VGluT2	Synaptic systems	Cat# 135 403; RRID:AB_887883)
Rabbit anti-GFP	Abcam	Cat# ab290; RRID:AB_303395
Alexa Fluor 488 goat anti-rabbit	Thermo Fisher Scientific	Cat# A-11008; RRID:AB_143165
Alexa Flour 594 goat anti-mouse	Thermo Fisher Scientific	Cat# A-11005; RRID:AB_2534073)
Alexa Fluor 647 goat anti-rabbit	Thermo Fisher Scientific	Cat# A-21236; RRID:AB_2535805)
Alexa Fluor 594-streptavidin	Thermo Fisher Scientific	Cat# S11227
Alexa Fluor 488-streptavidin	Thermo Fisher Scientific	Cat# S11223
Bacterial and Virus strains		
AAV5-CaMKIIa-hChR2(H134R)-eYFP	University of North Carolina vector core	Lot#: AV4316P
AAV5-EF1a-DIO-hChR2(H134R)-eYFP	University of North Carolina vector core	N/A
Chemicals, Peptides and Recombinant Proteins		
Kynurenic Acid	Sigma-Aldrich	Cat# K3375
CGP55845 hydrochloride	Tocris	Cat#1248
SR95531	Abcam	Cat# ab120042
Tetrodotoxin	Ascent	Cat# ab120055
4-aminopyridine	Tocris	Cat# 0940
Biocytin	Thermo Fisher Scientific	Cat# B-1592
Paraformaldehyde	Sigma-Aldrich	Cat# 158127
Red Retrobeads	Lumafluor Inc	N/A
Experimental models: Organisms/strains		
Mouse: C57BL/6JNarl	National Laboratory Animal Center (Taiwan)	# RMRC11005
Mouse: VGluT2-Cre: Slc17a6$^{tm2(cre)Lowl}$/J	The Jackson Laboratory	Stock #: 016963
Mouse: VGAT-Cre: Slc32al$^{tm2(cre)Lowl}$/J,	The Jackson Laboratory	Stock #: 028862
Mouse: Gad2-Cre: Gad2$^{tm2(cre)Zjh}$/J	The Jackson Laboratory	stock #: 010802
Software and algorithms		
GraphPad Prism 6	GraphPad	https://www.graphpad.com
ImageJ	ImageJ	https://imagej.net
CorelDrawX8	CorelDraw Graphic Suit	https://www.coreldraw.com
pClamp and Clampfit 10.3	Molecular Devices	https://www.moleculardevices.com
HBP Neuron Morphology Viewer	NeuroInformatics.NL	https://neuroinformatics.nl/HBP/morphology-viewer/
Neuromantic 1.6.3	University of Reading	https://www.reading.ac.uk/neuromantic/body_index.php
Python	Jupyter notebook	https://jupyter.org
Other		
The microsyringe pump	Kd Scientific	# KDS310
NanoFil 10uL syringe	World Precision Instruments	# NANOFIL

34G beveled NanoFil needle	World Precision Instruments	# NF34BV-2
Microslicer	Dosaka	# DTK-1000
Microtome	Leica	# SM2010R
MultiClamp 700B Microelectrode Amplifier	Molecular Devices	# MULTICLAMP 700B
Digitizer	Molecular Devices	# Digidata 1440A
Borosilicate Glass with Filament	Harvard Apparatus	# GC150F-7.5

7. REFERENCES

Abel T, Martin KC, Bartsch D, Kandel ER (1998) Memory suppressor genes: inhibitory constraints on the storage of long-term memory. Science 279:338–341.

Abraham W (2008) Metaplasticity: tuning synapses and networks for plasticity. Nat Rev Neursci 9:387.

Abraham WC, Bear MF (1996) Metaplasticity: the plasticity of synaptic plasticity. Trends Neurosci 19:126–130.

Acsády L, Kamondi A, Sik A, Freund T, Buzsáki G (1998) GABAergic cells are the major postsynaptic targets of mossy fibers in the rat hippocampus. J Neurosci 18:3386–3403.

Ahn JH, Chen BH Shin, BN Lee, TK, Cho JH, Kim IH, Park JH, Lee JC, Tae HJ, Lee CH, Won MH, Lee YL, Choi SY, Hong S (2016) Comparison of catalase immunoreactivity in the hippocampus between young, adult and aged mice and rats. Molecular medicine reports 14:851–856.

Altman J, Das GD (1965) Autoradiographic and histological evidence of postnatal hippocampal neurogenesis in rats. J Comp Neurol. 124:319–35.

Amaral DG, Scharfman HE, Lavenex P (2007) The dentate gyrus: fundamental neuroanatomical organization (dentate gyrus for dummies). Progress in brain research 163:3–22.

Armstrong C, Szabadics J, Tamás G, Soltész I (2011) Neurogliaform cells in the molecular layer of the dentate gyrus as feed-forward γ-aminobutyric acidergic modulators of entorhinal–hippocampal interplay. J Comp Neurol 519:1476–1491.

Bacci A, Huguenard JR (2006) Enhancement of spike-timing precision by autaptic transmission in neocortical inhibitory interneurons. Neuron 49:119–130.

Bannerman DM, Grubb M, Deacon RM, Yee BK, Feldon J, Rawlins JN (2003) Ventral hippocampal lesions affect anxiety but not spatial learning. Behav Brain Res 139, 197–213.

Barnes CA, McNaughton, BL, Mizumori, SJ, Leonard, BW, Lin LH (1990) Comparison of spatial and temporal characteristics of neuronal activity in sequential stages of hippocampal processing. Progress in brain research, 83, 287–300.

Bartos M, Vida I, Jonas P (2007) Synaptic mechanisms of synchronized gamma oscillations in inhibitory interneuron networks. Nat Rev Neurosci 8:45–56.

Behr J, Lyson KJ, Mody I (1998) Enhanced propagation of epileptiform activity through the kindled dentate gyrus. Journal of neurophysiology 79:1726–1732.

Berger B, Esclapez M, Alvarez C, Meyer G, Catala M (2001) Human and monkey fetal brain development of the supramammillary-hippocampal projections: a system involved in the regulation of theta activity. The Journal of comparative neurology 429:515–529.

Berron D, Schutze H, Maass A, Cardenas-Blanco A, Kuijf HJ, Kumaran D, Duzel E (2016) Strong Evidence for Pattern Separation in Human Dentate Gyrus. J Neurosci 36: 7569–7579.

Bi G, Poo M (2001) Synaptic modification by correlated activity: Hebb's postulate revisited. Annu. Rev Neurosci 24:139–166.

Bilkey DK, Goddard GV (1987) Septohippocampal and commissural pathways antagonistically control inhibitory interneurons in the dentate gyrus. Brain research 405, 320–325.

Bingman VP (1992) The importance of comparative studies and ecological validity for understanding hippocampal structure and cognitive function. Hippocampus 2:213–219.

Blackstad TW, Fuxe K, Hökfelt T (1967) Noradrenaline nerve terminals in the hippocampal region of the rat and the guinea pig. Z Zellforsch Mikrosk Anat 78:463–73.

Bland, BH, Oddie, SD (1998) Anatomical, electrophysiological and pharmacological studies of ascending brainstem hippocampal synchronizing pathways. Neuroscience and biobehavioral reviews 22:259–273.

Blasco-Ibanez JM, Martinez-Guijarro FJ, Freund TF (2000) Recurrent mossy fibers preferentially innervate parvalbumin-immunoreactive interneurons in the granule cell layer of the rat dentate gyrus. Neuroreport 11:3219–3225.

Bliss TV, Lomo T (1973) Long-lasting potentiation of synaptic transmission in the dentate area of the anaesthetized rabbit following stimulation of the perforant path. The Journal of Physiology 232:331–356.

Booker SA, Vida I (2018) Morphological diversity and connectivity of hippocampal interneurons. Cell and tissue research, 373:619–641.

Borhegyi Z, Leranth C (1997) Distinct substance P- and calretinin-containing projections from the supramammillary area to the hippocampus in rats; a species difference between rats and monkeys. Experimental brain research 115:369–374.

Borhegyi Z, Magloczky Z, Acsady L, Freund TF (1998) The supramammillary nucleus innervates cholinergic and GABAergic neurons in the medial septum-diagonal band of Broca complex. Neuroscience 82:1053–1065.

Boss BD, Peterson GM, Cowan WM (1985) On the number of neurons in the dentate gyrus of the rat. Brain Res 338:144–150.

Boulland JL, Jenstad M, Boekel AJ, Wouterlood FG, Edwards RH, Storm-Mathisen J, Chaudhry FA (2009) Vesicular glutamate and GABA transporters sort to distinct sets of vesicles in a population of presynaptic terminals. Cerebral cortex 19:241–248.

Boulland JL, Qureshi T, Seal RP, Rafiki A, Gundersen V, Bergersen LH, Fremeau RT, Edwards RH, Storm-Mathisen J, Chaudhry FA (2004) Expression of the vesicular glutamate transporters during development indicates the widespread corelease of multiple neurotransmitters. The Journal of comparative neurology 480:264–280.

Brun VH, Solstad T, Kjelstrup KB, Fyhn M, Witter MP, Moser EI, Moser MB (2008) Progressive increase in grid scale from dorsal to ventral medial entorhinal cortex. Hippocampus 18:1200–1212.

Buckmaster PS, Jongen-Relo AL (1999) Highly specific neuron loss preserves lateral inhibitory circuits in the dentate gyrus of kainate-induced epileptic rats. J Neurosci 19:9519–9529.

Buckmaster PS, Strowbridge BW, Kunkel DD, Schmiege DL, Schwartzkroin PA (1992) Mossy cell axonal projections to the dentate gyrus molecular layer in the rat hippocampal slice. Hippocampus 2, 349–362.

Buckmaster PS, Tam E, Schwartzkroin PA (1996) Electrophysiological correlates of seizure sensitivity in the dentate gyrus of epileptic juvenile and adult gerbils. Journal of neurophysiology 76:2169–2180.

Bucurenciu I, Bischofberger J, Jonas P (2010) A small number of open Ca2+ channels trigger transmitter release at a central GABAergic synapse. Nat Neurosci 13:19–21.

Buxhoeveden DP, Casanova MF (2002) The minicolumn hypothesis in neuroscience. Brain 125:935–951.

Buzsaki G (2005) Theta rhythm of navigation: link between path integration and landmark navigation, episodic and semantic memory. Hippocampus 15:827–840.

Buzsaki G, Moser EI (2013) Memory, navigation and theta rhythm in the hippocampal-entorhinal system. Nature neuroscience 16:130–138.

Callaway EM (2002) Cell type specificity of local cortical connections. Journal of neurocytology 31, 231–237.

Carandini M (2004) Amplification of trial-to-trial response variability by neurons in visual cortex. PLoS Biol 2, E264.

Carey M, Lisberger S (2002) Embarrassed, but not depressed: eye opening lessons for cerebellar learning. Neuron 35:223–226.

Chaudhry FA, Reimer RJ, Bellocchio EE, Danbolt NC, Osen KK, Edwards RH, Storm-Mathisen J (1998) The vesicular GABA transporter, VGAT, localizes to synaptic vesicles in sets of glycinergic as well as GABAergic neurons. J Neurosci 18:9733–9750.

Chen S, He L, Huang AJY, Boehringer R, Robert V, Wintzer ME, Polygalov D, Weitemier AZ, Tao Y, Gu M, Middleton SJ, Namiki K, Hama H, Therreau L, Chevaleyre V, Hioki H, Miyawaki A, Piskorowski RA, McHugh TJ (2020) A hypothalamic novelty signal modulates hippocampal memory. Nature 586:270–274.

Chudasama Y, Izquierdo A, Murray EA (2009) Distinct contributions of the amygdala and hippocampus to fear expression. The European journal of neuroscience 30:2327–2337.

Colombo M, Broadbent N (2000) Is the avian hippocampus a functional homologue of the mammalian hippocampus? Neuroscience and biobehavioral reviews 24:465–484.

Dale HH (1935) Pharmacology and nerve-endings. Proc. R. Soc. Med. 28:319 –332.

Damasio AR (1995) Descartes' Error: emotion, Reason, and the Human Brain (New York: G. P. Putnam's Sons).

Dan Y, Poo MM (2006) Spike timing-dependent plasticity: from synapse to perception. Physiological Reviews 86:1033–1048.

Davis RL (1996) Physiology and biochemistry of Drosophila learning mutants. Physiol Rev 76:299–317.

Deng W, Aimone JB, Gage FH (2010) New neurons and new memories: how does adult hippocampal neurogenesis affect learning and memory? Nat Rev Neurosci 11:339-50.

Dent JA, Galvin NJ, Stanfield BB, Cowan WM (1983) The mode of termination of the hypothalamic projection to the dentate gyrus: an EM autoradiographic study. Brain research 258:1–10.

Dragoi G, Harris KD, Buzsaki G (2003) Place representation within hippocampal networks is modified by long-term potentiation. Neuron 39:843–853.

Eccles JC (1957) The Physiology of Nerve Cells. Baltimore MD: John Hopkins Press.

Eichenbaum H (1997) Declarative memory: insights from cognitive neurobiology. Annu Rev Psychol 48:547–572.

Espinoza C, Guzman SJ, Zhang X, Jonas P (2018) Parvalbumin^{+} interneurons obey unique connectivity rules and establish a powerful lateral-inhibition microcircuit in dentate gyrus. Nature communications 9:4605.

Ewell LA, Jones MV (2010) Frequency-tuned distribution of inhibition in the dentate gyrus. J Neurosci 30:12597–12607.

Fattorini G, Antonucci F, Menna E, Matteoli M, Conti F (2015) Co-expression of VGLUT1 and VGAT sustains glutamate and GABA co-release and is regulated by activity in cortical neurons. J Cell Sci 128:1669–1673.

Feldman DE (2012) The spike-timing dependence of plasticity. Neuron 75:556–571.

Freund TF (2003) Interneuron Diversity series: Rhythm and mood in perisomatic inhibition. Trends in neurosciences 26:489–495.

Freund TF, Buzsaki G (1996) Interneurons of the hippocampus. Hippocampus 6:347-470.

Fricker D, Miles R (2001) Interneurons, spike timing, and perception. Neuron 32:771–774.

Fyhn M, Hafting T, Witter MP, Moser EI, Moser, MB (2008) Grid cells in mice. Hippocampus 18:1230–1238.

Ge S, Yang CH, Hsu KS, Ming GL, Song H (2007) A critical period for enhanced synaptic plasticity in newly generated neurons of the adult brain. Neuron 54:559–566.

Gilbert PE, Kesner RP, Lee I (2001) Dissociating hippocampal subregions: double dissociation between dentate gyrus and CA1. Hippocampus 11:626–636.

Gonzalo-Ruiz A, Morte L, Flecha JM, Sanz JM (1999) Neurotransmitter characteristics of neurons projecting to the supramammillary nucleus of the rat. Anat Embryol (Berl) 200:377–392.

Gruart A, Munoz MD, Delgado-Garcia JM (2006) Involvement of the CA3-CA1 synapse in the acquisition of associative learning in behaving mice. J. Neurosci. 26:1077–1087.

Gulyas AI, Miettinen R, Jacobowitz DM, Freund TF (1992) Calretinin is present in nonpyramidal cells of the rat hippocampus--I. A new type of neuron specifically associated with the mossy fiber system. Neuroscience 48:1–27.

Hafting T, Fyhn M, Molden S, Moser MB, Moser EI (2005) Microstructure of a spatial map in the entorhinal cortex. Nature 436:801–806.

Haglund L, Swanson LW, Kohler C (1984) The projection of the supramammillary nucleus to the hippocampal formation: an immunohistochemical and anterograde transport study with the lectin PHA-L in the rat. The Journal of comparative neurology 229:171–185.

Halasy K, Somogyi P (1993) Subdivisions in the multiple GABAergic innervation of granule cells in the dentate gyrus of the rat hippocampus. Eur J Neurosci 5:411–429.

Han ZS, Buhl EH, Lörinczi Z, Somogyi P (1993) A high degree of spatial selectivity in the axonal and dendritic domains of physiologically identified local-circuit neurons in the dentate gyms of the rat hippocampus. Eur J Neurosci 5:395–410.

Harley C (1991) Noradrenergic and locus coeruleus modulation of the perforant path-evoked potential in rat dentate gyrus supports a role for the locus coeruleus in attentional and memorial processes. Progress in brain research 88:307–321.

Hashimotodani Y, Karube F, Yanagawa Y, Fujiyama F, Kano M (2018) Supramammillary Nucleus Afferents to the Dentate Gyrus Co-release Glutamate and GABA and Potentiate Granule Cell Output. Cell Rep 25, 2704–2715.

Hebb DO (1949). The organization of behavior; a neuropsychological theory. New York: Wiley; 1949.

Hefft S, Jonas P (2005) Asynchronous GABA release generates long-lasting inhibition at a hippocampal interneuron–principal neuron synapse. Nat Neurosci 8:1319–1328.

Henze DA, Urban NN, Barrionuevo G (2000) The multifarious hippocampal mossy fiber pathway: a review. Neuroscience 98:407–427.

Henze, DA, Wittner, L, Buzsaki, G (2002) Single granule cells reliably discharge targets in the hippocampal CA3 network in vivo. Nature neuroscience 5:790–795.

Herculano-Houzel S (2012) The remarkable, yet not extraordinary, human brain as a scaled-up primate brain and its associated cost. Proc Natl Acad Sci 109:10661-8.

Hilgetag, CC, Medalla, M, Beul, SF, Barbas, H (2016) The primate connectome in context: Principles of connections of the cortical visual system. Neuroimage 134:685–702.

Hjorth-Simonsen, A, Jeune, B (1972) Origin and termination of the hippocampal perforant path in the rat studied by silver impregnation. J Comp Neurol 144:215–232.

Hökfelt T, Johansson O, Goldstein M. Chemical anatomy of the brain. Science. 1984 Sep 21;225(4668):1326–34.

Hosp, JA, Struber, M, Yanagawa, Y, Obata, K, Vida, I, Jonas, P, Bartos, M (2014) Morpho-physiological criteria divide dentate gyrus interneurons into classes. Hippocampus 24:189–203.

Hou, WH, Kuo, N, Fang, GW, Huang, HS, Wu, KP, Zimmer, A, Cheng, JK, Lien, CC (2016) Wiring Specificity and Synaptic Diversity in the Mouse Lateral Central Amygdala. J Neurosci 36:4549–4563.

Hsu, TT, Lee, CT, Tai, MH, Lien, CC (2015) Differential Recruitment of Dentate Gyrus Interneuron Types by Commissural Versus Perforant Pathways. Cerebral cortex 26:2715–2727.

Hurley, KM, Herbert, H, Moga, MM, Saper, CB (1991) Efferent projections of the infralimbic cortex of the rat. The Journal of comparative neurology 308:249–276.

Ikegaya Y, Saito H, Abe K (1996a) The basomedial and basolateral amygdaloid nuclei contribute to the induction of long-term potentiation in the dentate gyrus in vivo. The European journal of neuroscience 8:1833–1839.

Ikegaya Y, Saito H, Abe K (1996b) Dentate gyrus field potentials evoked by stimulation of the basolateral amygdaloid nucleus in anesthetized rats. Brain research 718:53–60.

Ikemoto S (2005) The supramammillary nucleus mediates primary reinforcement via GABA(A) receptors. Neuropsychopharmacology 30:1088–1095.

Ito HT, Moser EI, Moser MB (2018) Supramammillary Nucleus Modulates Spike-Time Coordination in the Prefrontal-Thalamo-Hippocampal Circuit during Navigation. Neuron 99:576–587.

Ito M, Shirao T, Doya K, Sekino Y (2009) Three-dimensional distribution of Fos-positive neurons in the supramammillary nucleus of the rat exposed to novel environment. Neurosci Res 64:397–402.

James W (1890) Principles of Psychology. Henry Holt, New York.

Jan LY, Jan YN (1982) Peptidergic transmission in sympathetic ganglia of the frog. J Physiol 327:219–246.

Jimenez JC, Su K, Goldberg, AR, Luna VM, Biane, JS, Ordek, G, Zhou, P, Ong SK, Wright, MA, Zweifel L, Paninski L, Hen R, Kheirbek, MA (2018) Anxiety cells in a hippocampal-hypothalamic circuit. Neuron 97, 670–683.

Jonas P, Bischofberger J, Fricker D, Miles R (2004) Interneuron Diversity series: Fast in, fast out--temporal and spatial signal processing in hippocampal interneurons. Trends Neurosci 27:30–40.

Jonas P, Bischofberger J, Sandkuhler J (1998) Corelease of two fast neurotransmitters at a central synapse. Science 281:419–424.

Jonides J, Lewis RL, Nee DE, Lustig CA, Berman MG, Moore KS. The mind and brain of short-term memory. Annu Rev Psychol 59:193–224.

Jurkowski MP, Bettio L, Woo EK, Patten A, Yau SY, Gil-Mohapel J (2020) Beyond the Hippocampus and the SVZ: Adult Neurogenesis Throughout the Brain. Frontiers in cellular neuroscience, 14:576444.

Kandel ER, Schwartz JH (1982) Molecular biology of learning: modulation of transmitter release. Science 218:433–443.

Kandel ER, Schwartz JH, Jessell TM, Siegelbaum SA, Hudspeth AJ, Mack S (2013) Principles of neural science (Fifth edition.). New York, N.Y.: McGraw-Hill Education LLC...

Kara P, Reinagel P, Reid RC (2000) Low response variability in simultaneously recorded retinal, thalamic, and cortical neurons. Neuron 27:635–646.

Kesner RP (2007) A behavioral analysis of dentate gyrus function. Prog Brain Res 163:567–576.

Kheirbek MA, Drew LJ, Burghardt NS, Costantini DO, Tannenholz L, Ahmari SE, Zeng H, Fenton AA, Hen, R (2013) Differential control of learning and anxiety along the dorsoventral axis of the dentate gyrus. Neuron 77:955–968.

Kirk IJ (1998) Frequency modulation of hippocampal theta by the supramammillary nucleus, and other hypothalamo-hippocampal interactions: mechanisms and functional implications. Neuroscience and biobehavioral reviews 22:291–302.

Kirk IJ, Mackay JC (2003) The role of theta-range oscillations in synchronising and integrating activity in distributed mnemonic networks. Cortex; a journal devoted to the study of the nervous system and behavior 39:993–1008.

Kirk IJ, McNaughton N (1991) Supramammillary cell firing and hippocampal rhythmical slow activity. Neuroreport 2:723–725.

Kirk IJ, McNaughton N (1993) Mapping the differential effects of procaine on frequency and amplitude of reticularly elicited hippocampal rhythmical slow activity. Hippocampus 3:517–525.

Kiss J, Csaki A, Bokor H, Kocsis K, Szeiffert G (1997) Topographic localization of calretinin, calbindin, VIP, substance P, CCK and metabotropic glutamate receptor immunoreactive neurons in the supramammillary and related areas of the rat. Neurobiology 5:361–388.

Kiss J, Csaki A, Bokor H, Shanabrough M, Leranth C (2000) The supramammillo-hippocampal and supramammillo-septal glutamatergic/aspartatergic projections in the rat: a combined [3H]D-aspartate autoradiographic and immunohistochemical study. Neuroscience 97: 657–669.

Klancnik JM, Phillips AG (1991) Modulation of synaptic plasticity in the dentate gyrus of the rat by electrical stimulation of the median raphe nucleus. Brain research 557, 236–240.

Klausberger T, Somogyi P (2008) Neuronal diversity and temporal dynamics: the unity of hippocampal circuit operations. Science 321:53–57.

Kocsis B (2006) The effect of descending theta rhythmic input from the septohippocampal system on firing in the supramammillary nucleus. Brain research 1086:92–97.

Kocsis B, Vertes RP (1994) Characterization of neurons of the supramammillary nucleus and mammillary body that discharge rhythmically with the hippocampal theta rhythm in the rat. J Neurosci 14:7040-7052.

Kocsis B, Vertes RP (1997) Phase relations of rhythmic neuronal firing in the supramammillary nucleus and mammillary body to the hippocampal theta activity in urethane anesthetized rats. Hippocampus 7:204-214.

Kohara K, Pignatelli M, Rivest AJ, Jung HY, Kitamura T, Suh J, Frank D, Kajikawa K, Mise N, Obata Y, Wickersham IR, Tonegawa S. Cell type-specific genetic and optogenetic tools reveal hippocampal CA2 circuits. Nat Neurosci 17:269-79.

Larimer P, Strowbridge BW (2008) Nonrandom local circuits in the dentate gyrus. J. Neurosci 28:12212–12223.

Lee CT, Kao MH, Hou WH, Wei YT, Chen CL, Lien CC (2016) Causal Evidence for the Role of Specific GABAergic Interneuron Types in Entorhinal Recruitment of Dentate Granule Cells. Sci Rep 6:36885.

Lensjo KK, Christensen AC, Tennoe S, Fyhn M, Hafting T (2017) Differential Expression and Cell-Type Specificity of Perineuronal Nets in Hippocampus, Medial Entorhinal Cortex, and Visual Cortex Examined in the Rat and Mouse. eNeuro 4.

Leranth C, Carpi D, Buzsaki G, Kiss J (1999) The entorhino-septo-supramammillary nucleus connection in the rat: morphological basis of a feedback mechanism regulating hippocampal theta rhythm. Neuroscience 88, 701-718.

Leranth C, Hajszan T (2007) Extrinsic afferent systems to the dentate gyrus. Progress in brain research 163:63-84.

Leranth C, Kiss J (1996) A population of supramammillary area calretinin neurons terminating on medial septal area cholinergic and lateral septal area calbindin-containing cells are aspartate/glutamatergic. J Neurosci 16:7699-710.

Leranth C, Nitsch R (1994) Morphological evidence that hypothalamic substance P-containing afferents are capable of filtering the signal flow in the monkey hippocampal formation. J Neurosci 14:4079-4094.

Leutgeb JK, Leutgeb S, Moser MB, Moser EI (2007) Pattern separation in the dentate gyrus and CA3 of the hippocampus. Science 315:961-966.

Li WC, Soffe SR, Roberts A (2004) Glutamate and acetylcholine corelease at developing synapses. Proceedings of the National Academy of Sciences of the United States of America 101:15488-15493.

Li Y, Stam FJ, Aimone JB, Goulding M, Callaway EM, Gage FH. Molecular layer perforant path-associated cells contribute to feed-forward inhibition in the adult dentate gyrus. Proc Natl Acad Sci 110:9106-11.

Liu G (2004) Local structural balance and functional interaction of excitatory and inhibitory synapses in hippocampal dendrites. Nature neuroscience 7:373-379.

Liu X, Ramirez S, Pang PT, Puryear CB, Govindarajan A, Deisseroth K, Tonegawa S (2012) Optogenetic stimulation of a hippocampal engram activates fear memory recall. Nature 484:381-385.

Liu YC, Cheng JK, Lien CC (2014) Rapid dynamic changes of dendritic inhibition in the dentate gyrus by presynaptic activity patterns. J Neurosci 34:1344-1357.

López-Ferreras L, Eerola K, Shevchouk OT, Richard JE, Nilsson FH, Jansson LE, Hayes MR, Skibicka KP (2020) The supramammillary nucleus controls anxiety-like behavior; key role of GLP-1R. Psychoneuroendocrinology 119:104720.

Magloczky Z, Acsady L, Freund TF (1994) Principal cells are the postsynaptic targets of supramammillary afferents in the hippocampus of the rat. Hippocampus 4:322-334.

Malenka RC (1994) Synaptic plasticity in the hippocampus: LTP and LTD. Cell 78:535–538.

Markwardt SJ, Dieni CV, Wadiche JI, Overstreet-Wadiche L (2011) Ivy/neurogliaform interneurons coordinate activity in the neurogenic niche. Nat Neurosci 14:1407.

Martin SJ, Grimwood PD, Morris RGM (2000) Synaptic plasticity and memory: an evaluation of the hypothesis. Annu. Rev. Neurosci. 23, 649–711.

McBain CJ, Fisahn A (2001) Interneurons unbound. Nature reviews Neuroscience 2:11-23.

McHugh TJ, Jones MW, Quinn JJ, Balthasar N, Coppari R, Elmquist JK, Lowell BB, Fanselow MS, Wilson MA, Tonegawa S. 2007. Dentate gyrus NMDA receptors mediate rapid pattern separation in the hippocampal network. Science 317:94–99.

McNaughton BL, Douglas RM, Goddard GV (1978) Synaptic enhancement in fascia dentata: co-operativity among coactive afferents. Brain Research 157:277–293.

McNaughton BL, Morris RGM (1987) Hippocampal synaptic enhancement and information storage within a distributed memory system. Trends in Neurosciences 10:408–415.

McNaughton N, Logan B, Panickar KS, Kirk IJ, Pan WX, Brown NT, Heenan A (1995) Contribution of synapses in the medial supramammillary nucleus to the frequency of hippocampal theta rhythm in freely moving rats. Hippocampus 5:534-545.

Meister ML, Buffalo EA (2018) Neurons in primate entorhinal cortex represent gaze position in multiple spatial reference frames. J Neurosci 38:2430-2441.

Merzenich MM, Sameshima K (1993) Cortical plasticity and memory. Curr Opin Neurobiol 3:187–196.

Meye FJ, Soiza-Reilly M, Smit T, Diana MA, Schwarz MK, Mameli M (2016) Shifted pallidal co-release of GABA and glutamate in habenula drives cocaine withdrawal and relapse. Nature neuroscience 19:1019-1024.

Ming GL, Song H (2011) Adult neurogenesis in the mammalian brain: significant answers and significant questions. Neuron, 70:687–702.

Moodley KK, Chan D (2014) The hippocampus in neurodegenerative disease. Frontiers of neurology and neuroscience 34:95-108.

Moser E, Moser MB, Andersen P (1993) Spatial learning impairment parallels the magnitude of dorsal hippocampal lesions, but is hardly present following ventral lesions. J Neurosci 13:3916-3925.

Moser EI, Moser MB, McNaughton BL (2017) Spatial representation in the hippocampal formation: a history. Nature neuroscience 20:1448-1464.

Nafstad PH (1967) An electron microscope study on the termination of the perforant path fibres in the hippocampus and the fascia dentata. Z Zellforsch Mikrosk Anat 76:532-42.

Nakanishi K, Saito H, Abe K (2001) The supramammillary nucleus contributes to associative EPSP-spike potentiation in the rat dentate gyrus in vivo. The European journal of neuroscience 13:793-800.

Nakashiba T, Cushman JD, Pelkey KA, Renaudineau S, Buhl DL, McHugh TJ, Rodriguez Barrera V, Chittajallu R, Iwamoto KS, McBain CJ, Fanselow MS, Tonegawa S (2012) Young dentate granule cells mediate pattern separation, whereas old granule cells facilitate pattern completion. Cell 149:188-201.

Nakashiba T, Young JZ, McHugh TJ, Buhl, DL, Tonegawa, S (2008) Transgenic inhibition of synaptic transmission reveals role of CA3 output in hippocampal learning. Science 319, 1260-1264.

Neves G, Cooke SF, Bliss TVP (2008) Synaptic plasticity, memory and the hippocampus: a neural network approach to causality. Nature Rev. Neurosci. 9:65–75.

Nitsch R, Leranth C (1993) Calretinin immunoreactivity in the monkey hippocampal formation--II. Intrinsic GABAergic and hypothalamic non-GABAergic systems: an experimental tracing and co-existence study. Neuroscience 55:797-812.

Nitsch R, Leranth C (1994) Substance P-containing hypothalamic afferents to the monkey hippocampus: an immunocytochemical, tracing, and coexistence study. Experimental brain research 101:231-240.

Ocana FM, Uceda S, Arias JL, Salas C, Rodriguez F (2017) Dynamics of Goldfish Subregional Hippocampal Pallium Activity throughout Spatial Memory Formation. Brain, behavior and evolution 90:154-170.

O'Keefe J, Dostrovsky J (1971) The hippocampus as a spatial map. Preliminary evidence from unit activity in the freely-moving rat. Brain research 34:171-175.

Otto T, Schottler F, Staubli U, Eichenbaum H, Lynch G (1991) Hippocampus and olfactory discrimination learning: effects of entorhinal cortex lesions on olfactory learning and memory in a successive-cue, go-no-go task. Behavioral neuroscience 105, 111-119.

Pan WX, McNaughton N (2004) The supramammillary area: its organization, functions and relationship to the hippocampus. Progress in neurobiology 74:127-166.

Paton JA, Nottebohm FN (1984) Neurons generated in the adult brain are recruited into functional circuits. Science 225:1046-8.

Patton PE, Mcnaughton B (1995) Connection matrix of the hippocampal-formation .1. The dentate gyrus. Hippocampus 5:245–286.

Pedersen NP, Ferrari L, Venner A, Wang JL, Abbott SBG, Vujovic N, Arrigoni E, Saper CB, Fuller PM (2017) Supramammillary glutamate neurons are a key node of the arousal system. Nat Commun 8:1405.

Pelkey KA, Chittajallu R, Craig MT, Tricoire L, Wester JC, McBain CJ (2017) Hippocampal GABAergic inhibitory interneurons. Physiol Rev 97:1619–1747.

Penttonen M, Kamondi A, Acsády L, Buzsáki G (1998) Gamma frequency oscillation in the hippocampus of the rat: intracellular analysis in vivo. Eur J Neurosci 10:718–728.

Pignatelli M, Beyeler A, Leinekugel X (2012) Neural circuits underlying the generation of theta oscillations. Journal of physiology 106:81-92.

Pouille F, Scanziani M (2001). Enforcement of temporal fidelity in pyramidal cells by somatic feed-forward inhibition. Science *293*, 1159–1163.

Prasad, JA, Chudasama, Y (2013) Viral tracing identifies parallel disynaptic pathways to the hippocampus. J Neurosci 33:8494-8503.

Ramaswamy S (2015) Exciting times for inhibition: GABAergic synaptic transmission in dentate gyrus interneuron networks. Frontiers in neural circuits 9:13.

Ramirez S, Liu X, MacDonald CJ, Moffa A, Zhou J, Redondo RL, Tonegawa S (2015) Activating positive memory engrams suppresses depression-like behaviour. Nature 522:335-339.

Ransome MI, Renoir T, Hannan AJ (2012) Hippocampal neurogenesis, cognitive deficits and affective disorder in Huntington's disease. Neural plasticity 2012:874387.

Reich DS, Victor JD, Knight BW, Ozaki T, Kaplan E (1997) Response variability and timing precision of neuronal spike trains in vivo. Journal of neurophysiology 77:2836-2841.

Reinagel P, Reid RC (2002) Precise firing events are conserved across neurons. J Neurosci 22:6837-6841.

Renouard L, Billwiller F, Ogawa K, Clément O, Camargo N, Abdelkarim M, Gay N, Scoté-Blachon C, Touré R, Libourel PA, Ravassard P, Salvert D, Peyron C, Claustrat B, Léger L, Salin P, Malleret G, Fort P, Luppi PH (2015) The supramammillary nucleus and the claustrum activate the cortex during REM sleep. Science advances, 1(3), e1400177.

Risold, PY, Swanson, LW (1997) Connections of the rat lateral septal complex. Brain research Brain research reviews 24:115-195.

Robert V, Therreau L, Chevaleyre V, Lepicard E, Viollet C, Cognet J, Huang AJ, Boehringer R, Polygalov D, McHugh TJ, Piskorowski RA (2021) Local circuit allowing hypothalamic control of hippocampal area CA2 activity and consequences for CA1. Elife 10:e63352.

Robinson, GB, Racine, RJ (1982) Heterosynaptic interactions between septal and entorhinal inputs to the dentate gyrus: long-term potentiation effects. Brain research 249:162-166.

Rodriguez, F, Lopez, JC, Vargas, JP, Broglio, C, Gomez, Y, Salas, C (2002) Spatial memory and hippocampal pallium through vertebrate evolution: insights from reptiles and teleost fish. Brain research bulletin 57:499-503.

Rodriguez-Exposito, B, Gomez, A, Martin-Monzon, I, Reiriz, M, Rodriguez, F, Salas, C (2017) Goldfish hippocampal pallium is essential to associate temporally discontiguous events. Neurobiology of learning and memory 139:128-134.

Root, DH, Mejias-Aponte, CA, Zhang, S, Wang, HL, Hoffman, AF, Lupica, CR, Morales, M (2014) Single rodent mesohabenular axons release glutamate and GABA. Nature neuroscience 17:1543-1551.

Root, DH, Zhang, S, Barker, DJ, Miranda-Barrientos, J, Liu, B, Wang, HL, Morales, M (2018) Selective Brain Distribution and Distinctive Synaptic Architecture of Dual Glutamatergic-GABAergic Neurons. Cell Rep 23:3465-3479.

Santin, LJ, Aguirre, JA, Rubio, S, Begega, A, Miranda, R, Arias, JL (2003) C-fos expression in supramammillary and medial mammillary nuclei following spatial reference and working memory tasks. Physiol. Behav. 78:733–739.

Sargolini, F, Fyhn, M, Hafting, T, McNaughton, BL, Witter, MP, Moser, MB, Moser, EI (2006) Conjunctive representation of position, direction, and velocity in entorhinal cortex. Science 312:758–762.

Savanthrapadian S, Meyer T, Elgueta C, Booker SA, Vida I, Bartos M (2014) Synaptic properties of SOM- and CCK-expressing cells in dentate gyrus interneuron networks. J Neurosci 34:8197–8209.

Scharfman, HE (2007) The CA3 "backprojection" to the dentate gyrus. Prog Brain Res 163:627–637.

Scharfman, HE (2016). The enigmatic mossy cell of the dentate gyrus. Nat. Rev. Neurosci.17, 562–575.

Scharfman, HE, Myers, CE (2012) Hilar mossy cells of the dentate gyrus: a historical perspective. Frontiers in neural circuits 6:106.

Schmidt-Hieber C, Jonas P, Bischofberger J (2004) Enhanced synaptic plasticity in newly generated granule cells of the adult hippocampus. Nature 429:184–187.

Scoville, WB, Milner, B (1957) Loss of recent memory after bilateral hippocampal lesions. Journal of neurology, neurosurgery, and psychiatry 20:11-21.

Segal, M, Landis, S (1974) Afferents to the hippocampus of the rat studied with the method of retrograde transport of horseradish peroxidase. Brain Res 78:1–15.

Senzai Y, Buzsáki G (2017) Physiological properties and behavioral correlates of hippocampal granule cells and mossy cells. Neuron 93, 691-704.

Seo DO, Zhang ET, Piantadosi SC, Marcus DJ, Motard LE, Kan BK, Gomez AM, Nguyen TK, Xia L, Bruchas MR (2021) A locus coeruleus to dentate gyrus noradrenergic circuit modulates aversive contextual processing. Neuron 109:2116–2130.

Shabel, SJ, Proulx, CD, Piriz, J, Malinow, R (2014) Mood regulation. GABA/glutamate co-release controls habenula output and is modified by antidepressant treatment. Science 345:1494-1498.

Shadlen, MN, Newsome, WT (1998) The variable discharge of cortical neurons: implications for connectivity, computation, and information coding. J Neurosci 18:3870–3896.

Shepard, PD, Mihailoff, GA, German, DC (1988) Anatomical and electrophysiological characterization of presumed dopamine-containing neurons within the supramammillary region of the rat. Brain research bulletin 20:307-314.

Silveira, MCL, Sandner, G, Graeff, FG (1993) Induction of fos immunoreactivity in the brain by exposure to the elevated plus-maze. Behav. Brain Res. 56:115–118.

Small, SA, Schobel, SA, Buxton, RB, Witter, MP, Barnes, CA (2011) A pathophysiological framework of hippocampal dysfunction in ageing and disease. Nature reviews Neuroscience 12:585-601.

Solstad, T, Boccara, CN, Kropff, E, Moser, MB, Moser, EI (2008) Representation of geometric borders in the entorhinal cortex. Science 322:1865-1868.

Somogyi, J (2006) Functional significance of co-localization of GABA and Glu in nerve terminals: a hypothesis. Current topics in medicinal chemistry 6:969-973.

Soriano, E, Frotscher, M (1994) Mossy cells of the rat fascia dentata are glutamate-immunoreactive. Hippocampus 4:65-69.

Soussi, R, Boulland, JL, Bassot, E, Bras, H, Coulon, P, Chaudhry, FA, Storm-Mathisen, J, Ferhat, L, Esclapez, M (2015) Reorganization of supramammillary-hippocampal pathways in the rat pilocarpine model of temporal lobe epilepsy: evidence for axon terminal sprouting. Brain structure & function 220:2449-2468.

Soussi, R, Zhang, N, Tahtakran, S, Houser, CR, Esclapez, M (2010) Heterogeneity of the supramammillary-hippocampal pathways: evidence for a unique GABAergic

neurotransmitter phenotype and regional differences. The European journal of neuroscience 32:771-785.

Squire LR (1987) Memory and Brain. Oxford University Press, New York.

Squire LR (2004) Memory systems of the brain: a brief history and current perspective. Neurobiol Learn Mem 82:171–177.

Stachenfeld, KL, Botvinick, MM, Gershman, SJ (2017) The hippocampus as a predictive map. Nature neuroscience 20:1643-1653.

Stam, CJ, van Straaten, EC (2012) The organization of physiological brain networks. Clinical neurophysiology : official journal of the International Federation of Clinical Neurophysiology 123:1067-1087.

Stanfield, BB, Cowan, WM (1984) An EM autoradiographic study of the hypothalamo-hippocampal projection. Brain research 309:299-307.

Stone SS, Teixeira CM, Devito LM, Zaslavsky K, Josselyn SA, Lozano AM, Frankland PW (2011) Stimulation of entorhinal cortex promotes adult neurogenesis and facilitates spatial memory. J Neurosci 31:13469-84.

Strange, BA, Witter, MP, Lein, ES, Moser, EI (2014) Functional organization of the hippocampal longitudinal axis. Nature reviews Neuroscience 15:655-669.

Sulzer, D, Rayport, S (2000) Dale's principle and glutamate corelease from ventral midbrain dopamine neurons. Amino acids 19:45-52.

Swanson, LW (1982) The projections of the ventral tegmental area and adjacent regions: a combined fluorescent retrograde tracer and immunofluorescence study in the rat. Brain research bulletin 9:321-353.

Swanson, LW (2018) Brain maps 4.0-Structure of the rat brain: An open access atlas with global nervous system nomenclature ontology and flatmaps. The Journal of comparative neurology 526:935-943.

Swanson, LW, Cowan, WM (1979) The connections of the septal region in the rat. The Journal of comparative neurology 186:621-655.

Takács VT, Cserép C, Schlingloff D, Pósfai B, Szőnyi A, Sos KE, Környei Z, Dénes Á, Gulyás AI, Freund TF, Nyiri G (2018) Co-transmission of acetylcholine and GABA regulates hippocampal states. Nat Commun 9(1):2848.

Tamminga, CA, Stan, AD, Wagner, AD (2010) The hippocampal formation in schizophrenia. Am J Psychiatry 167:1178-1193.

Taube, JS, Muller, RU, Ranck, JB, Jr. (1990). Head-direction cells recorded from the postsubiculum in freely moving rats. I. Description and quantitative analysis. J Neurosci 10:420-435.

Thinschmidt, JS, Kinney, GG, Kocsis, B (1995) The supramammillary nucleus: is it necessary for the mediation of hippocampal theta rhythm? Neuroscience 67:301-312.

Thompson RF, Krupa DJ (1994) Organization of memory traces in the mammalian brain. Annu Rev Neurosci 17:519–550.

Treves A, Tashiro A, Witter MP, Moser EI (2008) What is the mammalian dentate gyrus good for? Neuroscience 154:1155-1172.

Tritsch NX, Ding JB, Sabatini BL (2012) Dopaminergic neurons inhibit striatal output through non-canonical release of GABA. Nature 490:262–266.

Tulving E, Schacter DL (1990) Priming and human memory systems. Science 247:301 306.

Turrigiano, G.G., and Nelson, S.B. (2004). Homeostatic plasticity in the developing nervous system. Nature reviews Neuroscience 5, 97-107.

Tyan L, Chamberland S, Magnin E, Camiré O, Francavilla R, David LS, Deisseroth K, Topolnik L (2014) Dendritic inhibition provided by interneuron-specific cells controls the firing rate and timing of the hippocampal feedback inhibitory circuitry. J Neurosci 34:4534–4547.

Vaaga CE, Borisovska M, Westbrook GL (2014) Dual-transmitter neurons: Functional implications of co-release and co-transmission. Curr. Opin. Neurobiol 29: 25–32.

van Groen T, Wyss JM (1990) Extrinsic projections from area CA1 of the rat hippocampus: olfactory, cortical, subcortical, and bilateral hippocampal formation projections. The Journal of comparative neurology 302, 515-528.

Vann SD, Brown MW, Aggleton JP (2000) Fos expression in the rostral thalamic nuclei and associated cortical regions in response to different spatial memory tests. Neuroscience 101:983–991.

Vertes RP (1992) PHA-L analysis of projections from the supramammillary nucleus in the rat. The Journal of comparative neurology 326, 595-622.

Vertes RP (2015) Major diencephalic inputs to the hippocampus: supramammillary nucleus and nucleus reuniens. Circuitry and function. Progress in brain research 219:121-144.

Vertes RP, Kocsis B (1997) Brainstem-diencephalo-septohippocampal systems controlling the theta rhythm of the hippocampus. Neuroscience 81:893-926.

Vertes RP, Martin GF, Waltzer R (1986) An autoradiographic analysis of ascending projections from the medullary reticular formation in the rat. Neuroscience 19:873-898.

Vertes RP, McKenna JT (2000) Collateral projections from the supramammillary nucleus to the medial septum and hippocampus. Synapse 38:281-293.

Vivar C, Potter MC, Choi J, Lee JY, Stringer TP, Callaway EM, Gage FH, Suh H, van Praag H (2012) Monosynaptic inputs to new neurons in the dentate gyrus. Nat Commun 3:1107.

Vivar C, van Praag H (2013) Functional circuits of new neurons in the dentate gyrus. Frontiers in neural circuits 7:15.

Vreeswijk CV, Sompolinsky H (1996) Chaos in neuronal networks with balanced excitatory and inhibitory activity. Science 274:1724-1726.

Wang KY, Wu JW, Cheng JK, Chen CC, Wong WY, Averkin RG, Tamás G, Nakazawa K, Lien CC (2021) Elevation of hilar mossy cell activity suppresses hippocampal excitability and avoidance behavior. Cell Rep. 36:109702.

West MJ (1990) Stereological studies of the hippocampus: a comparison of the hippocampal subdivisions of diverse species including hedgehogs, laboratory rodents, wild mice and men. Progress in brain research 83, 13-36.

Wheeler ME, Petersen SE, Buckner RL (2000) Memory's echo: vivid remembering reactivates sensory-specific cortex. Proc Natl Acad Sci 97:11125–11129.

Whitlock JR, Heynen AJ, Shuler MG, Bear MF (2006) Learning induces long-term potentiation in the hippocampus. Science 313:1093–1097.

Woodruff AR, Sah P (2007) Inhibition and synchronization of basal amygdala principal neuron spiking by parvalbumin-positive interneurons. Journal of neurophysiology 98:2956-2961.

Yassa MA, Stark CE (2011) Pattern separation in the hippocampus. Trends in neurosciences 34, 515-525.

Yeh CY, Asrican B, Moss J, Quintanilla LJ, He T, Mao X, Cassé F, Gebara E, Bao H, Lu W, Toni N, Song J (2018) Mossy Cells Control Adult Neural Stem Cell Quiescence and Maintenance through a Dynamic Balance between Direct and Indirect Pathways. Neuron 99:493-510.

Yuan M, Meyer T, Benkowitz C, Savanthrapadian S, Ansel-Bollepalli L, Foggetti A, Wulff P, Alcami P, Elgueta C, Bartos M (2017) Somatostatin-positive interneurons in the dentate gyrus of mice provide local- and long-range septal synaptic inhibition. eLife 6:e21105.

Zaitsev AV (2013) Classification and function of GABAergic interneurons of the mammalian cerebral cortex. Biochem. Moscow Suppl. Ser. A 7:245–259.

Zhang SJ, Ye J, Miao C, Tsao A, Cerniauskas I, Ledergerber D, Moser MB, Moser EI (2013) Optogenetic dissection of entorhinal-hippocampal functional connectivity. Science 340: 1232627.

Zucker HR, Ranganath C (2015) Navigating the human hippocampus without a GPS. Hippocampus 25:697-703.

CURRICULUM VITAE

Ajibola, Musa Iyiola, M.Sc
Taiwan International Graduate Program
National Yang Ming Chiao Tung University and Academia Sinica,
Institute of Neuroscience
No. 155, Section 2, LiNong Street, Beitou District
Taipei 112, Taiwan
Tel: +886 (09) 6565-5454; E-mail: musaiyiola@gmail.com

EDUCATION/TRAINING

INSTITUTION AND LOCATION	DEGREE	YEAR(s)	FIELD OF STUDY
University of Ilorin, Nigeria	B.Sc.	2007-2010	Anatomy
University of Ilorin, Nigeria	M.Sc.	2011-2013	Anatomy
National Yang Ming Chiao Tung University	Ph.D.	2015-2021	Neuroscience

Personal Statement

Humans learn from experience and perceive ongoing behaviors based on experience. This is essential for the survival of animals and humans. My overarching interest is to understand the circuit mechanisms underlying cognitive and emotional behaviors and how these can be explored to better understand neurological disorders to provide helps to patients. I would also like to understand how the interactions between the cortical and subcortical brain areas inspire complex behaviors such as cognition and emotion. In my research, I focus on understanding physiological relevance of subcortical inputs from the hypothalamic to the hippocampus.

Honors and Scholarships

- 2021: Winner of outstanding international student scholarship of National Yang Ming Chiao Tung University
- 2020: Recipient of research performance fellowship of Academia Sinica
- 2018: Winner of outstanding thesis award at 2018 Annual thesis competition of National-Yang-Ming University
- 2018: Recipient of best poster travel grants award of TIGP-INS 2018 retreat to attend 2018 Federation of European neuroscience (FENS) forum in Berlin, Germany.
- 2015-2018: Ph.D. scholarship of Taiwan International Graduate Program (TIGP) in Interdisciplinary Neuroscience.

- 2015: IBRO travel grant award to attend 2015 society of Neuroscience (sfn) meeting in San diego, USA
- 2014: IBRO travel grant award to attend society of African neuroscience (SONA) meeting in Durban, South Africa.
- 2010: A recipient of Overall Best Graduating Student Award, Faculty of Basic Medical Sciences, College of Health Sciences, University of Ilorin, Nigeria. 2009/2010 Academic Session.

Workshops/Training Programmes/Conferences Attended

- 11th FENS forum of Neuroscience, Berlin, Germany.
- 2018 annual meeting of Neuroscience Society of Taiwan (NST), Tainan, Taiwan.
- 2018 EMBO conference on neural development, Academia Sinica, Taipei, Taiwan
- 2017 annual meeting of Neuroscience Society of Taiwan (NST), Taipei, Taiwan.
- 2015 EMBO conference on neural development, Academia Sinica, Taipei, Taiwan.
- A participant at 12th International Meeting of Society of Neuroscientists of Africa, Durban, South Africa, 26 – 30th March, 2015. Theme: ***Brain science".***

Positions and Employment

- Assistant lecturer at Kampala International University, Western-campus, Ishaka-Bushenyi, Uganda. (2013–2015)

Other Experience and Professional Memberships

- 2017 – Present: The Chinese Physiological Society, Taiwan
- 2014 – Present: Society for Neuroscience (SfN), USA
- 2017 – Present: Neuroscience Society of Taiwan (NST)
- 2014 – Present: Neuroscience Society of Nigeria (NSN)

Peer-reviewed publications

1. **Ajibola MI**, Wu JW, Abdulmajeed WI, Lien CC (2021) Hypothalamic Glutamate/GABA Cotransmission Modulates Hippocampal Circuits and Supports Long-Term Potentiation. ***J Neurosci*** 41:8181–8196.

2. Aminu I, Sulaiman N, Oyewole A, Chengetanai S, Williams V, **Ajibola MI**, Folarin R, Muhammad A, Shittu S, Ajao MS, (2018). Chlorpyrifos- and Dichlorvos-Induced Oxidative and Neurogenic Damage Elicits Neuro-Cognitive Deficits and Increases Anxiety-Like Behavior in Wild-Type Rats. ***Toxics*** 6:71.
3. **Ajibola MI**, Ibrahim RB, Masud MA, Safiriyu A, Imam A, Etibor T (2015) Neurodegenerative potential of *Ocimum gratissimum*: a histological and biochemical study. ***Anatomy journal of Africa*** 4:563–570.
4. Etibor AE, **Ajibola MI,** Mohammad OB, Safiriyu AA, Akinola OB, Ezekiel A. Caxton-Martins (2015). Datura metel administration distorts medial prefrontal cortex histology of wistar rats. ***World Journal of Neuroscience*** 5:282–291.
5. Aminu I, Abideen L, Oyewole LA, **Ajibola MI,** Williams V, Chengetanai S, Shittu TS, Ajao MS (2018) Nigella sativa conserved hippocampal oxidative and neurogenic activities to salvage neuro-cognitive integrities in chlorpyrifos insult. ***Scientific Africa*** 1, e00008.